REPORT DOCUMENTATION PAGE

Form Approved
OMB No 0704 0188

1. AGENCY USE ONLY (Leave blank)	2. REPORT DATE	3. REPORT TYPE AND DATES COVERED
	9 DEC 93	THESIS/DISSERTATION

4. TITLE AND SUBTITLE
ERROR GROWTH IN POOR ECMWF FORECASTS OVER THE CONTIGUOUS UNITED STATES

5. FUNDING NUMBERS
1

6. AUTHOR(S)
NORMAN RAY MODLIN

7. PERFORMING ORGANIZATION NAME(S) AND ADDRESS(ES)
AFIT Student Attending: TEXAS A&M UNIVERSITY

8. PERFORMING ORGANIZATION REPORT NUMBER
AFIT/CI/CIA- 93-154

9. SPONSORING/MONITORING AGENCY NAME(S) AND ADDRESS(ES)
DEPARTMENT OF THE AIR FORCE
AFIT/CI
2950 P STREET
WRIGHT-PATTERSON AFB OH 45433-7765

10. SPONSORING/MONITORING AGENCY REPORT NUMBER

11. SUPPLEMENTARY NOTES

12a. DISTRIBUTION/AVAILABILITY STATEMENT
Approved for Public Release IAW 190-1
Distribution Unlimited
MICHAEL M. BRICKER, SMSgt, USAF
Chief Administration

12b. DISTRIBUTION CODE

13. ABSTRACT (Maximum 200 words)

14. SUBJECT TERMS	15. NUMBER OF PAGES 80
	16. PRICE CODE

17. SECURITY CLASSIFICATION OF REPORT	18. SECURITY CLASSIFICATION OF THIS PAGE	19. SECURITY CLASSIFICATION OF ABSTRACT	20. LIMITATION OF ABSTRACT

ERROR GROWTH IN POOR ECMWF FORECASTS OVER THE CONTIGUOUS UNITED STATES

A Thesis

by

NORMAN RAY MODLIN

Submitted to the Office of Graduate Studies of
Texas A&M University
in partial fulfillment of the requirements for the degree of

MASTER OF SCIENCE

December 1993

Major Subject: Meteorology

ERROR GROWTH IN POOR ECMWF FORECASTS OVER THE CONTIGUOUS UNITED STATES

A Thesis

by

NORMAN RAY MODLIN

Submitted to Texas A&M University
in partial fulfillment of the requirements
for the degree of

MASTER OF SCIENCE

Approved as to style and content by:

James P. McGuirk
(Chair of Committee)

Dusan Djuric
(Member)

Steven A. Jennings
(Member)

Edward J. Zipser
(Head of Department)

December 1993

Major Subject: Meteorology

ABSTRACT

Error Growth In Poor ECMWF Forecasts

Over The Contiguous United States. (August 1993)

Norman Ray Modlin, B. S., North Carolina State University

Chair of Advisory Committee: Dr. James P. McGuirk

Successive improvements to the European Center for Medium-range Weather Forecasting model have resulted in improved forecast performance over the Contiguous United States (CONUS). While the overall performance of the model in this region was found to have improved during the period of the 1981-1990 winter seasons, the number of poor forecasts increased over this time.

This study uses the Root Mean Square (RMS) error to measure the performance of 5-day 500 mb winter forecasts over the CONUS. Poor and good forecasts were defined in terms of the 10-year distribution of the RMS values between the 1981 and 1990 winter seasons.

Subjective analysis of a subset of poor forecasts yielded no obvious patterns of error growth, location or propagation in the evolution of poor forecasts. A tendency was noted for *in situ* amplification of forecast errors. Additionally, successive forecasts verifying on the same day were found to have similar error patterns, with increased amplitudes at longer forecast lengths. This implies that the initial conditions are not a significant source of the error in poor forecasts.

Empirical Orthogonal Function (EOF) analysis of error growth in time and space revealed significant differences between poor and good forecasts. Good forecasts were found to have the majority of RMS growth on day 1 while poor forecasts did not experience rapid error growth until days 3 and 4. For poor forecasts, the leading EOFs revealed a wave pattern down stream of the Rocky Mountains. This pattern evolved and propagated throughout the forecast period until it dominated the 5-day error field. No

similar pattern was revealed in the error fields of good forecasts. This pattern suggests a dynamic link between the Rockies and the zonal wind, although no link with the 500 mb geostrophic wind could be established.

DEDICATION

This thesis is dedicated to my wife Lilah and son Christopher. They have been loving, supportive, entertaining, comforting, instructive, helpful and sometimes critical as needed. Most of all, they have always been there, even when I couldn't because of the demands of research. Many thanks are due to them for their past support and many more will be forthcoming for what they offer to me in the future. Thanks a lot, Lilah and Chris.

ACKNOWLEDGMENTS

This work would not have been possible without the assistance, knowledge and support provided by many people along the way. Special thanks are due to the European Center for Medium-range Weather Forecasting for making this data set available to the scientific community. This work is in no way intended as a criticism of their tremendous efforts in the field of medium and extended range weather forecasting. Rather it is intended as an effort to identify areas for possible improvement to the model. Thanks to Dr. James P. McGuirk for serving as my committee chair and for guiding this research. Capt Patrick M. Hayes, USAF and LT Don T. Conlee, USN shared much of their patience and computer expertise as I learned to operate the different systems at Texas A&M and within the Department of Meteorology. They also provided much knowledge of personal computers which was used to prepare this thesis. Mr. Gordon D. Carrie also offered additional computer knowledge as well as serving as computer program debugger *extraordinaire*. Thanks also to my classmates at Texas A&M. Final appreciation goes to the Air Force Institute of Technology for providing me the opportunity to continue my education via this Master's Degree program.

TABLE OF CONTENTS

Page

LIST OF FIGURES

LIST OF TABLES

CHAPTER I

INTRODUCTION

Weather forecasting has been greatly advanced in the latter portion of this century due to the advent of Numerical Weather Prediction (NWP) models. Despite tremendous advances in NWP, the goal of a perfect forecast model can not be realized for many reasons. Among them is the fact that the models use discrete observations and numerical methods to analyze and predict continuous meteorological fields and processes. As a consequence, errors in these forecasts are an unpleasant, yet unavoidable result. By studying the error characteristics of the operational NWP models, we may be able to recognize in advance if a model is producing suspicious forecast results. Additionally, the identification of these characteristics is essential in order to modify and improve their performance over time. Knowledge of the shortcomings of an NWP model, such as the European Center for Medium-Range Weather Forecasting (ECMWF) model studied here, is necessary to accurately interpret the results of the model and to identify forecasts that perform poorly. Specifically, this study will investigate the growth of 500 mb errors over the Contiguous United States, hereafter referred to as the CONUS. The focus of the error growth study will involve 5-day forecasts which are identified as poor performers in terms of Root Mean Square (RMS) error over this region. Comparisons are also made with good performing forecasts at this level and forecast length. The error growth is studied in both space and time.

The objectives of this research are presented in Chapter II. Chapter III discusses the evolution of the forecast model and reviews previous studies of forecast model errors. The data used in this research is described in Chapter IV, as well as the procedures to be used. In Chapter V, a climatology of error fields is developed, using both the absolute

---

The style used is that of *Monthly Weather Review*.

errors and the RMS error. Chapter VI presents the growth of the forecast errors in time and space, as well as the sensitivity of the growth of errors to differing initial conditions. Finally, Chapter VII summarizes all results from the research presented. The Appendix lists the valid dates of the poor and good 5-day forecasts that comprise the data sets used in the analyses of this study.

CHAPTER II

RESEARCH OBJECTIVE

The objective of this research is to document the occurrence and temporal and spatial structure of 500 mb forecast errors in poor 5-day forecasts over the contiguous United States. The distribution of errors, both forecast and RMS, are investigated to provide clues as to the preferred locations of error occurrence. Also, regional differences in the long-term distribution of RMS errors are quantified. The evolution of these errors are described in terms of typical spatial and temporal modes. It is hypothesized that there are preferred modes or patterns for these errors and that differences exist between the error modes of poor and good forecasts. It is also hypothesized that the error patterns and their growth are sensitive to the antecedent 500 mb pattern used as initial conditions for a particular run. By documenting the existence and growth of these error modes and their sensitivities, this research identifies areas of deficiency in the ECMWF model, assists in the identification of poorly evolving forecasts and provides input for future improvements.

The objectives of this research will be met by:

1. The construction of a climatology of the error fields.
2. A subjective study of error evolution, to include a case study.
3. Empirical Orthogonal Function (EOF) analysis of forecast error growth in both time and space.
4. A comparison of the EOF results for poor and good forecast categories.
5. A comparison of the EOF results for different time periods in the evolution of the ECMWF model.

CHAPTER III

BACKGROUND

Ever since the pioneering attempt at NWP by Richardson (1922), forecasts have been verified against the existing analyses to gauge the accuracy of the prediction and to identify and correct areas of deficiency. Retrospective looks such as Platzman (1967) and Lynch (1992) have shown that Richardson's model could not overcome problems with the data used as initial conditions. Recognition of such limitations has resulted in successively improved models, up through the current ECMWF model. As with previous models, this one has been studied repeatedly to determine its error characteristics.

Analysis of the error characteristics of the ECMWF must be viewed in light of the changes made to the model over time, which are intended to reduce the total forecast error. These changes are documented by Trenberth and Olson (1988). The most significant changes include the following:

a. Change from a grid-point to T63 spectral model in April 1983.

b. Inclusion of envelope orography in February 1984.

c. Extensive change to the model's analysis procedures in May 1984.

d. Modifications to radiative parameterization in December 1984.

e. Increase in horizontal resolution to T106 and modification to parameterizations of convection, clouds and condensation in May 1985.

f. Increased vertical resolution from 16 to 19 levels in May 1986.

g. Revised use of observations and data selection methods which improved the analysis procedure in September 1986.

Lorenz (1982) performed a study of 500 mb height forecasts versus analysis using data from the 1980-81 winter season operational ECMWF grid-point model. This study analyzed the global root mean square (RMS) errors in the forecast verification using the height fields in spectral format. He noted that we have a good understanding of the

dynamical processes which govern atmospheric motions, which is essential in order to predict the atmosphere's future state. However, the atmosphere itself is unstable with respect to small-scale perturbations. Therefore, observations which accurately measure large-scale features, but contain uncertainties at smaller scales, will lead to forecasts containing large-scale errors comparable to those which would exist if large-scale errors were present in the initial data.

Lorenz (1989) studied simulations of a simple chaotic forecast system in an effort to determine which has the greater effect on overall system performance; improvements to the analysis procedures or improvements to the forecast model. The simulation forecast model used sets of equations for which the solution could be computed and used as exact initial data. Analysis and model errors were then added to the data and forecast system, respectively, and then reduced singly and in combination. Improvements to the analysis procedure alone were found to bring the analysis more in line with the initial data, while increasing the difference between the analysis and forecasts. The analysis improvements were found to be most effective at shorter time ranges. Forecast model improvements, when viewed alone, reduced the total error as compared to the initial data, while reducing the forecast to analysis difference. Model improvements were most effective at longer time ranges. The greatest benefits to the overall system were achieved in concert, that is model improvements were more effective if the analysis had been previously improved, and vice versa. While these results may seem intuitive, Lorenz (1989) states that the results may not directly apply to the ECMWF system, because the simulations were not based on real atmospheric behavior and since daily ECMWF error behavior may not be independent of preceding days or the initial state.

The systematic error characteristics of the spectral ECMWF were reported by Arpe and Klinker (1986). The spectral model was chosen to replace the grid-point model because the spectral model more accurately predicts the movement of short waves (Girard and Jarraud 1982) while achieving greater computational efficiency (Simmons 1983). For

the period April 1983 - April 1985, Arpe and Klinker (1986) found that the spectral model correctly identified the positions of 500 mb troughs in 10-day forecasts, but incorrectly forecast their amplitudes. The errors exhibit a wave number 2 pattern with 500 mb heights under forecast over Northern Europe and the Bering Strait, and heights over forecast over Canada and Siberia. This error pattern was found to develop from the onset of the 10-day forecast period, with the error growing in place continually through the period. An error dipole pattern was found to exist near the main mountain ranges. This dipole continued, although reduced in amplitude, after the introduction of envelope orography in February 1984. Arpe and Klinker (1986), as well as Arpe (1989), found that the error fields exhibited an equivalent barotropic characteristic, although the error amplitudes did increase with height. Additionally, Arpe (1989) found that the most significant reductions of systematic error were achieved by modifications to the convective and radiative parameterizations in December 1984 and May 1985, respectively, with the most significant improvements noted in the winter season. This study also noted that the ECMWF model has poor skill in predicting blocking situations.

The work of Lorenz (1982) was extended by Dalcher and Kalnay (1987). Their study separated total forecast mean square error into systematic and random components. This work found that systematic errors were dominated by low total wave numbers and that the error growth rate increases monotonically with total wave number. Dalcher and Kalnay (1987) also advocate the measurement of error growth at finite times versus the Lorenz (1982) concept of "doubling time of small errors," since the determination of small errors can lead to extrapolation difficulties in a discrete data set. The current study is concerned with error growth measured at finite times.

A detailed study of the ECMWF model performance over the CONUS was accomplished by Netterville (1991). This study identified specific ECMWF 5-day forecasts of 500 mb height which performed poorly over the CONUS. The period of study was the 1981-1990 winter seasons. Poor forecast performances were identified in

terms of the RMS error of the forecast over the CONUS, and its relation to the annual distribution of these RMS values. The significant finding was that all cases of poor 5-day forecasts were found to have anomalous height departures at the initial time of the forecast in one of the three known Northern Hemisphere blocking regions. However, the presence and recognition of the blocking patterns alone was judged inadequate to determine *a priori* the skill of individual 5-day ECMWF forecast over the CONUS. Additionally, Netterville (1991) noted that both the winter season 5-day mean RMS error and its variability over the CONUS region decreased over the period of study, indicating increased forecast performance. However the annual number of poor 5-day forecasts increased toward the end of the period of study. This result indicates that the distribution of RMS errors at 5 days may not be normal, but instead may be skewed toward larger values. However, this issue was not addressed directly by Netterville (1991).

In summary, much work has been accomplished to document the systematic error characteristics of the ECMWF model. As systematic errors were identified, successive improvements to the model were incorporated in order to reduce these errors. These improved models have also been studied to document the effects of the changes. Error evolution has been studied both theoretically and empirically, but on a global basis. Evolution of errors over a limited region, specifically for specific classes of forecast performance, has not been presented.

This study will incorporate the results from these previous studies, most notably those of Netterville (1991), in order to measure the time evolution of the error field for poor forecast performances, its deviation from known systematic errors and atmospheric modes, as well as the sensitivity of the error evolution to initial conditions. However, while Netterville (1991) focused on the relationship between initial conditions and forecast performance, the research presented here will study evolutionary factors between the time of the initial conditions and the resulting 5-day forecast.

CHAPTER IV

DATA AND PROCEDURES

A. Data

The data set used in this study consists of 500 mb analyses and forecasts for the 1981-1990 winter seasons based on the global operational ECMWF model. A winter season is defined as a 100 day period beginning on 1 Dec of the previous year; that is, 1 Dec 1980 starts the 100 days of the 1981 winter season. For each of the 100 days, the verifying analysis for 00 UTC is available, as well as the ten forecasts for this valid time which were initiated 1-10 days prior. This format is commonly referred to as the "Lorenz format" and is further described by Lorenz (1982). The data are archived on magnetic tape as global coefficients of spherical harmonics with triangular truncation at total wave number 40. The spectral coefficients were converted to conventional heights (meters) using routines obtained from ECMWF and mapped onto a 3.75 by 3.75 degree grid over the Northern Hemisphere in this study for ease of computation. The resulting grid points over the Northern Hemisphere are shown in Fig. 1. In keeping with Netterville (1991), the region of interest is the CONUS region bounded by 60 W, 131.25 W, 22.5 N and 56.25 N. This region with corresponding grid points is shown in Fig. 2.

B. Procedures

Forecast performance at 5-days over the CONUS is judged in terms of the RMS statistic. Forecast performance will be analyzed using the following tasks:

a. Calculate the absolute errors over the Northern Hemisphere for the entire data set.

b. Compute the RMS value for the CONUS for all forecasts.

c. Construct 10-year histograms of the RMS values and compute the basic statistics of the distribution.

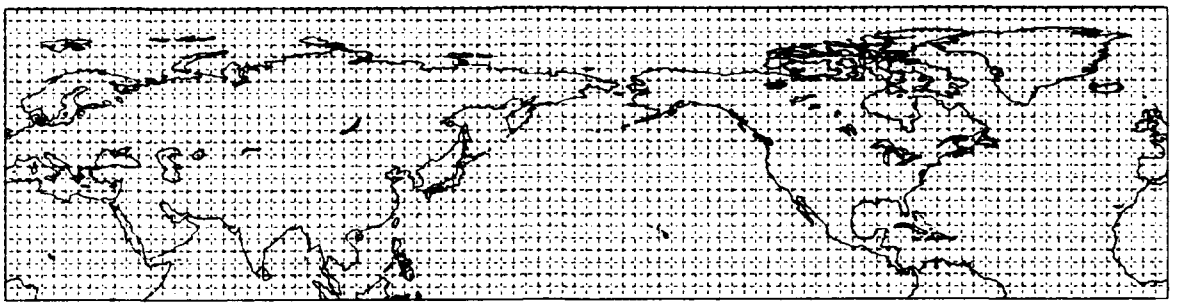

Figure 1. Northern Hemisphere with 3.75 by 3.75 degree grid.

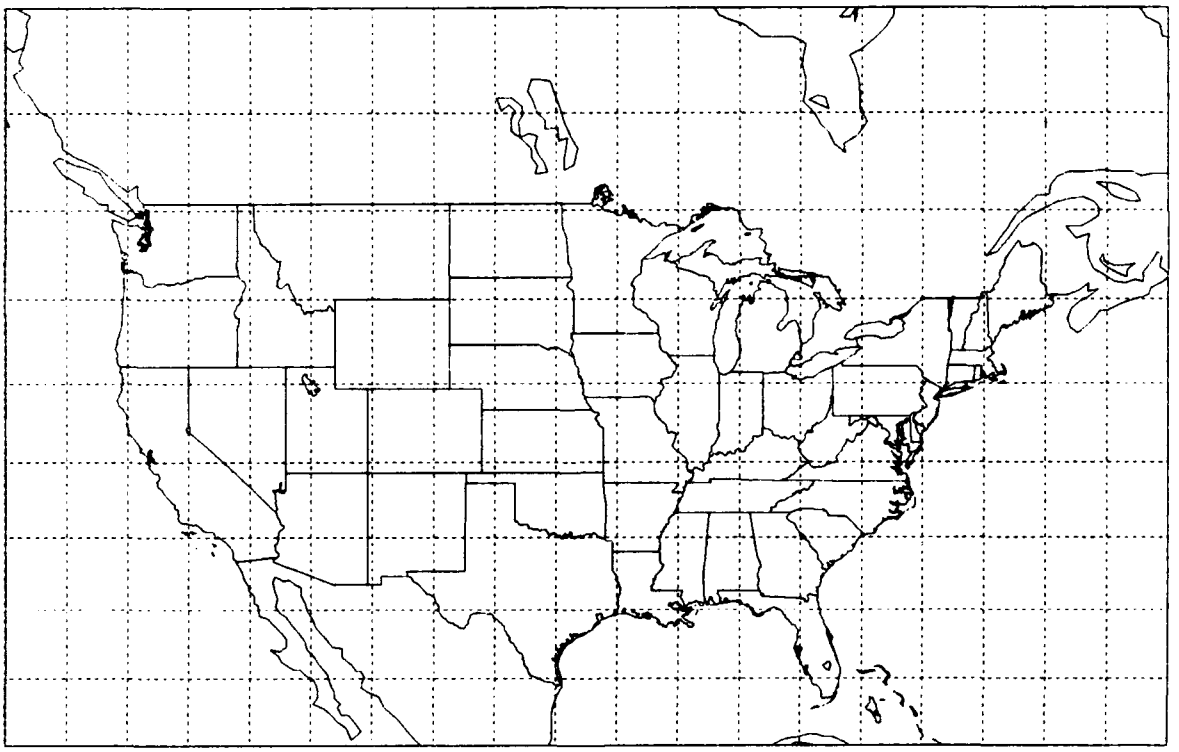

Figure 2. CONUS region of interest with 3.75 by 3.75 degree grid.

d. Define critical values for poor and good forecasts based on the 10-year distribution of RMS values.

The distribution of RMS error over the CONUS will be compared with other regions of the Northern Hemisphere. This regional variation in forecast performance will be studied in the following manner:

a. Perform steps b. - d. above for the other selected region.

b. Perform statistical tests for significance between the RMS distributions of the two regions.

Poor forecast error growth through time will be diagnosed using the following procedures:

a. A sample of poor forecasts will be examined subjectively for the origin, growth and location of error patterns.

b. The sample set will be examined for differences in error fields of poor forecasts produced by initial conditions of neighboring days.

c. Significant results and patterns, if any, from a. and b. will be examined throughout the entire data set.

d. Empirical Orthogonal Function (EOF) analysis will be performed over time on the RMS values of forecast evolution for both good and poor forecast cases.

Spatial patterns of error growth will be examined by the use of EOF analysis. Two types of EOF analysis will be performed. These analyses will be performed on the correlation and covariance matrices of the error fields. Additionally, both EOF analyses are performed with and without the mean error field. The correlation EOF analysis is used to extract error modes which are smoothed based on the standard deviation of each data point. The correlation EOFs accent areas of high variability, because they are not smoothed about the standard deviations. By leaving in the mean error field, the EOFs represent deviations about the mean error. However, by removing or correcting for the mean error, the dominant EOF is the mean error field and the remaining EOFs are

subordinate to the mean pattern. The EOF analysis will be accomplished in the following manner:

a. Perform EOF analysis on the error fields of poor and good forecasts.

b. Examine any differences which exist between these analyses.

The possible effects of bias in the case selection, as well as the effects of successive model improvements will be analyzed as follows:

a. Segregate the poor forecasts based on the operational version of the model which was used to produce them.

b. Perform EOF analysis on the error fields of these new data sets.

c. Compare the modes revealed from each version of the model with each other and with the modes revealed in the 10 year analysis.

A possible cause of the poor forecasts will be investigated by the following:

a. Compute the mean 500 mb zonal wind speeds over different geographical regions for the length of the forecast period.

b. Plot the distribution of the mean zonal wind speeds against the corresponding 5-day RMS values.

c. Examine the differences between the distributions of the zonal wind speeds for poor and good forecasts.

C. Equations

Throughout the course of this study, several equations and statistical tests will be used. They are summarized below.

In keeping with Netterville (1991), the RMS error was chosen as the standard of performance used to judge forecasts. The familiar formula for this measure is as follows:

$$\text{RMS} = \left[\frac{1}{n}\sum_{1}^{n}\left(X_f - X_o\right)^2\right]^{1/2} \qquad (1)$$

where X_f = forecast height at a grid point, X_o = observed height at a grid point and n = number of grid points in the region of interest.

The χ^2 goodness-of-fit test (Ott 1988) is used to determine the statistical significance of a distribution across several categories. The formula for this statistical test is:

$$\chi^2 = \sum_{1}^{i}\left[\frac{(n_i - E_i)^2}{E_i}\right] \qquad (2)$$

where i = the number of categories, n_i = the observed number in category i and E_i = the expected number in category i. The null hypothesis for this test is that all probabilities for each category are equal to a specified set of probabilities. The null hypothesis is rejected if χ^2 exceeds a critical value which is based on the number of categories and the desired level of confidence.

The geostrophic wind equation is used to compute a value of the mean zonal wind over the region of interest. The form of this equation from Holton (1993) is:

$$\bar{u} = -\frac{1}{f}\frac{\partial \Phi}{\partial y} \qquad (3)$$

where $\bar{u}$ is the mean zonal wind, f is the Coriolis parameter and $\frac{\partial \Phi}{\partial y}$ is the gradient of mean 500 mb geopotential heights over a specified latitudinal band. The geopotential heights are computed from the 500 mb height data.

CHAPTER V

DISTRIBUTION OF ERRORS

Prior to determining patterns of error growth, it was decided to look at the distributions of the actual forecast errors. This was done to determine the relative importance of the CONUS within the overall distribution of errors. Additionally, the distribution of the CONUS RMS values was revisited to study its statistical characteristics and seek improved criteria for defining poor forecasts. Finally, the distribution of RMS error values over a portion of the Pacific Ocean was studied to determine if differences exist between geographical regions.

A. Distribution of forecast errors

Since the critical error values used by Netterville (1991) are on the order of 100 meters for 5-day forecasts, this number is used as a representative value to measure the distribution of errors. For each grid point over the Northern Hemisphere, counts were made of the number of days with 100 meter errors of each sign, as well as for the absolute value of the error. These frequency plots for the 5-day forecast are depicted in Fig. 3.

Several features are apparent upon inspection of Fig. 3a. Most notable are the maxima located near Newfoundland and in the Southern Gulf of Alaska. These maxima affect the extreme northeast and northwest corners, respectively, of the CONUS area of interest. The CONUS region itself lies in a relative minimum of absolute error frequency. These two maxima correspond to previously documented climatological regions of explosive cyclogenesis (Roebber 1984, Uccellini 1990, Alberta et. al. 1991). The maximum over Newfoundland is dominated by positive forecast errors (Fig. 3b), which indicates that the main problem for this region is the over forecast of 500 mb heights. Another positive maximum is present over central Canada, which corresponds to the result of Arpe and Klinker (1986). Conversely, the Gulf of Alaska maximum is dominated by negative errors, (Fig 3c), indicating the preference for over development of cyclones or

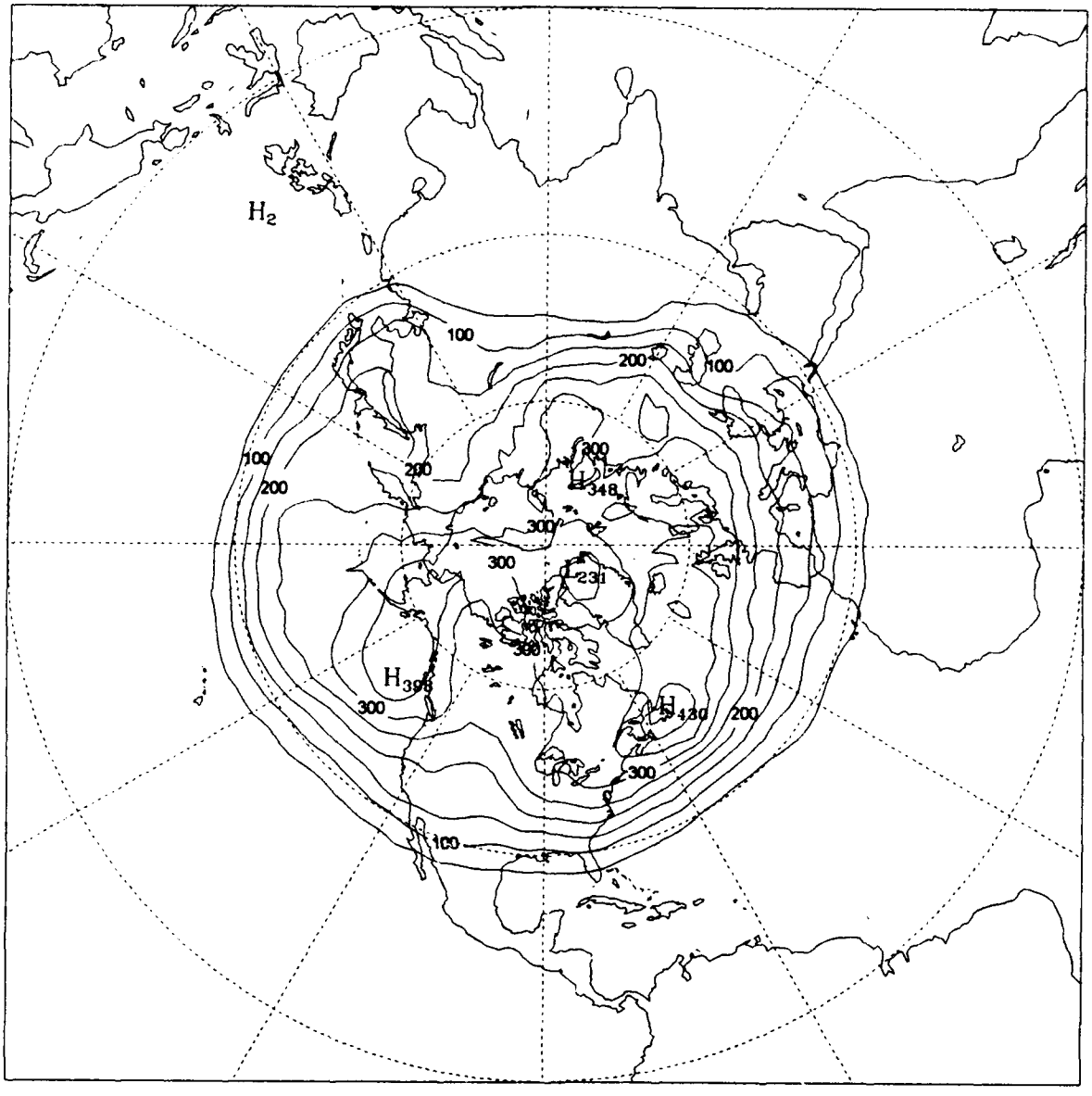

a.

Figure 3. Frequency of 5-day 500 mb forecast errors of 100 meters or more for the 1981-1990 winter seasons. (a.) Absolute errors, (b.) positive errors and (c.) negative errors. Contour interval is 50 occurrences.

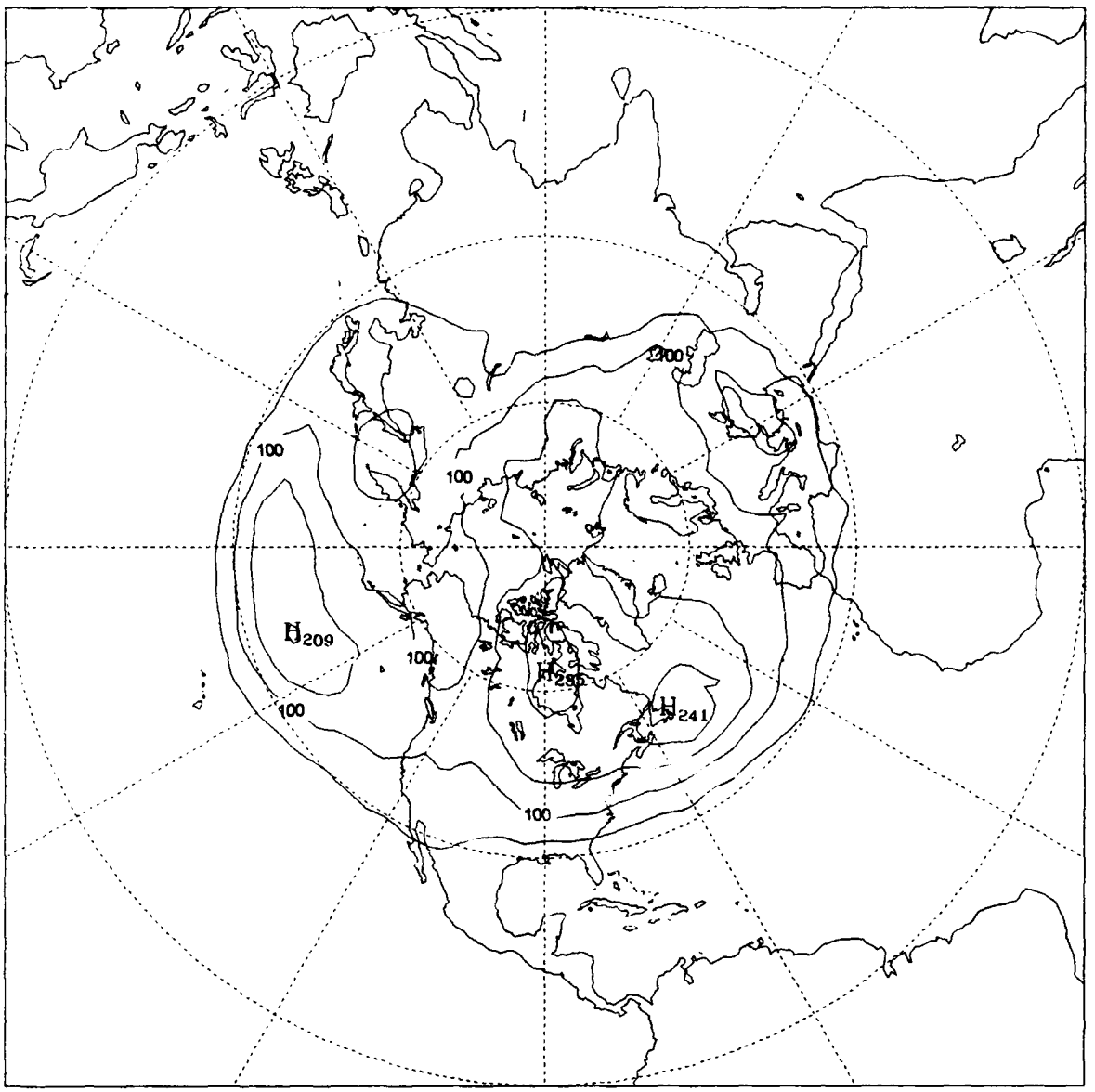

b.

Figure 3. (Continued).

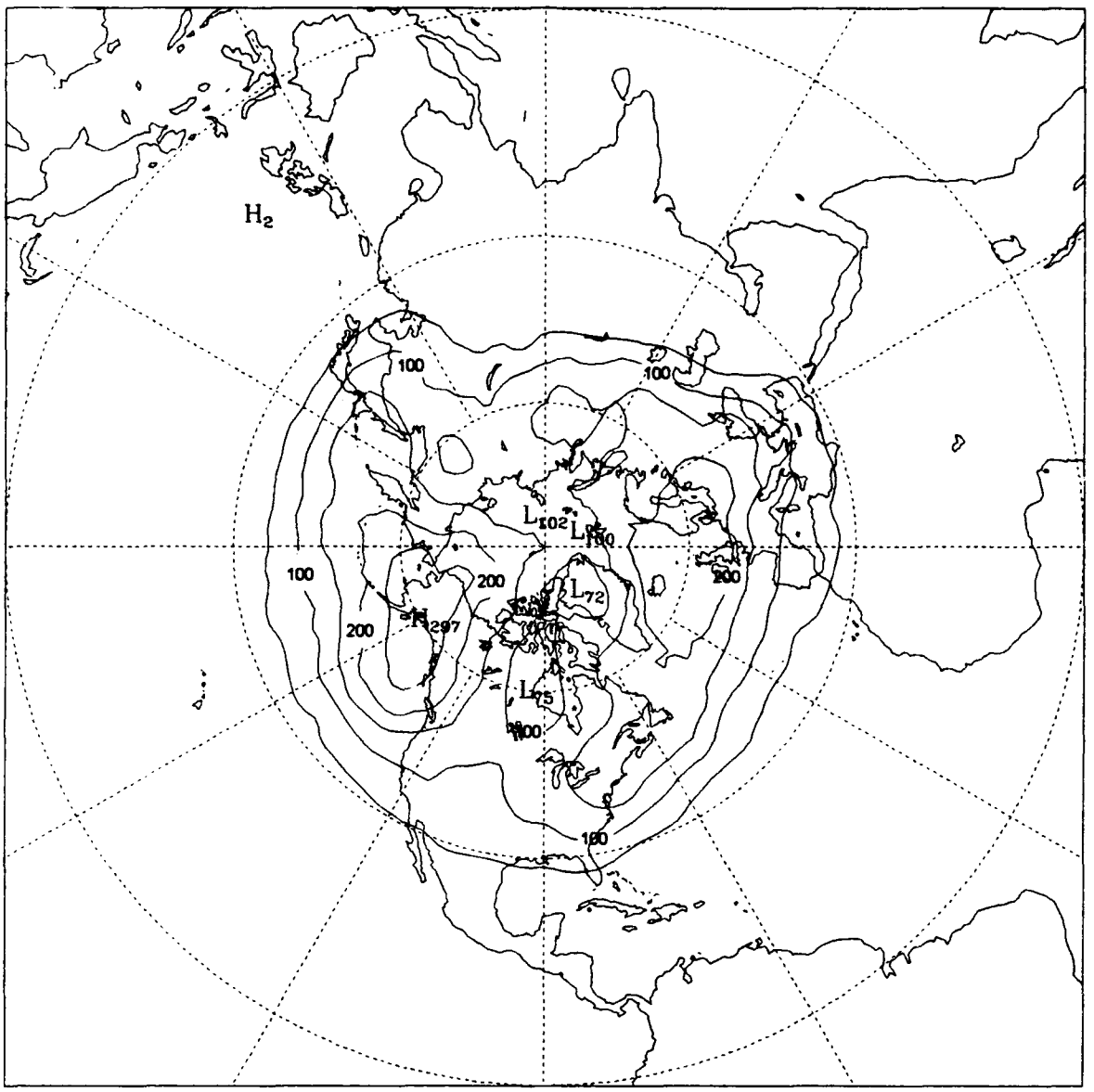

c.

Figure 3. (Continued).

underdevelopment of anticyclones in the region. This negative maximum is slightly displaced eastward from the result of Arpe and Klinker (1986). The regions of maximum positive errors over the Pacific Ocean and northeastern North America and negative errors over the Gulf of Alaska are aligned with the dominant storm tracks in these regions. Over the hemisphere, the steepest gradient of this error frequency distribution also occurs through the mid-latitudes, the region of transient, synoptic scale cyclones. Conversely, the distributions in the tropics and polar regions are relatively uniform, owing to the low frequency dynamics of these regions. Together, these results indicate that the most important regions of error are collocated with the regions of greatest activity or variability in the atmosphere.

Within the CONUS, the error frequency pattern is relatively zonal, especially in the Southeast, and increases poleward. However, a localized minima exists along and in the lee of the Rocky Mountains, primarily in the negative phase (Fig. 3c). This result shows that cyclones are forecast well in this region, even though the region is a preferred location for maximum cyclonic development (Roebber 1984). However, this performance may be enhanced by noting that little if any winter season explosive cyclogenesis occurs in the region (Roebber 1984).

B. Distribution of RMS errors

Netterville (1991) presented time series of the RMS values over the CONUS to show their daily variability. However, he did not discuss the overall distribution of these values with respect to the critical values which he used to define a poor forecast. His use of the annual mean RMS plus one standard deviation for that year, while attempting to allow for model changes and improvements, created something of a paradox. The annual mean RMS values, as well as its annual variability (as measured by the standard deviation), generally decreased over the 10-year period, indicating improved model performance. Concurrently, the number of cases which he defined as poor increased in the latter half of the period of investigation relative to the first half of the period. The resulting paradox is

that, as the model performs better overall, the number of "poor performances" increases. This increase in the number of poor forecasts is with respect to a decreasing criterion (mean RMS error) defining poor forecasts. Thus what Netterville (1991) actually shows is that as time has passed, the number of forecasts with RMS errors greater than one standard deviation (for that season) has increased. Thus the distribution of forecast errors about the seasonal mean has become slightly more skewed with time.

The annual histograms of RMS values (not shown) were studied for their statistical characteristics. None of the years revealed any significant bimodal distributions and the critical values used by Netterville (1991) were not located within any local maxima in the distribution. Thus his criteria for the definition of poor forecasts is rather arbitrary. The 10-year composite distribution for day 5 (Fig. 4) shows a near normal distribution, albeit slightly skewed toward the higher RMS values.

In the interest of judging all forecasts by the same criteria, poor forecasts were redefined in terms of the 10-year RMS statistics. For later comparisons, poor and good forecast RMS critical values were defined to be the 10-year mean RMS plus and minus the 10-year standard deviation, respectively. This yields critical values of RMS values greater than 104.49 m for poor forecasts and less than 56.40 m for good forecasts. The annual number of poor forecasts using this criteria is shown in Table 1, while the distribution for good forecasts is shown in Table 2. Using this criteria for the selection of cases removes the aforementioned paradox, i. e. , the number of poor forecasts generally decreases with time just as the RMS measure of performance also decreases. This criterion for poor and good forecasts was used to categorize forecasts for this research. One result of this definition is that the set of poor forecasts are biased towards the earlier years of the data set. Conversely, the good forecasts will be skewed toward the later years of the period. Notably, the earlier period contains the grid-point and T63 spectral models, while the latter half of the record was produced by the higher resolution T106 spectral model (Trenberth and Olson 1988). Additionally, the modifications to the radiative, convective,

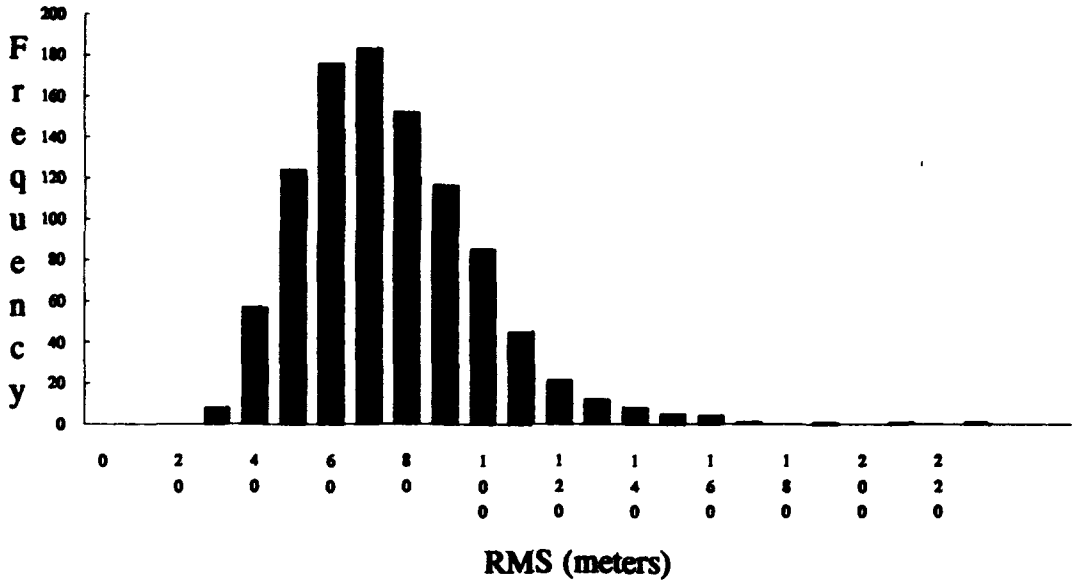

Figure 4. Distribution of CONUS 5-day RMS values.

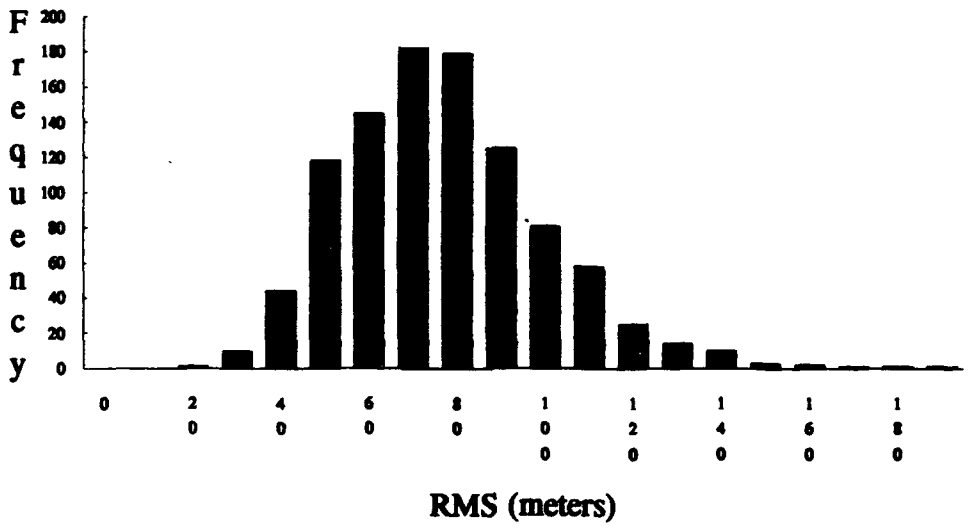

Figure 5. Distribution of Pacific 5-day RMS values.

cloud and condensation parameterizations introduced in 1984 and 1985 were found to be the most significant in terms of reducing the systematic error of the model (Arpe 1989). The differences of these two data sets will be considered when investigating the differences between the two categories.

The RMS values were also computed over a region of equal size over the Pacific Ocean. The region is bounded by the same latitudes as the CONUS region (22.5 - 56.25 degrees N) and by longitudes 135 W and 153.75 E. The 10-year frequency distribution of these RMS errors is shown in Fig.. 5. Poor and good forecasts were defined in the same manner as over the CONUS (regional 10-year mean RMS plus or minus one standard deviation). This yielded critical values of 105.11m (59.19m) for poor (good) forecasts. The annual distributions of the poor and good forecasts for the Pacific region are also contained in Tables 1 and 2. For the Pacific region, 151 poor forecast cases and 36 good forecast cases were identified. As with the distribution over the CONUS, the Pacific region distribution is relatively normal and skewed slightly toward higher values.

The RMS errors were computed over both geographical regions to see if regional differences exist in their distribution. The null hypothesis that the two distributions are different was tested using the Student's two-tailed t-test with unequal variances (Ott 1988). The resulting p-value from this test is greater than .1, indicating that there is a greater than 1 in 10 chance of selecting the two distributions at random. Therefore, there is insufficient evidence to reject the null hypothesis. Failure to reject the null hypothesis lends support to the assumption the forecasts for the CONUS and the Pacific do not present different problems, at least when viewed from an RMS standpoint. Because the two regions are seemingly similar, no further interest was expressed in the errors over the Pacific region and the remainder of this research will deal with the errors over the CONUS.

Table 1. Annual distribution of poor 5-day forecast cases for the CONUS and Pacific regions. See text for definition of poor forecasts.

YEAR	CONUS	PACIFIC
1981	22	19
1982	22	35
1983	14	9
1984	11	15
1985	20	18
1986	9	9
1987	9	9
1988	7	12
1989	11	16
1990	10	9
Total	**135**	**151**

Table 2. Annual distribution of good 5-day forecast cases for the CONUS and Pacific regions.

YEAR	CONUS	PACIFIC
1981	9	3
1982	4	2
1983	11	3
1984	13	2
1985	9	2
1986	23	4
1987	16	5
1988	23	7
1989	14	2
1990	26	6
Total	**148**	**36**

CHAPTER VI

GROWTH OF FORECAST ERRORS

Based on the separation of the ECMWF forecasts into poor and good categories as measured by the 5-day RMS error over the CONUS, the growth of forecast errors will now be examined. This examination will reveal the dominant modes of error growth, both in time and space. Additionally, it will reveal differences between the dominant modes of poor and good forecasts. This chapter presents the methods used in this search and the results of the examination.

A. Growth from initial conditions

Plots of the error fields were screened subjectively to identify any patterns that might exist in the evolution in the fields. Initially, the 5-day forecast error fields were studied and classified subjectively by patterns in these fields. However, it was found that no dominant pattern existed which provided useful information about the error growth. Patterns determined subjectively ranged from error dipoles over the CONUS to hemispheric error trains. These error dipoles exhibited no preferred orientation.

It was also decided to trace the growth of the error fields through time from the initial conditions. Netterville (1991) found that the initial conditions by themselves were not an adequate predictor of forecast skill. With this study, it was hoped to detect some kind of transient feature which produces a large error field and the resulting large RMS value.

To accomplish this, a subset of the poor forecast cases was studied. From the 135 poor 5-day CONUS forecasts identified in the previous chapter, 18 were selected at random. The verifying 500 mb analysis and corresponding 5-day 500 mb forecast for one of the cases is shown in Fig. 6. This particular forecast exhibits several common forecast problems. For instance, the 5-day forecast (Fig 6b.) attempts to move the

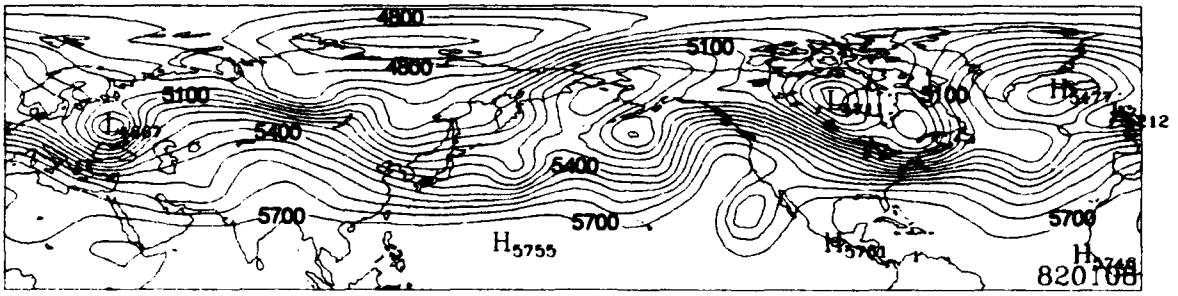

a.

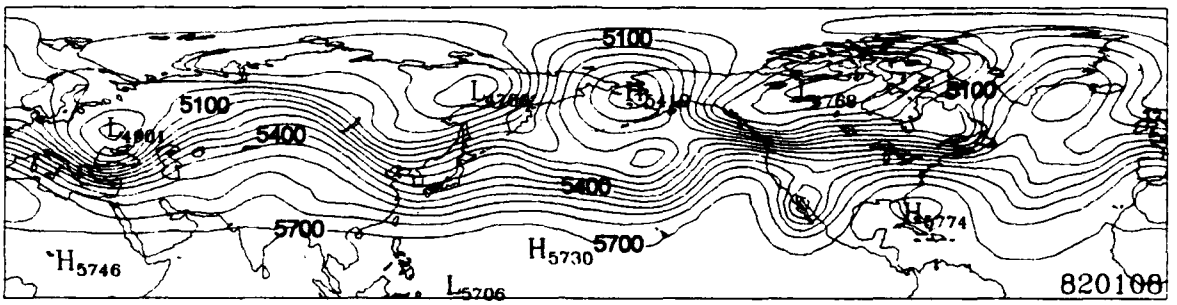

b.

Figure 6. 500 mb forecast initiated 3 Jan 82 and valid 8 Jan 82. (a.) Verifying analysis and (b.) 5-day forecast. Contour intervals are 60 meters.

cutoff low southwest of Baja California too far eastward. Additionally, the 5-day forecast exhibits a zonal flow over the Northern CONUS, versus the verifying northwesterly flow over the northwestern CONUS. The 5-day forecast also incorrectly placed a high pressure center over Florida as well as over developing the high pressure center north of the Aleutians.

Using analogous definitions (10-year mean plus standard deviation of RMS), the forecasts for days 1-4 were judged for their performance. Of the 135 poor 5-day CONUS forecast cases, the forecasts for days 1-4 were also judged to be poor 25.8, 34.4, 39.1 and 57.8 percent of the time, respectively. These results indicate that the greatest proportion (42.2%) of 5-day forecasts become poor on the fifth day. Additionally, it is interesting to note that one fourth of the poor 5-day forecasts are already poor forecasts on the first day of evolution. It also shows that poor 5-day forecasts tend to become poor at some point in the middle, rather than near the beginning, of its evolution. This result has also been documented by Lyons (1992).

A case study of error field evolution is shown in Fig. 7. This figure shows the daily evolution of the error field as forecast from the initial conditions which produced the poor 5-day CONUS forecast valid 8 Jan 82. This valid date is the same as the case shown in Fig. 6. This particular set of initial conditions produced poor forecasts on days 1, 2, 4, 5 and 6. The main forecast problems, or dominant errors, become apparent in this case by the third and fourth days. By day 3, the region of negative errors, or under forecast heights associated with the premature eastward movement of the low pressure center is apparent over Southern and Baja California. Likewise, so are the positive errors, or over forecast heights, further to the west in the region where the low pressure actually should be. A negative/positive/negative error pattern stretching from the Aleutians to the Canadian-United States border becomes most apparent between days 3 and 4. This error train is associated with incorrectly forecast

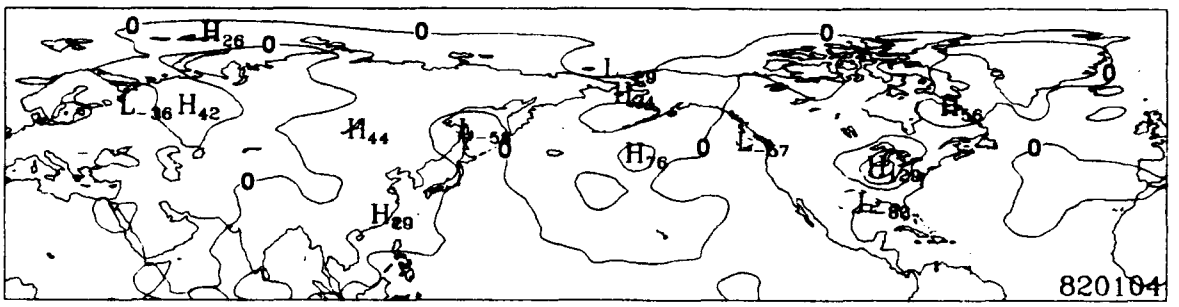

a.

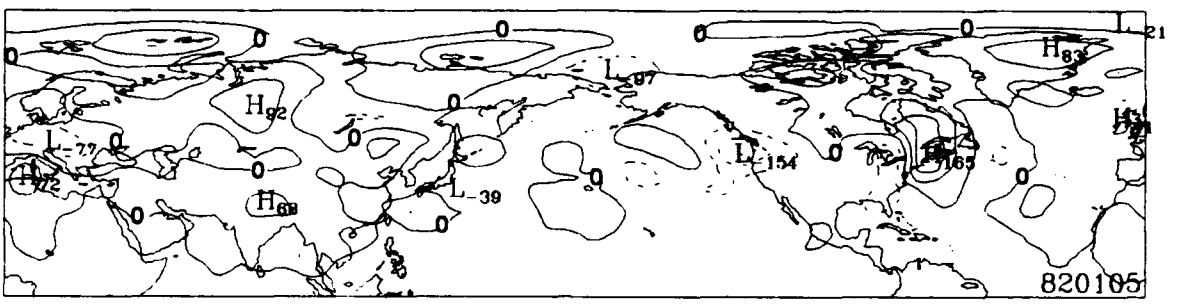

b.

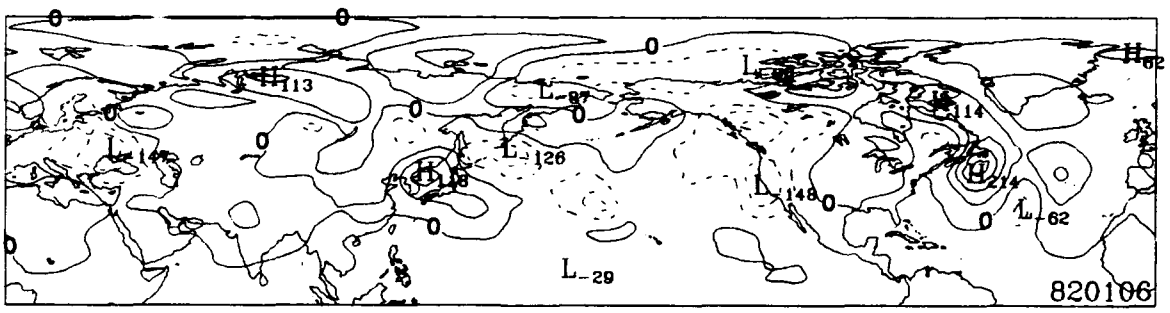

c.

Figure 7. Daily forecast errors evolving from the initial conditions which produce a poor 5-day forecast valid 8 Jan 82. (a.) Day 1, (b.) day 2, (c.) day 3, (d.) day 4, (e.) day 5 and (f.) day 6 errors. Contour intervals are (a.), (b.) and (c.) 50 meters and (d.), (e.) and (f.) 100 meters. Negative contours are dashed.

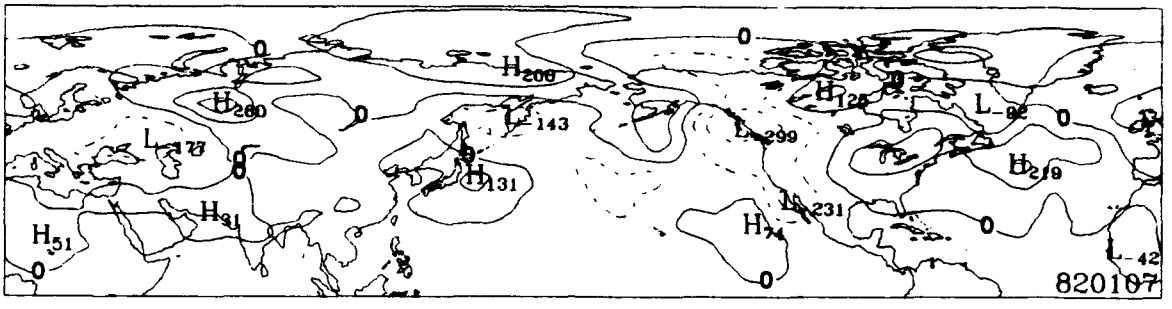

d.

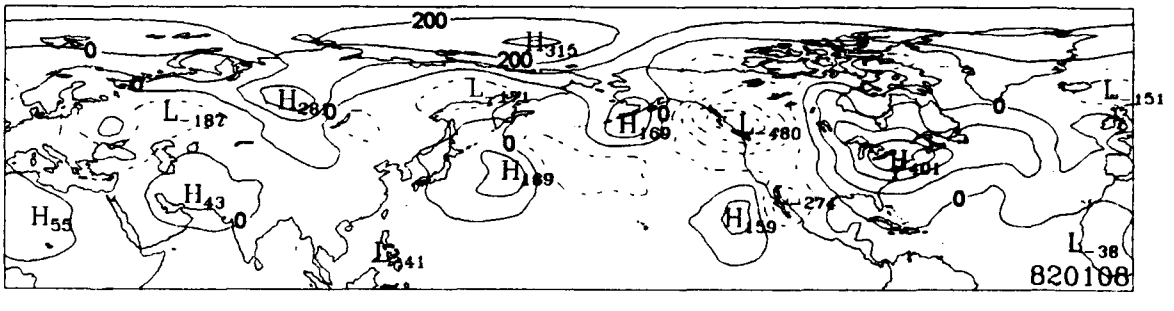

e.

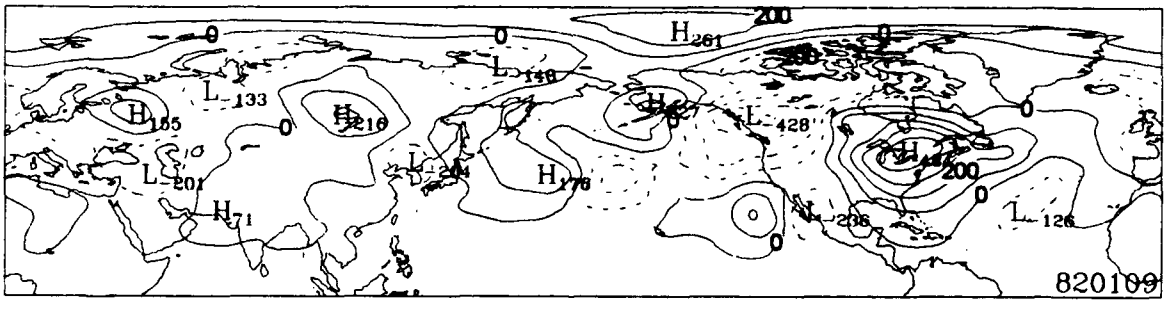

f.

Figure 7. (Continued).

high pressure center north of the Aleutians and the northwesterly versus zonal flow along the Canadian-United States border.

Two possibilities exist in the evolution of the error fields. The first is that the errors over the CONUS would result from a transient pattern of error growth. Such a transient feature might originate from a geographical region or regions which are poorly sampled by the ground-based observational network, such as the tropical East Pacific Ocean. An alternative result would be to find that the error patterns grow largely in place as previously documented by Arpe and Klinker (1986).

In this case study, as in most of this subset, the error fields were found to amplify in situ rather than as a result of any transient feature. No obvious growth was found to move out of the tropical East Pacific. However, there were some cases which exhibited prominent errors in this region. In fact, even though the poor forecasts were defined based on performance over the CONUS, there were many instances through the entire data set in which the maximum error amplitude was found well outside the CONUS region. No correlation can be made between these distant error maxima and the error patterns over the CONUS, as their positions spanned the entire Northern Hemisphere mid-latitudes. Likewise, they were found to occur both as mid-latitude error wave trains and as stand alone features.

The study of the subset of poor forecasts did not produce any "smoking gun" pattern of error growth. The main conclusion was that the eventual error pattern of the poor 5-day forecasts grows in place with the bulk of the growth occurring after the third or fourth day of the forecast. Additionally, it does not appear that the errors are the result of any transient feature or one that originates in a poorly sampled region. Because of the limited results of this study, it was not applied to the entire catalog of poor forecasts and other avenues of research were followed.

B. Sensitivity to initial conditions

In addition to the study of error growth described above, the sensitivity of error growth of the ECMWF model to the initial conditions was examined. To accomplish this, the same subset of poor 5-day forecast dates was used and the 4- and 6-day forecast error fields were studied. These forecasts were also valid on the same date as the poor 5-day forecasts. This study was performed to determine if the performance of the ECMWF is sensitive to the data used as initial conditions for the model. The underlying hypothesis is that the forecast for a given date will improve as the forecast length is shortened and worsen as the forecast length is lengthened. More specifically, if the initial conditions are important, the likelihood is small that the initial errors will be the same for three consecutive days. The forecasts which were initiated based on the surrounding initial conditions should not also be poor forecasts. Additionally, this examination will determine if there is a difference in the dominant error pattern over the CONUS among the three forecast lengths, or if the patterns are similar.

The 4-, 5- and 6-day forecast error fields from one of the subset cases is presented in Fig. 8. The valid date of all three forecasts is the same as that of Fig. 7. Visual inspection of these three forecast error fields reveals that there are not significant changes in the locations of major errors for the forecast valid date at the three forecast lengths. Specifically, the high/low error dipole near Baja and the negative/positive portion of the positive/negative/positive error train along the Canadian-United States border are evident on all three days. The fact that all three days produce errors in similar locations indicates that the initial conditions are not that important in producing a forecast for this valid date. There were, however, noticeable differences in the amplitudes of the error centers. This was especially true of the 4-day errors over the CONUS itself. Generally, the 4-day forecasts for the valid dates in the subset performed better than the 5- and 6-day forecasts. This trend was noted throughout the entire sample subset. In fact, for the valid dates of poor 5-day

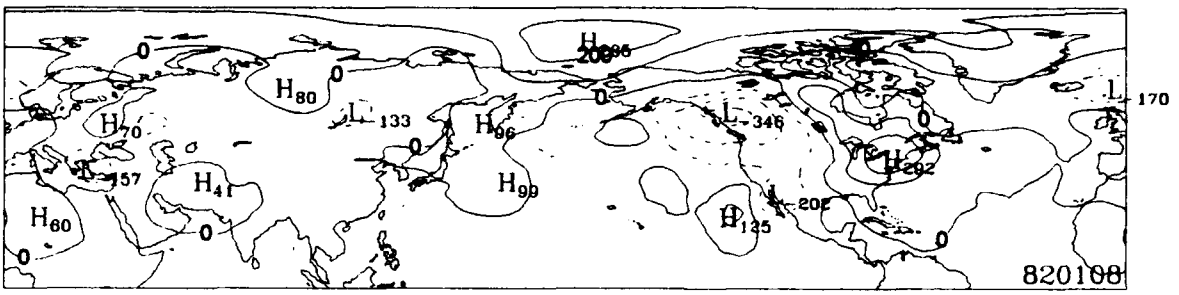

a.

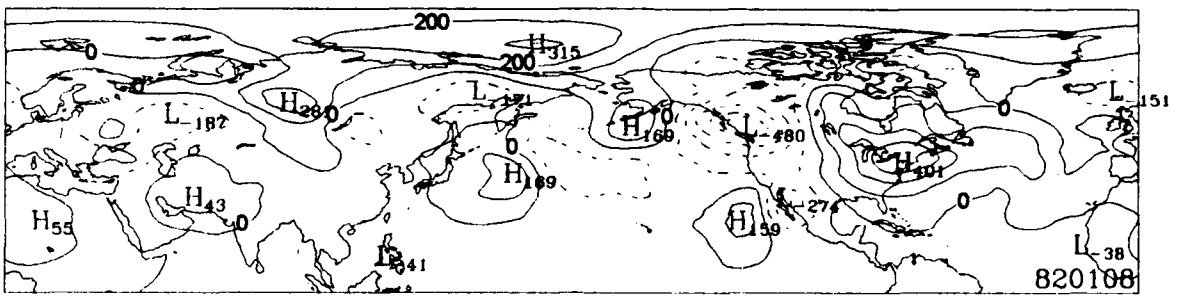

b.

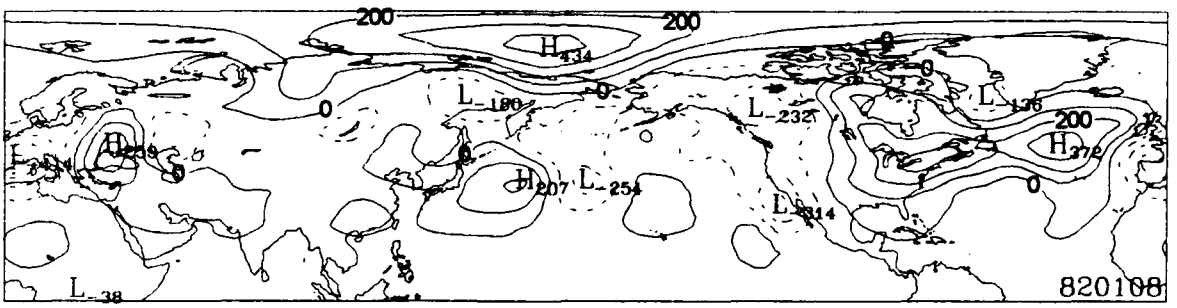

c.

Figure 8. Comparison of 4-, 5- and 6-day forecast errors which verify on 8 Jan 82.

forecasts, 53% of the corresponding 6-day forecasts were also deemed poor, while only 42% of the equivalent 4-day forecasts were poor performers. All three days produced poor forecasts in only 29.6% of the cases. Therefore, extensive runs of poor forecasts do not appear to be a frequent occurrence.

C. Empirical Orthogonal Function analysis of errors

The research presented thus far is limited by the fact that it is highly subjective. Additionally, due to high variability in 500 mb patterns, the appearance of a limited number of dominant error patterns would have been somewhat fortuitous. Therefore, more objective methods of analysis must be used to reveal the underlying patterns of error growth. Empirical Orthogonal Function (EOF) analysis is used to gain objective results.

EOF analysis has become a standard tool of exploratory data analysis (Richman 1986, Preisendorfer 1988). This method of analysis is used to decompose mathematically a data set into its dominant modes, while also determining the weight or significance of these modes. Modes are selected by using matrix operations to compute the eigenvectors of a data correlation matrix. The eigenvectors of this matrix define the modes of the data set, while the accompanying eigenvalues represent the respective weights of the eigenvectors. The weight of the eigenvectors represent the percentage of the total variance of the data set explained by that eigenvector.

EOF analysis is applied through in the following two procedures: First, the temporal growth of the RMS errors is analyzed over the length of the forecast period. Secondly, the spatial EOFs of the forecast error fields are computed for each day of the forecast period. The temporal EOFs show the dominant patterns of error growth rate. The spatial EOFs highlight patterns and regions of high and low error growth rates. EOF decomposition of individual forecast days (forecasts for day 1, 2, 3, etc.) highlight the evolving patterns of error growth. One of the interesting results is that the dominant error patterns changes from shorter to longer forecasts. In both the

temporal and spatial cases, comparisons are made between the results derived from the poor forecast cases and from the good forecasts. Such comparisons point out the differences in the two categories and possibly reveal a cause for the poor forecasts.

The spatial EOF analysis is restricted to the CONUS region of the gridded data. This region contains 200 grid points. To reduce computational demands, the number of grid points used in the EOF routine was reduced. The results discussed below are computed using 50 grid points over the CONUS. The 50 points represent every other longitude and latitude, beginning in the northwest corner of the CONUS region. This results in an effective grid point spacing of 7.5 degrees within the region. The use of this coarse spacing is still expected to resolve any major patterns, since the major errors in the field have typical length scales greater than 7.5 degrees.

1. Temporal EOF analysis

As part of the EOF analysis of RMS error growth, the mean growth curve of the RMS values was derived for all forecasts, as well as for the 135 poor (5-day RMS errors greater than 104.49 meters) and 148 good (5-day RMS errors less that 56.4 meters) forecast cases. Figure 9a summarizes the mean value of RMS error as a function of forecast length for each category.

Inspection of the curves shows that the RMS error growth rate of all forecasts is essentially linear, with an increase of about 15 meters per day through 5 days, decreasing to 12 meters per day on day 6. This is inconsistent with the normal concept of exponential growth rate and error doubling time. The implication of this linear growth rate is that the errors are not, on average, the results of a simple linear instability with a fixed error growth rate. However, neither the set of poor or good forecasts parallels this growth curve. For the collection of poor forecasts, the growth is still linear for days 1 and 2, but with a growth rate of about 20 meters per day. However, after day 2, the growth curve increases in slope, with a maximum growth rate of 30 meters per day between days 3 and 5. After this time, the growth of the

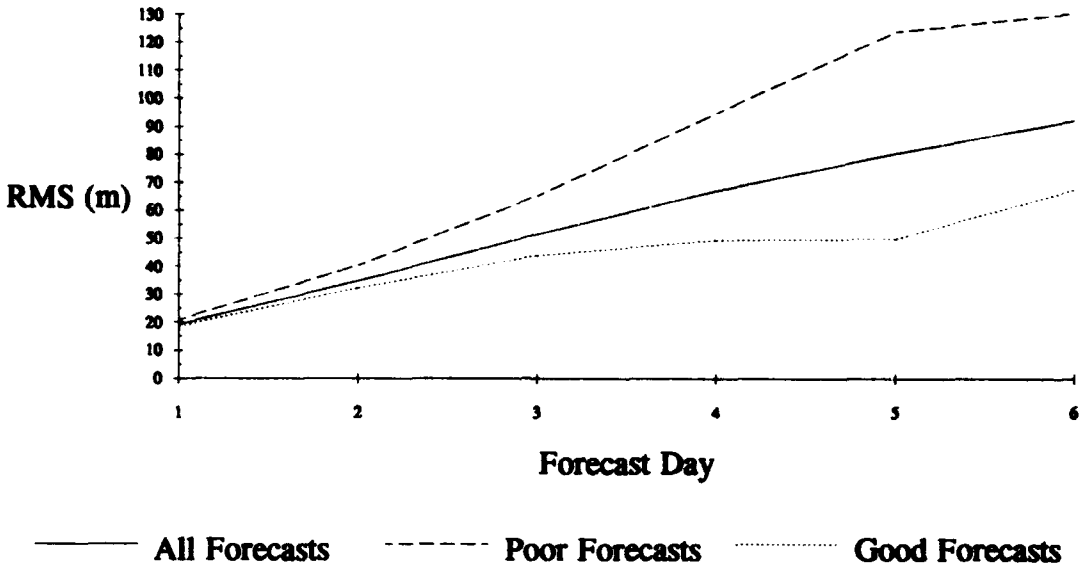

a.

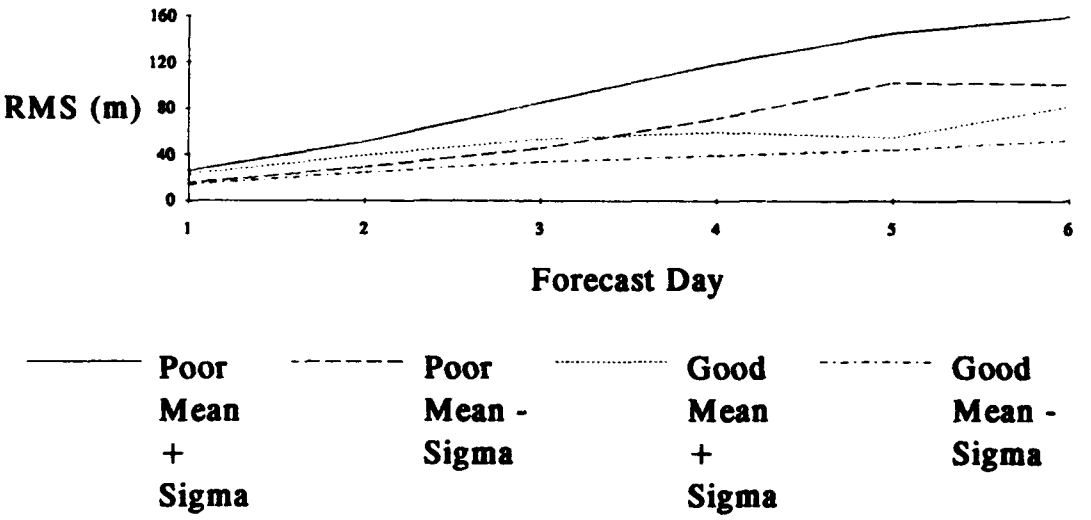

b.

Figure 9. Mean growth of the CONUS RMS error by forecast day and category. (a.) Means RMS values and (b.) plus and minus one sigma for poor and good forecasts.

RMS error is not as dramatic. These growth rates may owe their increase over time to some kind of linear instability. This result indicates that the RMS of poor 5-day forecasts increases most significantly on the synoptic time scale. The growth of errors for good forecasts is less dramatic, as the most growth (10-14 meters per day) occurs by day 3. After this day, daily growth is reduced to 6 meters or less per day through day 5. This result shows that, while the majority of RMS error in good forecasts occurs prior to day 3, the opposite is true for poor forecasts, indicating that poor forecasts do not become decidedly poor until midway through the 5-day forecast. Additionally, the collection of poor forecasts has a much greater variability (as expressed by its standard deviation around the mean of poor forecasts) than the collection of good forecasts (Fig. 9b). The restricted variability of the good forecasts effectively provides a lower bound on RMS performance, while the higher variability of the poor forecast population allows for much more extreme values in this category. The two forecast categories are essentially separated by day 4 of the forecast period. Further, the fact that the mean of the 135 poor forecasts moves further away from the overall mean, and have a greater variability than the 148 poor forecasts, is further evidence that the overall distribution of 5-day RMS values is not a normal or Gaussian distribution.

The EOF analysis of all forecasts for a 6-day period yields eigenvectors with proportions presented in Fig. 10. This EOF analysis removed the mean error growth rate. Therefore, the EOFs explain only the deviations from the mean error growth rate. The proportions in Fig. 10 represent the percent of variance explained by the individual eigenvectors or EOFs. If each EOF were to explain equal proportions of the total variance, their percentage would be 16.6% (1 part out of 6), since there are 6 EOFs. Only EOFs 1 and 2 (Fig. 11) represent percentages greater than 1 out of 6 and are deemed significant. A scatter plot of the amplitudes of EOF 1 versus EOF 2 is presented in Fig. 12. A χ^2 test was performed using the null hypothesis that the

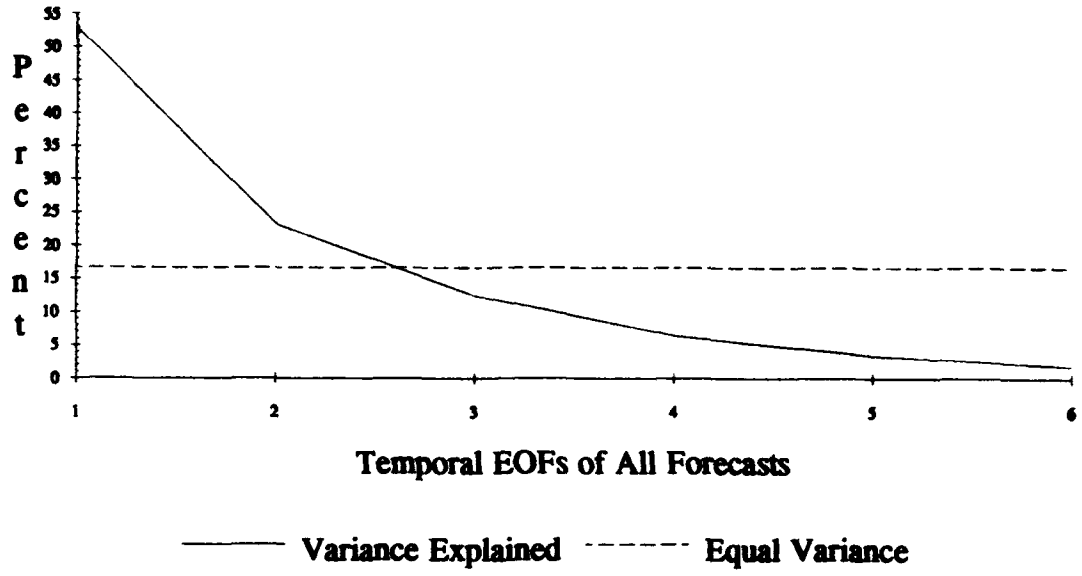

Figure 10. Percentage of variance explained by the temporal EOFs of CONUS RMS error growth.

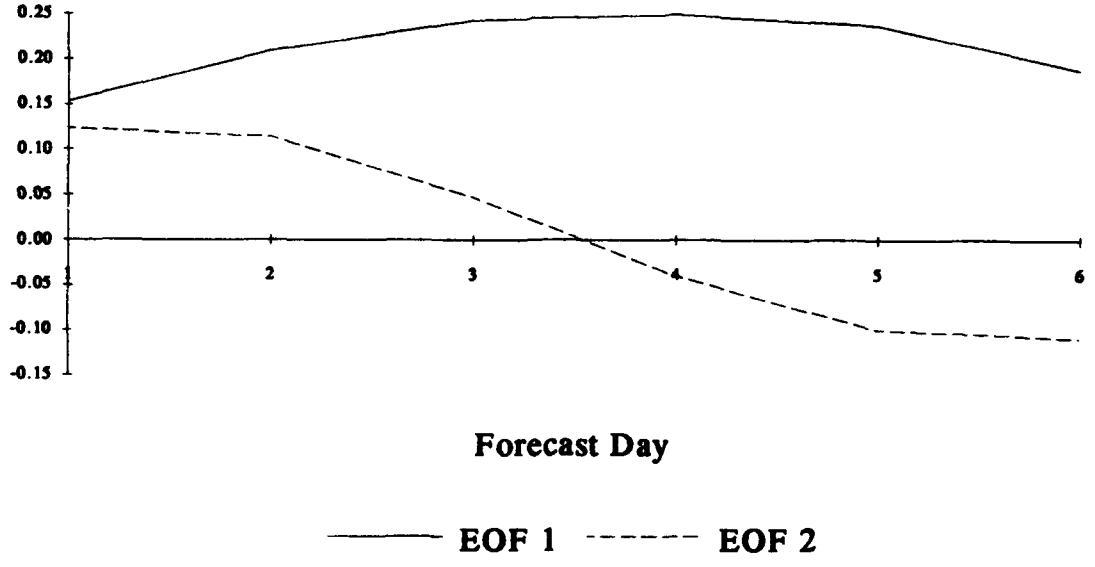

Figure 11. First two temporal EOFs of CONUS RMS error growth.

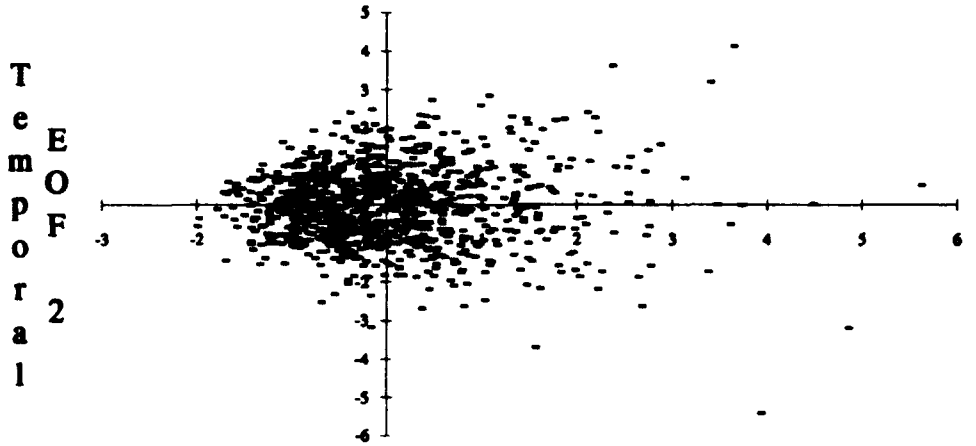

Figure 12. Scattergram of the amplitudes of temporal EOF 1 versus EOF 2 for all forecasts.

distribution in Fig. 12 is different from a completely random distribution of the amplitudes. The random distribution assumes that one fourth of the amplitudes fall in each quadrant. The p-value for this test is greater than .1. This p-value indicates that the two distributions could be selected at random more than 10% of the time. Therefore, the null hypothesis that the distribution is different than a random distribution can not be rejected.

Within each quadrant, in addition to counting the total number of cases, the number of poor forecasts was also determined by plotting the EOF 1 and EOF 2 amplitudes of just the poor forecasts. It was noted that while only 21.4% of all forecasts were found in the quadrant of positive EOF 1 and negative EOF 2, 76.6% of the poor 5-day forecasts were located within this region (Fig. 13). The null hypothesis that this distribution is the same as a random distribution was tested. Again using the

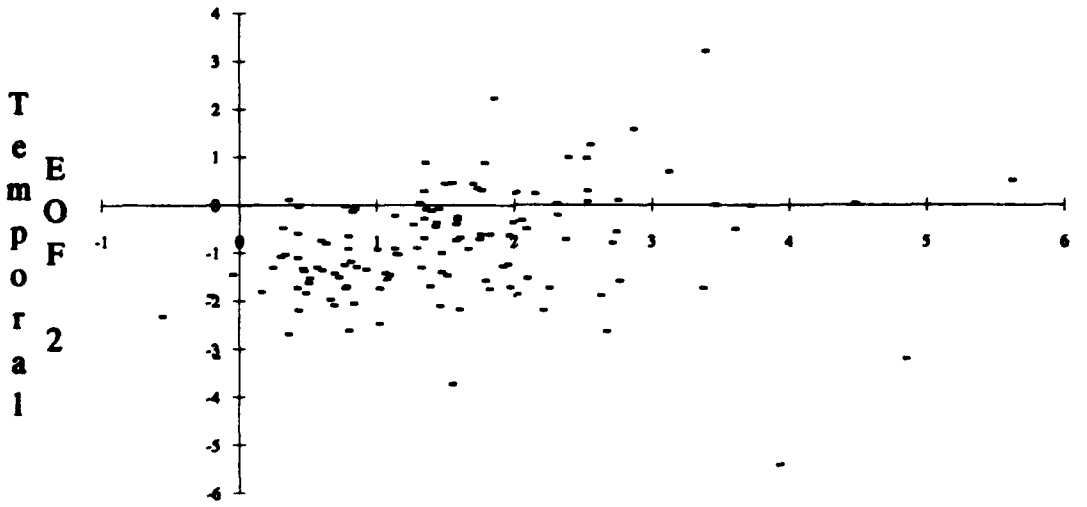

Figure 13. Scattergram of the amplitudes of temporal EOF 1 versus EOF 2 for the subset of poor forecasts.

χ^2 test, this result has a p-value less than .001, representing a less than 1 in 1000 probability of selecting such a distribution at random. Therefore, the null hypothesis that the distribution of the amplitudes of EOFs 1 and 2 of poor forecasts is rejected. The combination of positive EOF 1 and negative EOF 2 is a significant pattern of RMS error growth deviation from the mean in poor forecasts.

Analysis of this combination of EOFs 1 and 2 shows that EOF 1, representing 52.8% of the RMS error variance, is relatively flat. The daily contribution of this EOF does not vary greatly from day to day, although it does increase slightly through day 4 and then decreases somewhat on days 5 and 6. This decrease actually represents a return toward the mean RMS error growth rate. Since the EOF is relatively flat, it shows that much of the deviation from the mean growth rate is already present on day

1. The decrease in the later dates is due to the tendency of the model to converge back to its own climatology.

On the other hand, EOF 2, because of its negative phase, initially represents a tendency for poor forecasts to remain below or near the mean curve for the first 3 days of the period. As the forecast period goes beyond days 3 and 4, the contribution from this EOF becomes positive, indicating that poor forecasts with large negative EOF 2 grow most rapidly in the latter part of the forecast. The change in phase of this EOF is directly related to the period of greatest RMS growth of the 135 poor forecasts.

Conversely, the distribution of the amplitudes of EOFs 1 and 2 for the 148 good forecasts was determined (Fig. 14). The result was equally as impressive as the distribution of poor forecasts, in that most of the good forecasts were concentrated in the opposite quadrant from the poor cases. The combination of negative EOF 1 and positive EOF 2 contained 28.0% of all forecasts but 79.9% of the good forecasts. Again, the null hypothesis that this distribution is the same as a random distribution was tested using the χ^2 test. The resulting p-value is again less than .001, indicating that this is a significant combination of EOFs. In this case, the opposite sign of EOF 1 largely explains the deviation of the good forecasts to a location below the mean error growth curve, as opposed to the poor forecasts which deviate to a location above the mean curve. Additionally, EOF 2 differentiates between the rapid growth of RMS error on days 3 and 4 of poor forecasts and the very slow growth of RMS error on the same days of the poor forecasts. This dichotomy indicates that the departure from the mean RMS growth curve for good forecasts is exactly the opposite as that of the poor forecast growth.

While the EOF analysis presented above demonstrates the significant modes of RMS error departure from the mean error growth rate, it does so at the expense of removing the actual mean growth pattern. Because of this, the EOF analysis was recalculated for all forecasts without removing the mean error growth rate. The

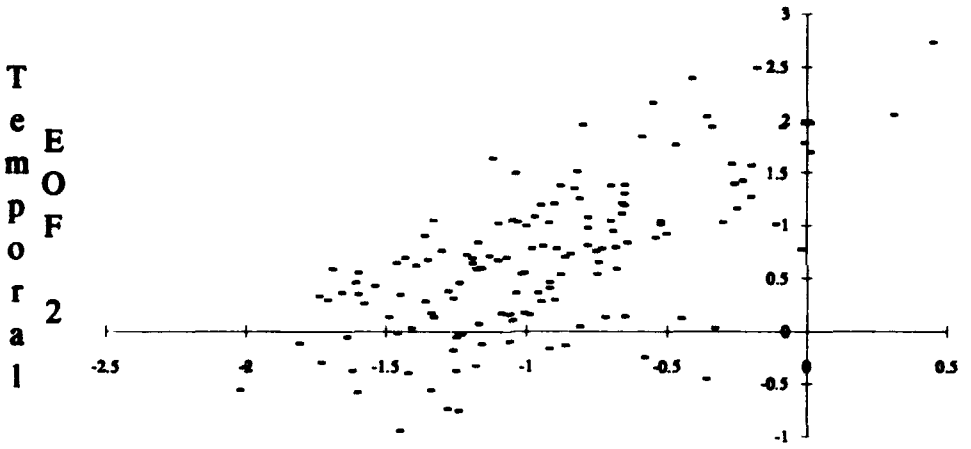

Temporal EOF 1

Figure 14. Scattergram of the amplitudes of temporal EOF 1 versus EOF 2 for the subset of good forecasts.

resulting eigenvectors are presented in Fig. 15. In this analysis, the mean pattern of growth is dominant and the remaining eigenvectors represent the departures from the mean, similar to the discussion above. The weights of the eigenvectors for this analysis are 96.3, 1.7, 0.1, 0.5, 0.3 and 0.1% respectively. These values indicate that the mean pattern represents the bulk of all RMS error variance and the deviations are a much smaller 3.7% of the total.

2. Spatial EOF analysis

The research presented thus far has shown that the greatest amount of error growth in poor 5-day forecasts, as judged by the RMS values and their growth, occurs between days 3 and 5. This corresponds to the time period for synoptic scale meteorological processes. In order to determine if the error fields of poor and good 5-day forecasts are related to synoptic scale processes, these fields are analyzed spatially via the EOF procedure. This procedure is performed for the error fields of each day in

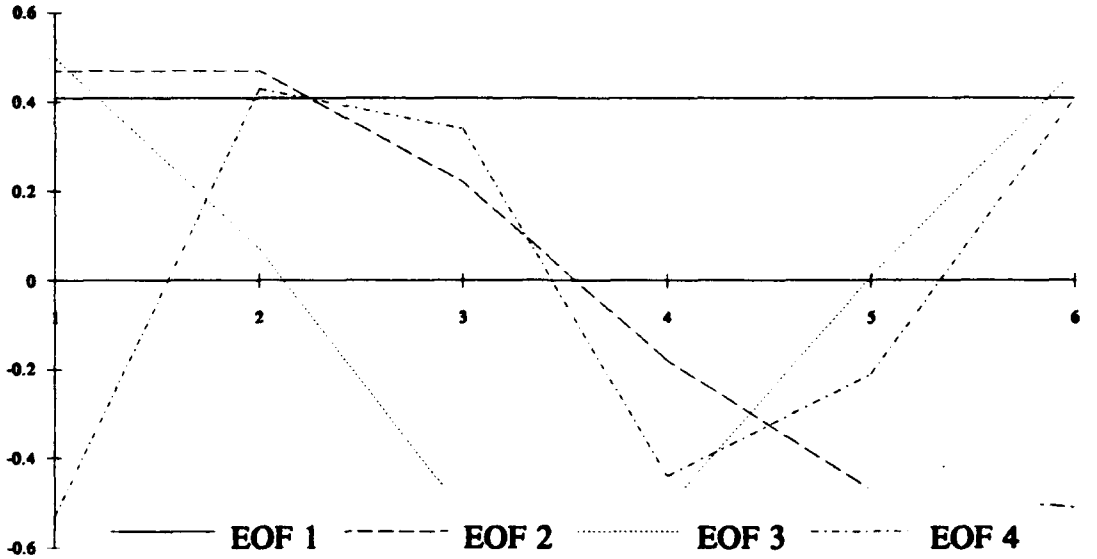

Figure 15. Leading temporal EOFs of CONUS RMS error growth after correcting for mean growth.

the evolving poor 5-day forecast. As a result, the dominant evolutionary patterns appear, and their changes through the forecast period (both in spatial patterns and dominance) described.

As discussed previously, the spatial EOFs are computed using a reduced set of grid points (50 vs. 200) within the CONUS region of interest. On day 5, the resulting 50 EOFs explain portions of the total variance of poor and good forecasts as shown in Fig. 16. From the graph, it is apparent that the first few EOFs combine to explain much more of the total variance in poor forecasts than in good forecasts. In fact, the graphs for days 1-4 (only day 5 is shown in Fig. 16) reveal that the dominance associated with the leading EOFs increases with time. For good forecasts, there are no such dominant leading EOFs. Since these are already defined as good forecasts, it is reasonable to expect that there is not a dominant pattern of error; that is, the good forecasts are not flawed by specific patterns of error growth. As with the temporal

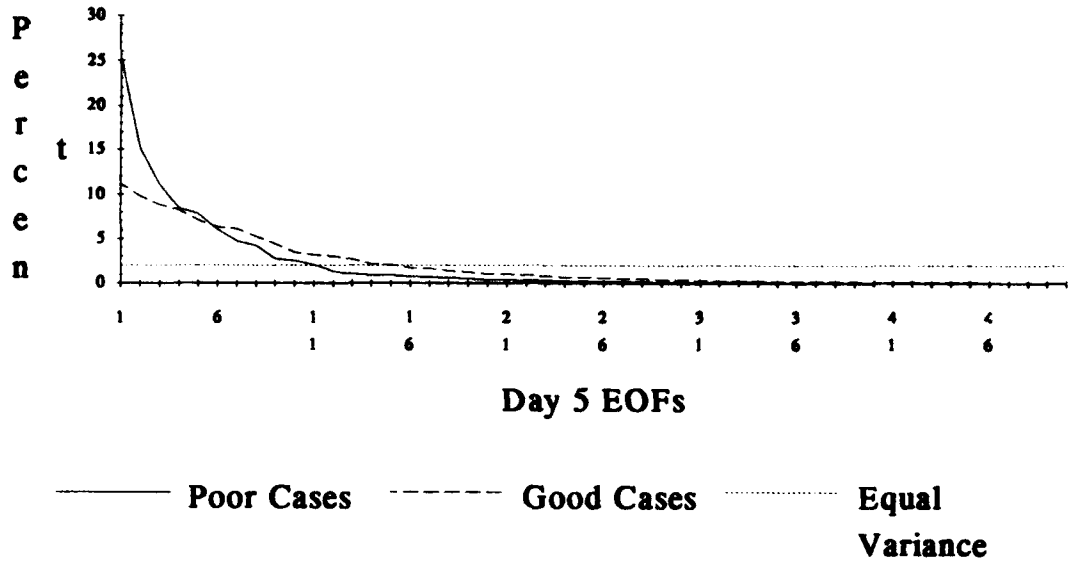

Figure 16. Percentage of variance of the day 5 CONUS error fields explained by the spatial EOFs calculated from the correlation matrix for 128 poor forecasts. The dotted line gives the average variance explained at each grid point, for reference.

analysis, these fields and the resulting EOFs are not corrected for the mean daily error field. Therefore, the EOFs represent the deviations of the error field about the mean error field of the respective day. This should not be a problem, since the mean error at individual points is close to zero; that is, there is only weak systematic bias of the forecasts over the CONUS region. The results are first presented for the spatial EOF analysis performed on the error fields of the subset of poor forecasts.

The first two EOFs from day 1 of the poor forecasts are presented in Fig. 17. The pattern of EOF 1 is simply a single phase with all points of the same sign. This single phase, relatively flat field is similar to what normally results from EOF analysis of geophysical data. Even though this field is relatively flat, there is a weak maximum

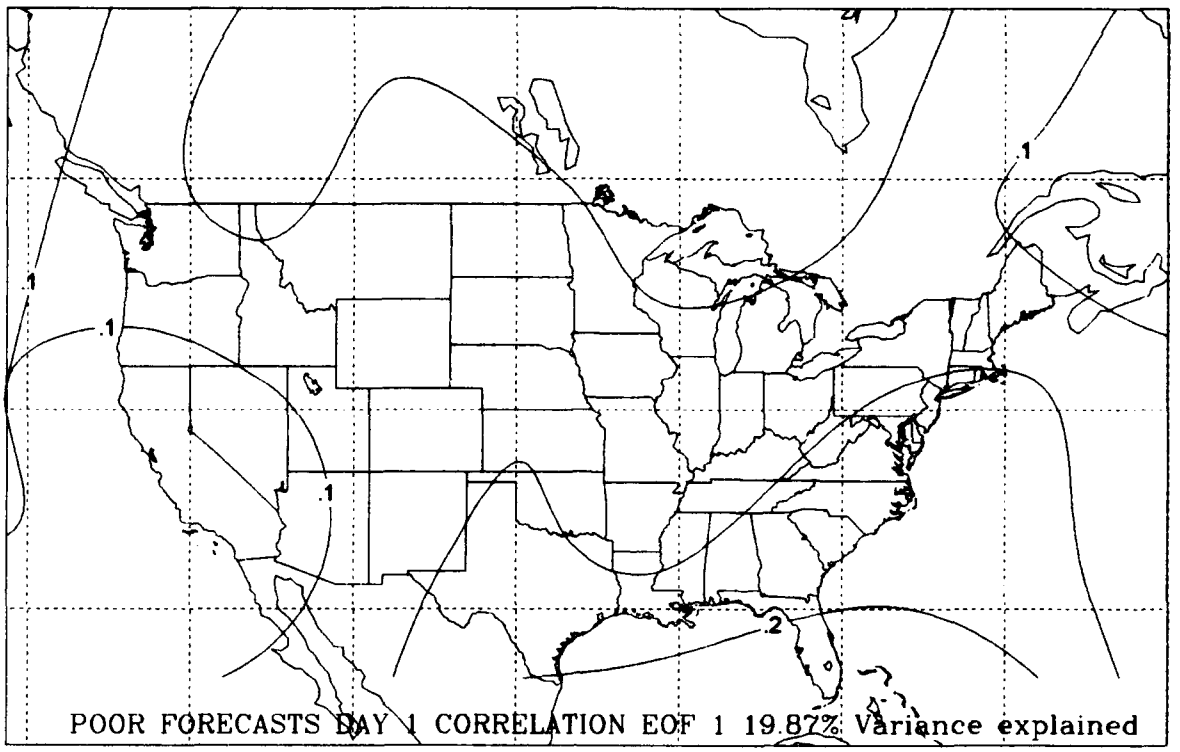

a.

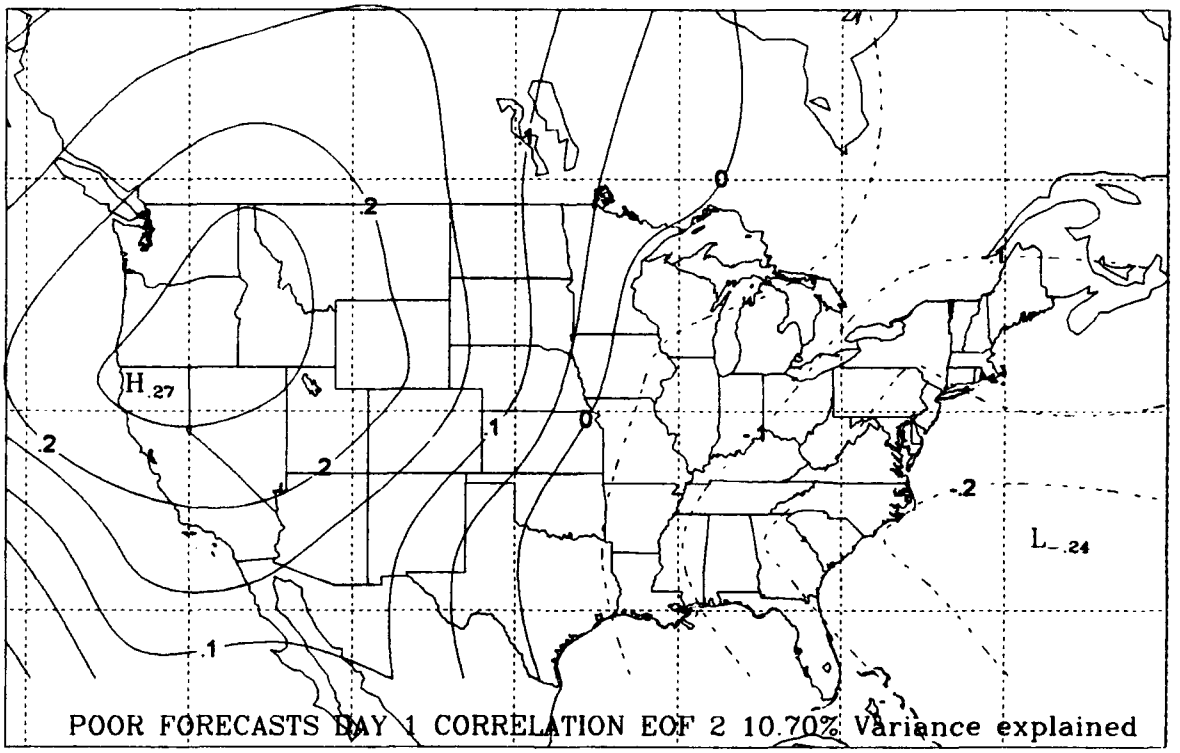

b.

Figure 17. Leading correlation EOFs of the day 1 error field of poor forecasts. Contour interval is .05. Negative contours are dashed.

along the southeast border of the region. The second EOF reveals a dipole pattern aligned northwest to southeast over the region. This pattern is also fairly normal in the context of EOF analysis. The scale of this wave pattern is at least 12,000 km, or twice the domain width. Together, these two patterns combine to explain 30% of the total error field variance.

Analysis of the leading EOFs on day 2 of the poor forecast runs (Fig. 18) begins to reveal a systematic evolution of the error field. The dipole pattern which was the second EOF on day 1 is now the leading EOF, although its contribution to total variance has increased from 10% to only 14%. The second EOF is essentially a single phase pattern, except for one grid point over Arizona. This pattern is similar to the leading pattern of day 1. Within this pattern, the earlier weak maximum over the Southeast has become more evident as an axis of maximum amplitude extending into the Ohio Valley. Additionally, the dominance of this pattern has been reduced by one third, as it is now responsible for only 12% of the total variance. Even though the same patterns exist on the first two days, their combined relevance is reduced, while they have also switched positions with each other. The third EOF begins to reveal an interesting feature. This EOF is the quadrature, or 90 degree phase shift of the first EOF. This is evident since the regions of maximum and minimum amplitude of EOF 1 are aligned along gradient regions of EOF 3, and vice versa. The two phases of these two EOFs combine to reveal all four phases of a standing wave pattern, which explains 25% of the variance of the error fields on this day. The switching of the first two EOFs, along with the appearance of the quadrature pattern are is indicative of the changes underway in the evolution of the forecast error fields.

The leading patterns on day 3 are shown as Fig. 19. The leading pattern is once again the dipole over the CONUS, which has increased in dominance to over 19% and become much better resolved. The dipole has also lost much of its northwest to southeast orientation and is now aligned almost zonally. The quadrature pattern is now

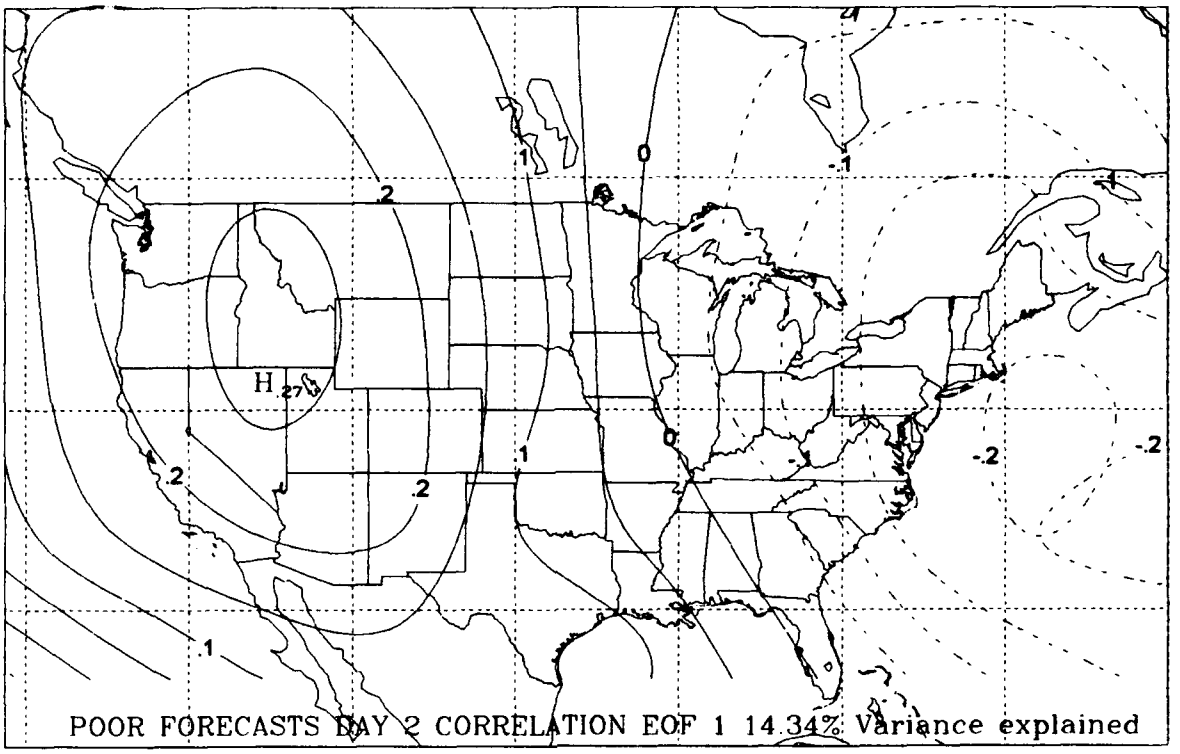

a.

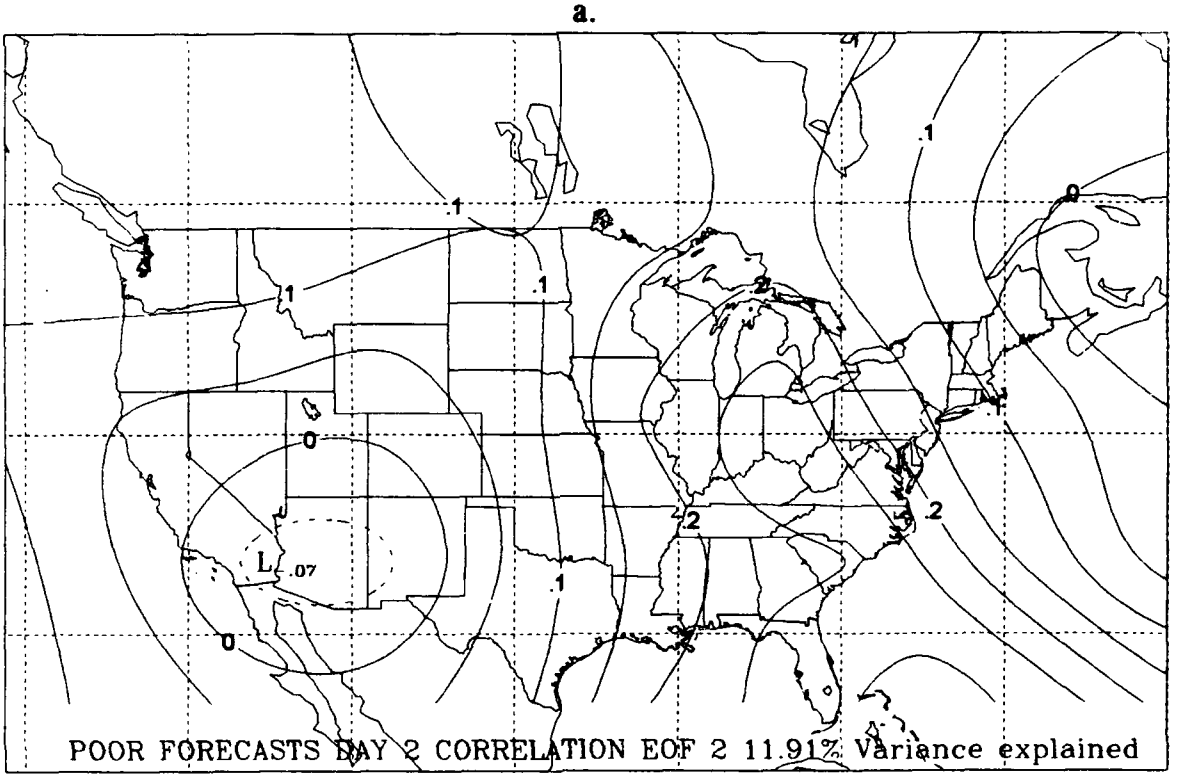

b.

Figure 18. Leading correlation EOFs of the day 2 error field of poor forecasts.

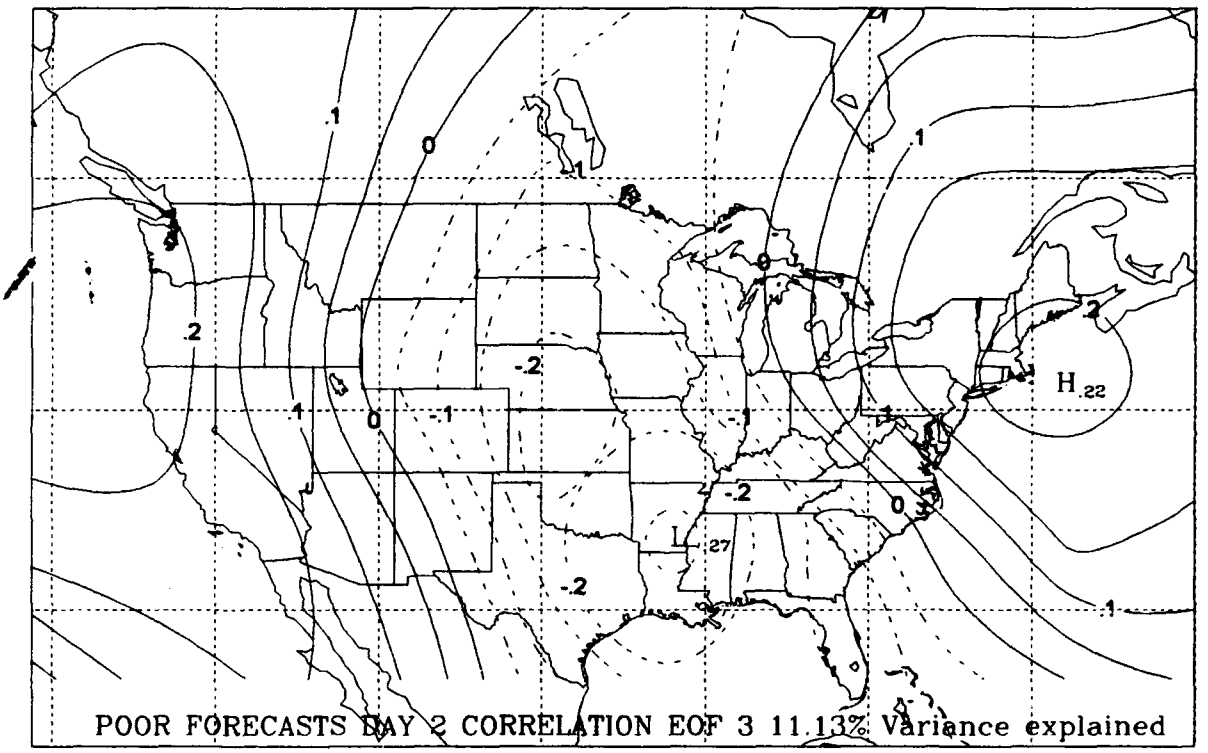

c.

Figure 18. (Continued).

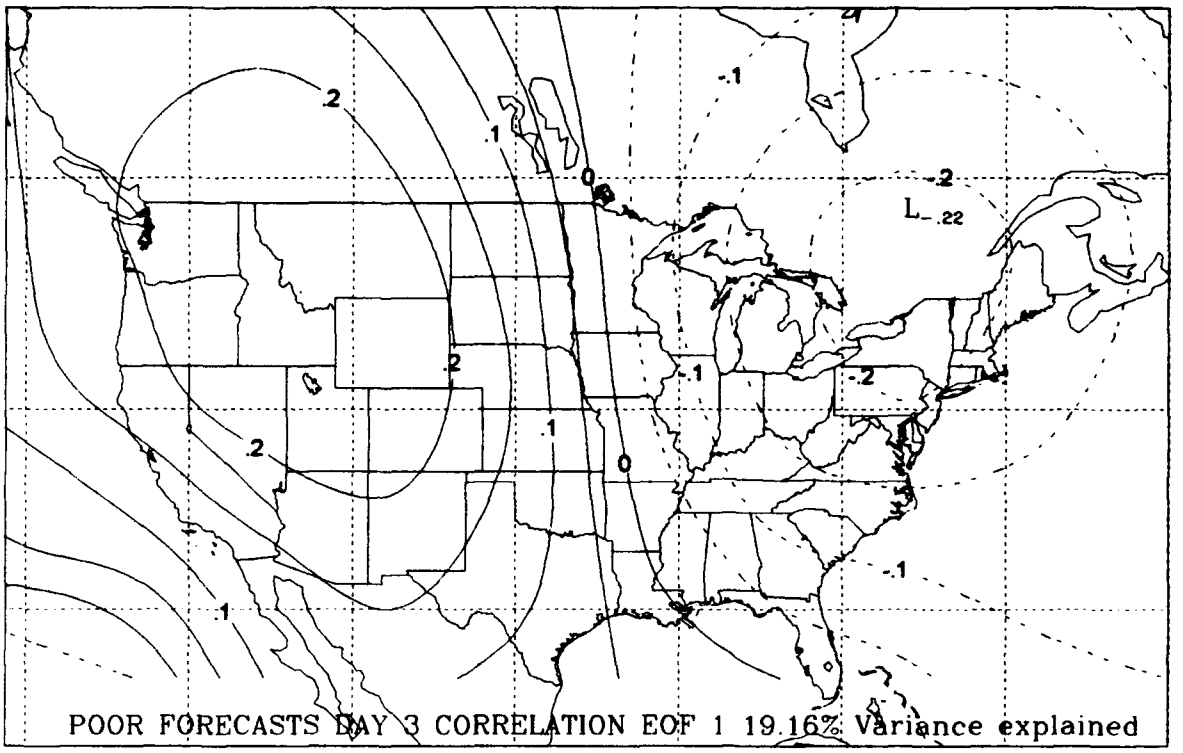

a.

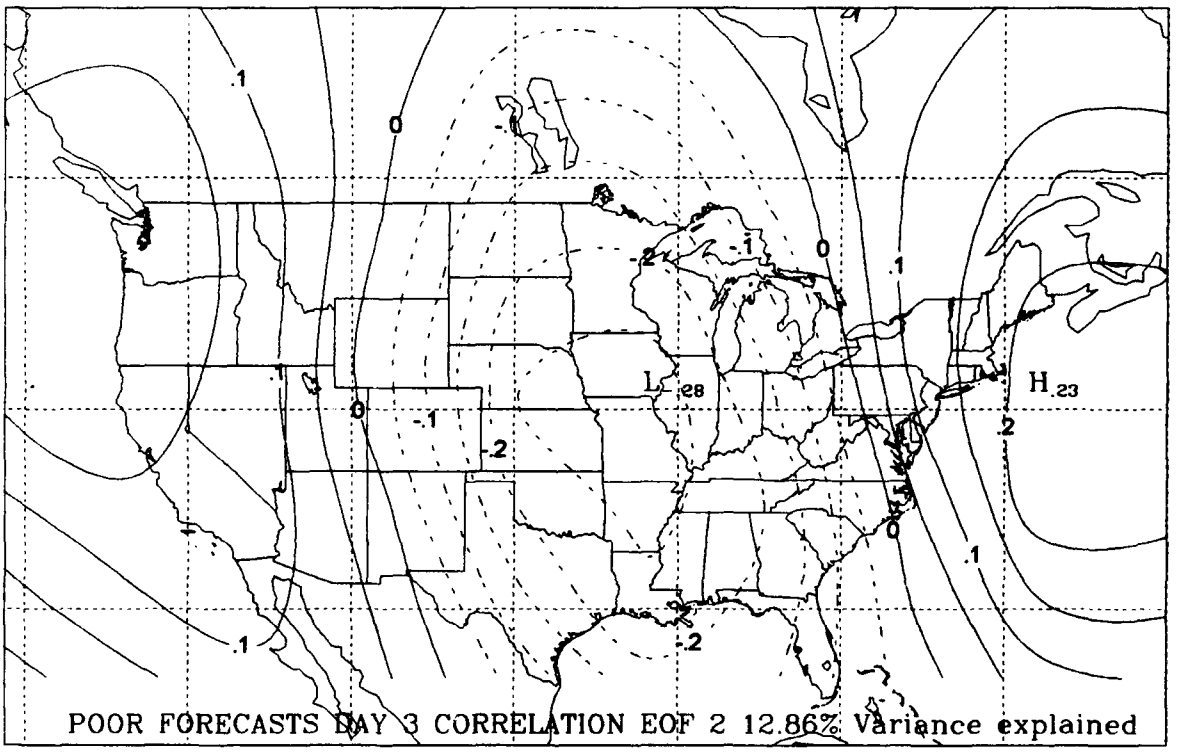

b.

Figure 19. Leading correlation EOFs of the day 3 error field of poor forecasts.

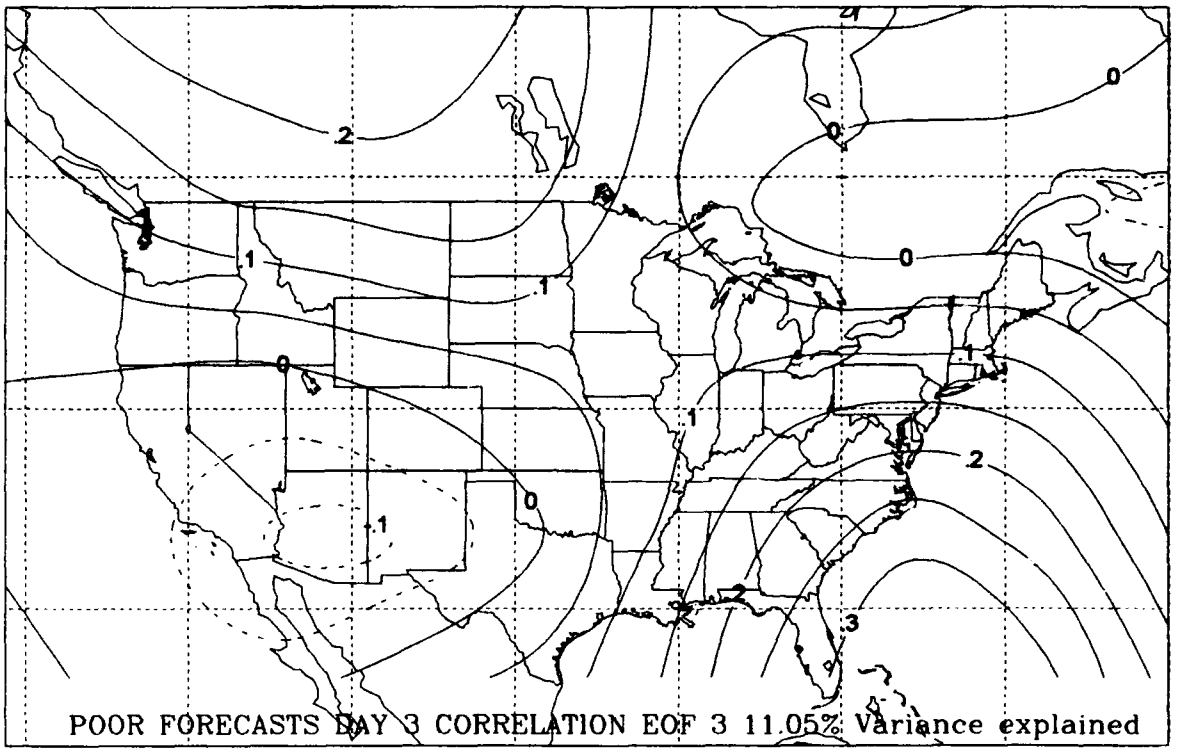

c.

Figure 19. (Continued).

the second EOF, and the combination of these two patterns increases in dominance to 32%. Thus, this wave pattern now explains about one third of the total variance. The single phase pattern which was present in the first two days is not as readily apparent by day 3. It might be found most closely in EOF 3, although this pattern has a greater negative area than was found in EOF 2 on day 2. Additionally, since EOFs 2 and 3 explain nearly the same percentage of the variance (12.86% versus 11.05%), there is some mixing of signal between the two.

The leading EOFs of day 4 (Fig. 20) indicate that the combination of patterns which emerged on day 3 have continued to do so. The dipole and its quadrature have separated from the remaining patterns and now combine to explain 40% of the total variance in the error fields. These two continue to be the leading modes on day 5 (Fig.

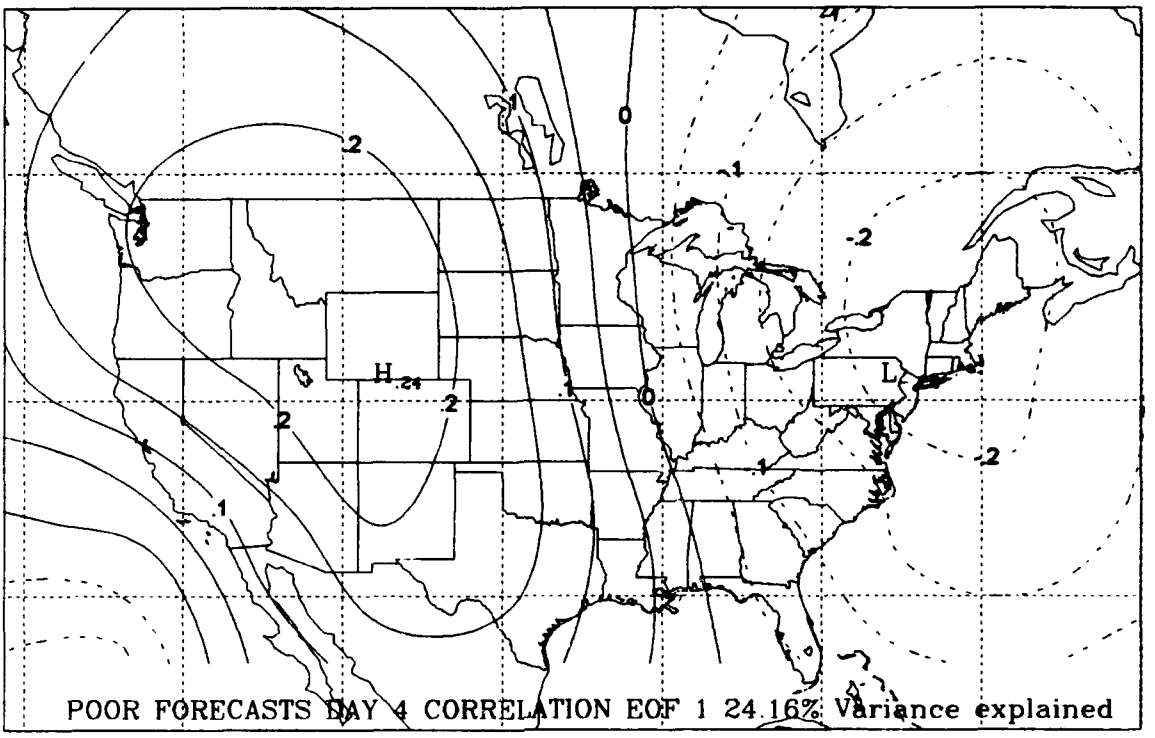

a.

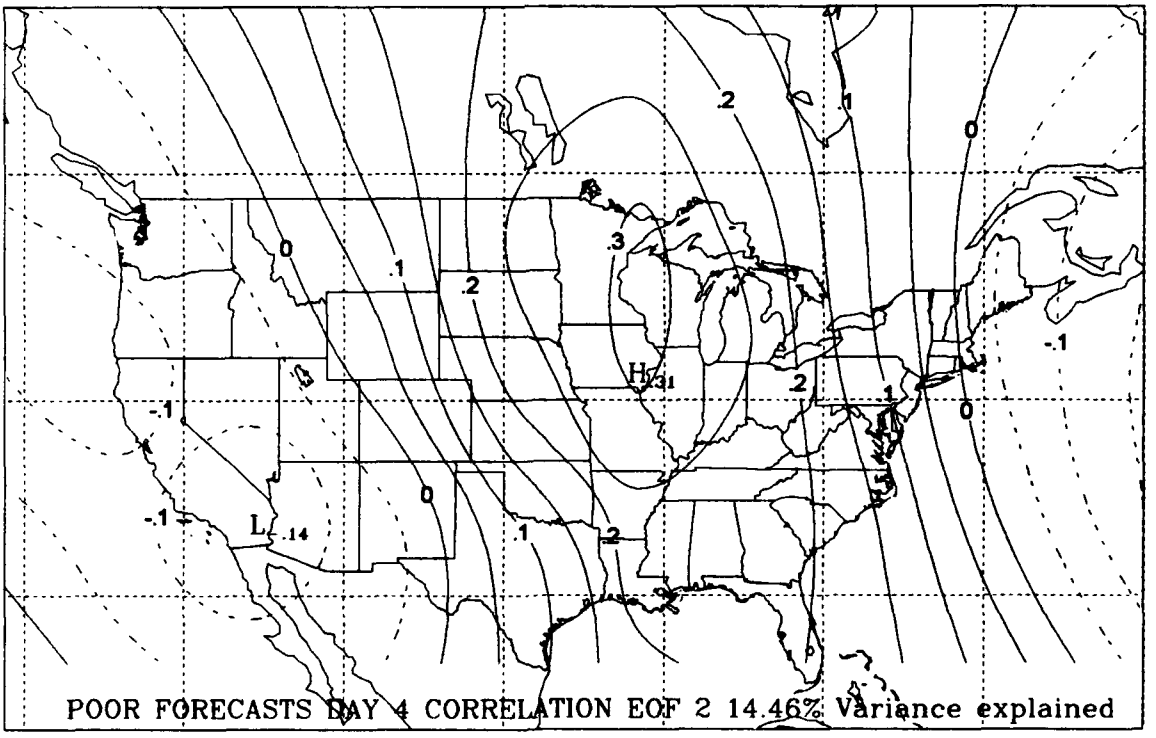

b.

Figure 20. Leading correlation EOFs of the day 4 error field of poor forecasts.

21), with similar contributions to the variance of the error fields. The single phase pattern from days 1 and 2 is not found among the first 5 EOFs on either day, indicating that it no longer contributes strongly to the error fields.

The evolution of EOFs for the set of good forecasts takes a different course and reveals their differences from the EOFs of the poor forecasts. On day 1 (Fig. 22), the leading pattern is nearly identical to that of the poor forecasts: a single phase, relatively flat field which explains 20% of the total variance. However, the dipolar pattern of EOF 2, while being somewhat weaker, has a more pronounced northwest to southeast orientation than did this pattern in poor forecasts. On day 2 (Fig. 23), the two patterns switch dominance, as they did in poor forecasts. Additionally, the wave pattern for good forecasts is in quadrature with the leading wave pattern of the poor forecasts. However, the closeness of this contribution to variance by EOFs 1 and 2, both in relation to each other and to the remaining EOFs, reveal that neither is a very dominant feature, as in poor forecasts. The mixing of these patterns is further evidenced by days 4 and 5, when they once again switch positions (Figs. 24 and 25). Finally, it is noted that the quadrature pattern, which was clearly evident in the poor forecasts, is not as dominant among the first 5 EOFs of any day in the good forecast subset.

The EOF analysis as discussed above was performed by analyzing the correlation matrix of the error fields. As a result, the patterns which are revealed have been smoothed by the standard deviations of the individual points in the error field. The EOF analysis was once performed again, this time using the values contained in the covariance matrix or the error fields. The resulting EOFs from this analysis are patterns which additionally emphasize the variance of the forecast error at all individual points in the error fields. Some of the results from this second analysis will be discussed below and compared to the previous results.

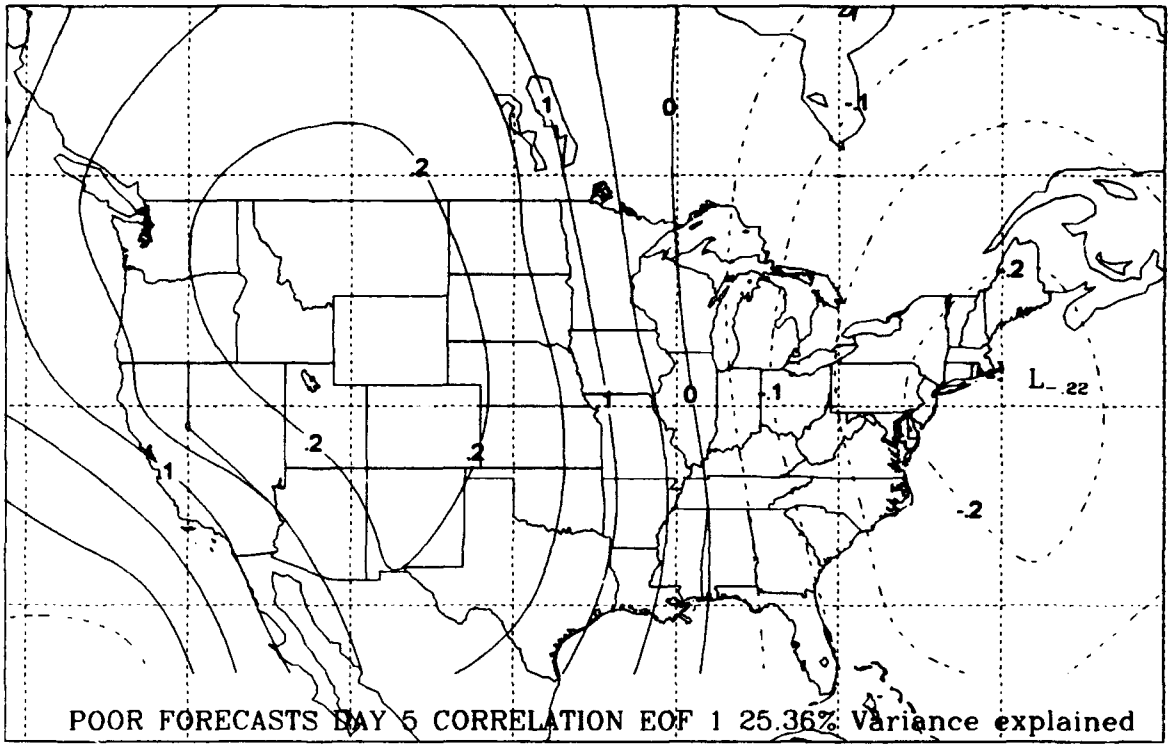

a.

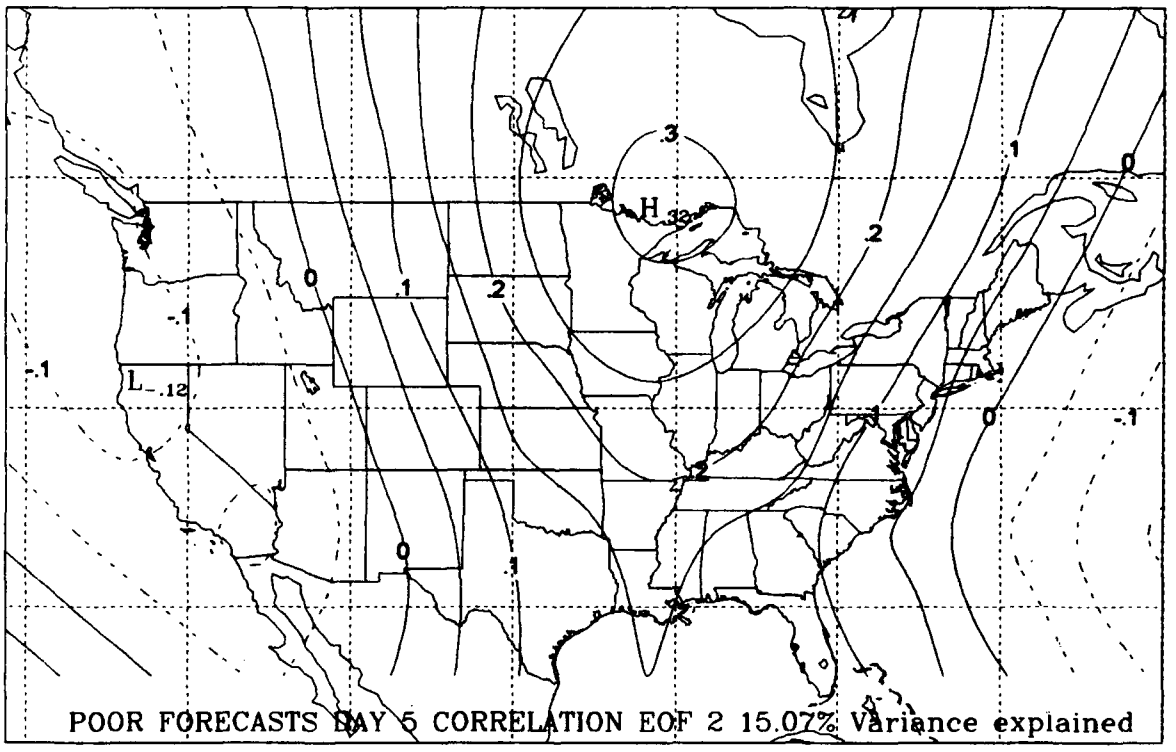

b.

Figure 21. Leading correlation EOFs of the day 5 error field of poor forecasts.

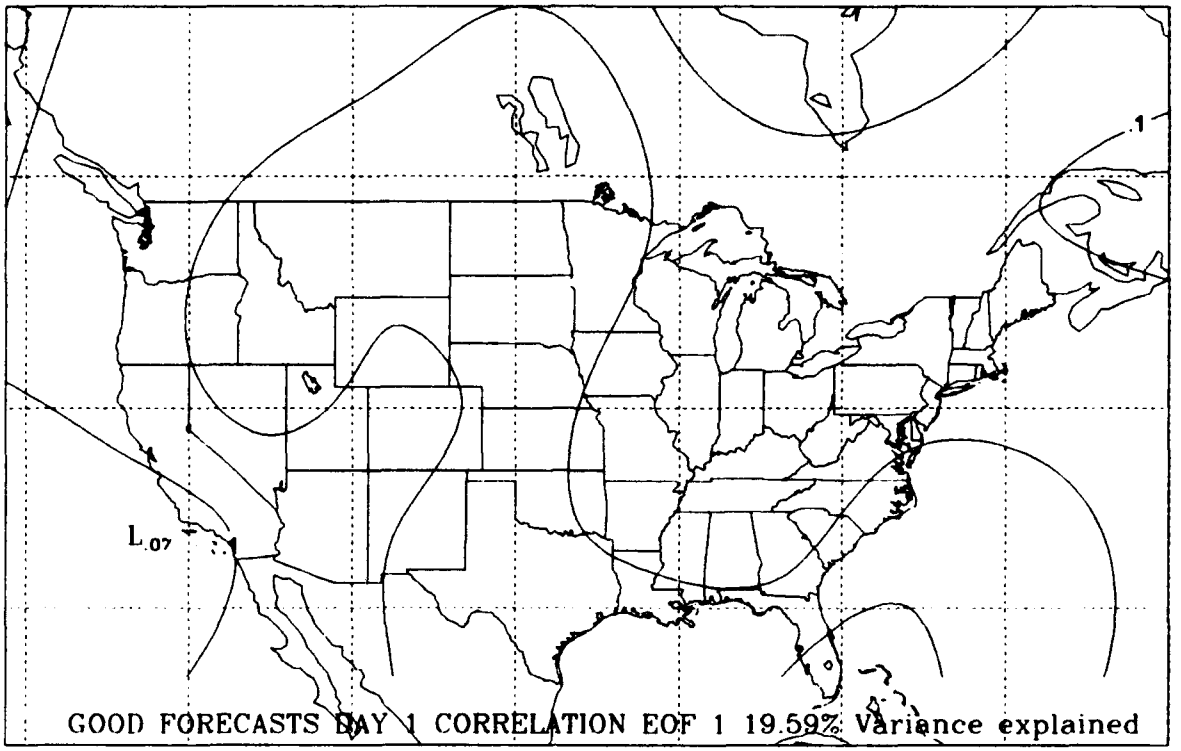

a.

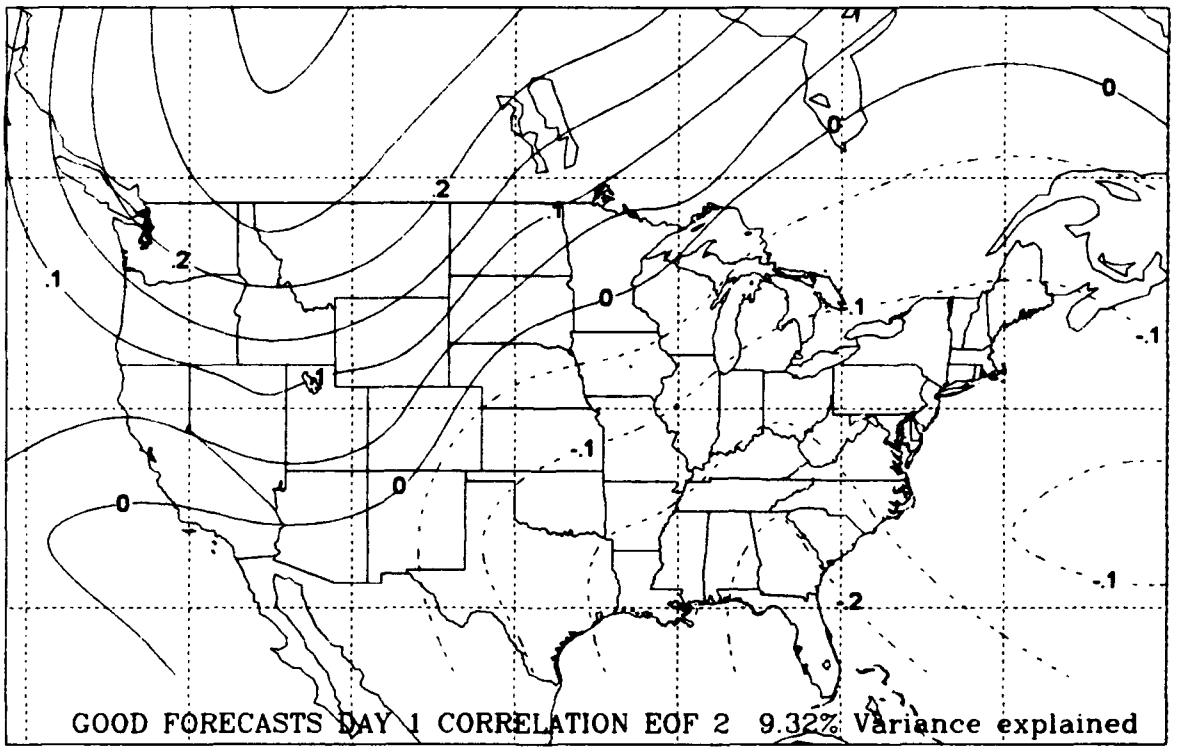

b.

Figure 22. Leading correlation EOFs of the day 1 error field of good forecasts.

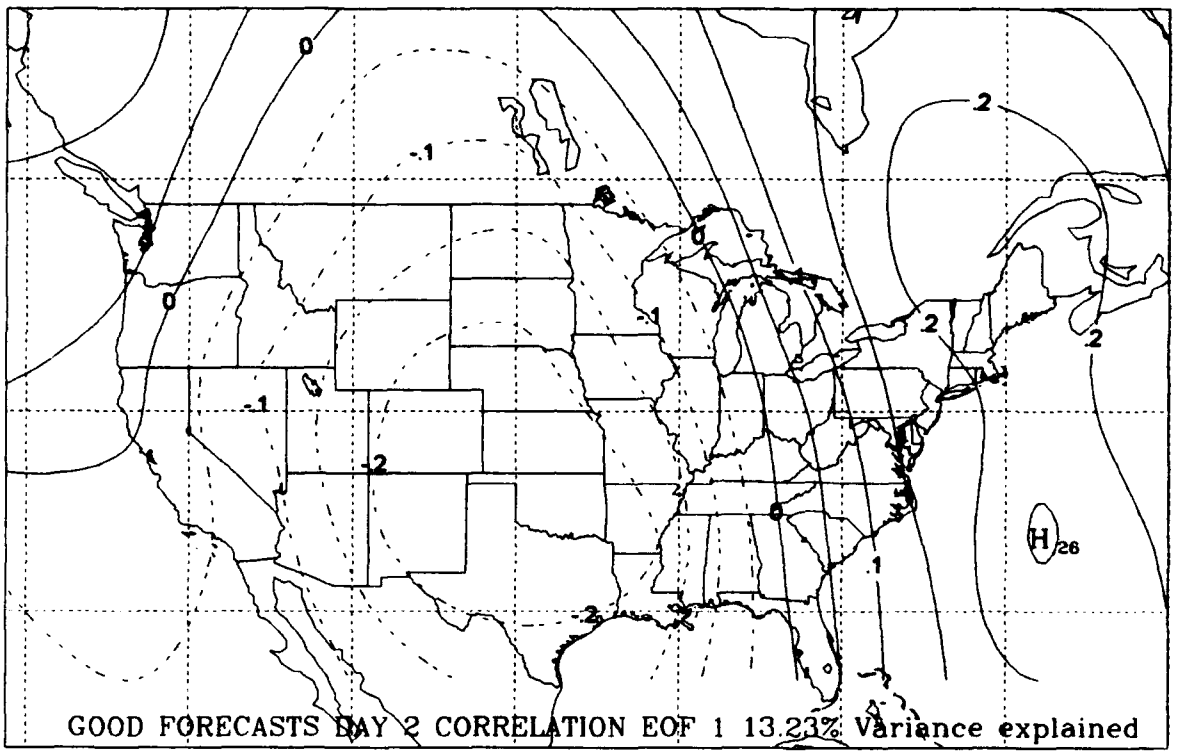

a.

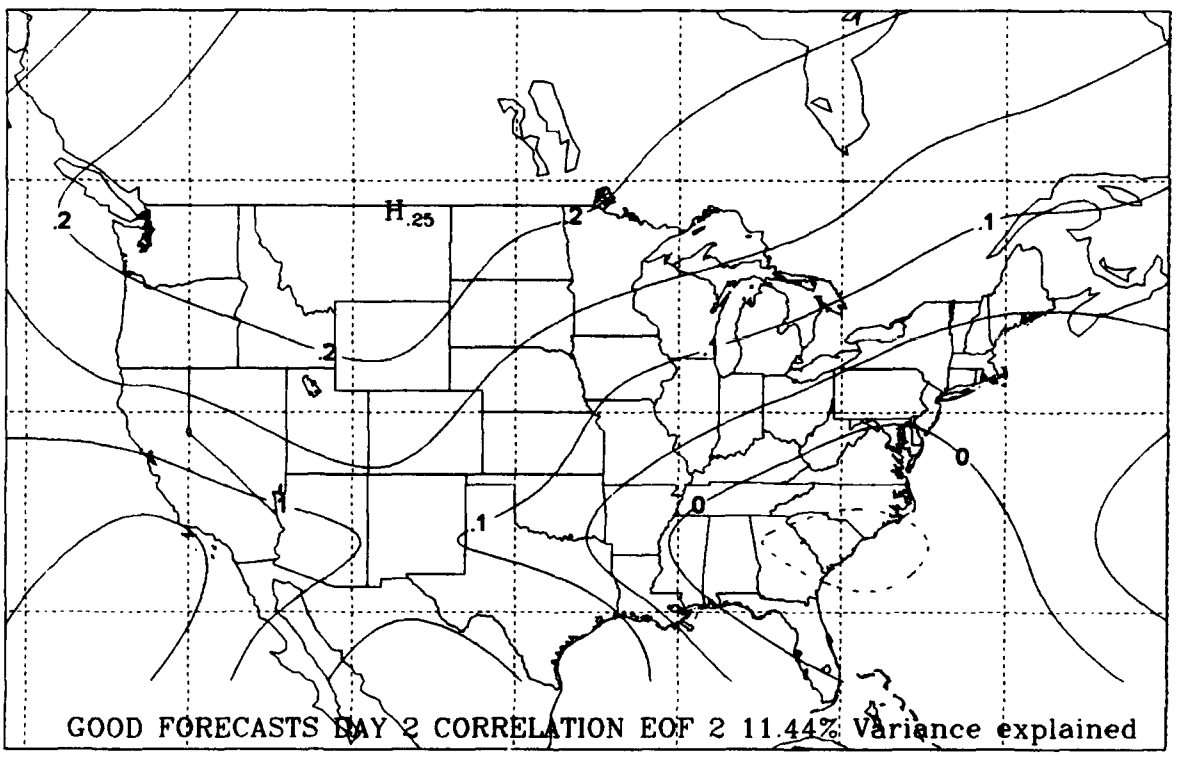

b.

Figure 23. Leading correlation EOFs of the day 2 error field of good forecasts.

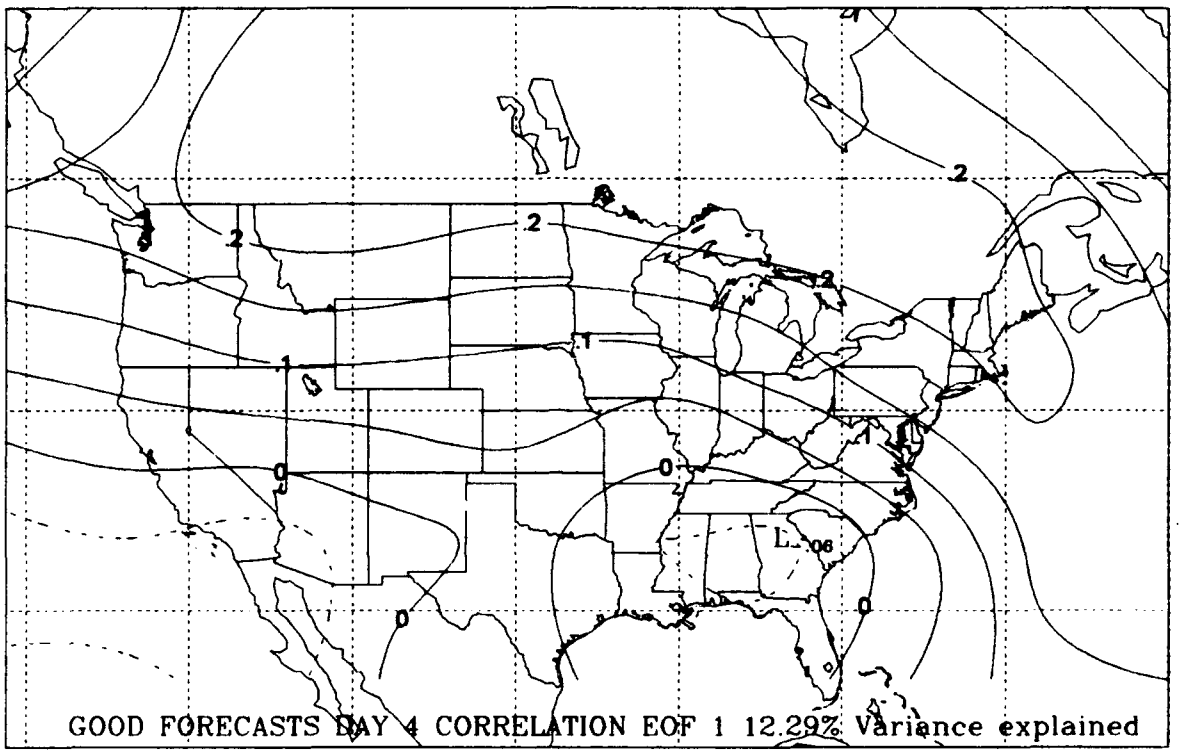

a.

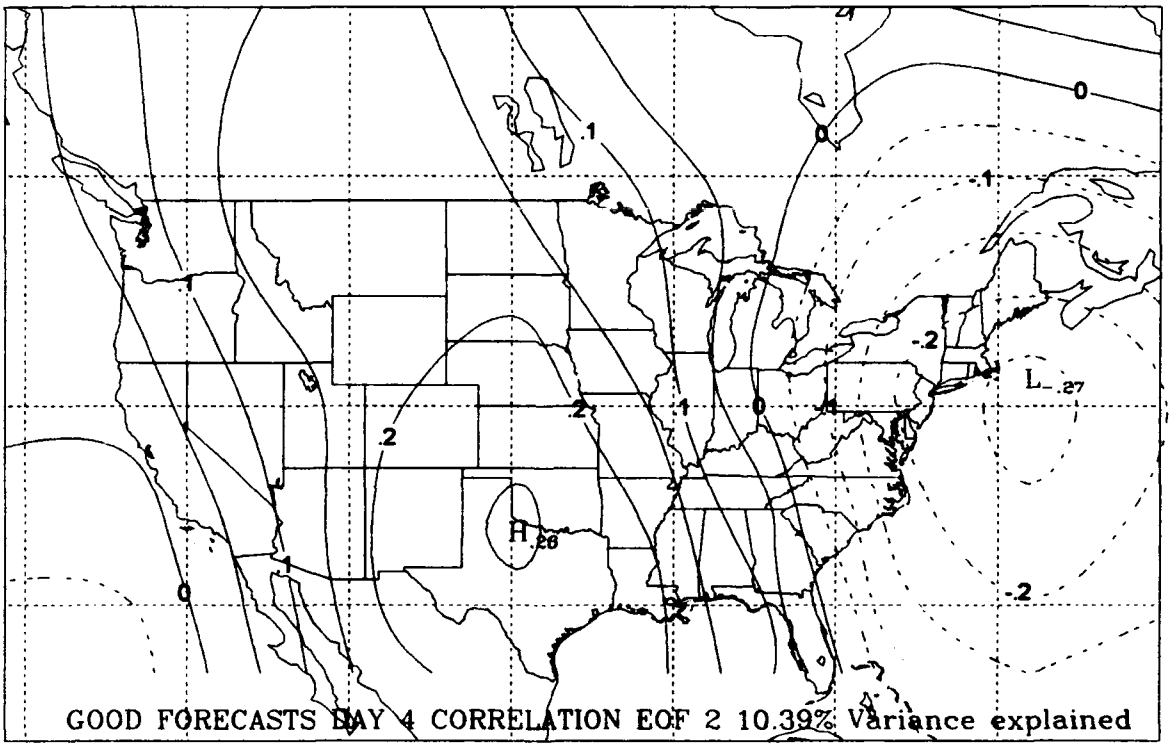

b.

Figure 24. Leading correlation EOFs of the day 4 error field of good forecasts.

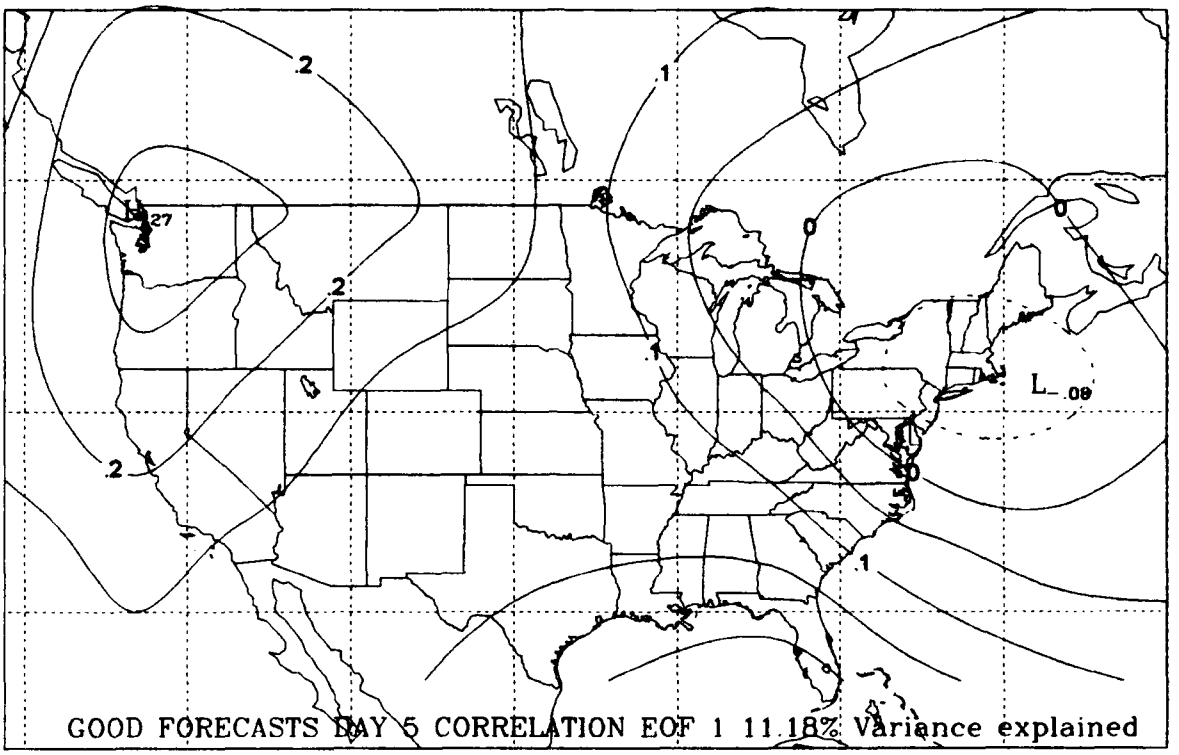

a.

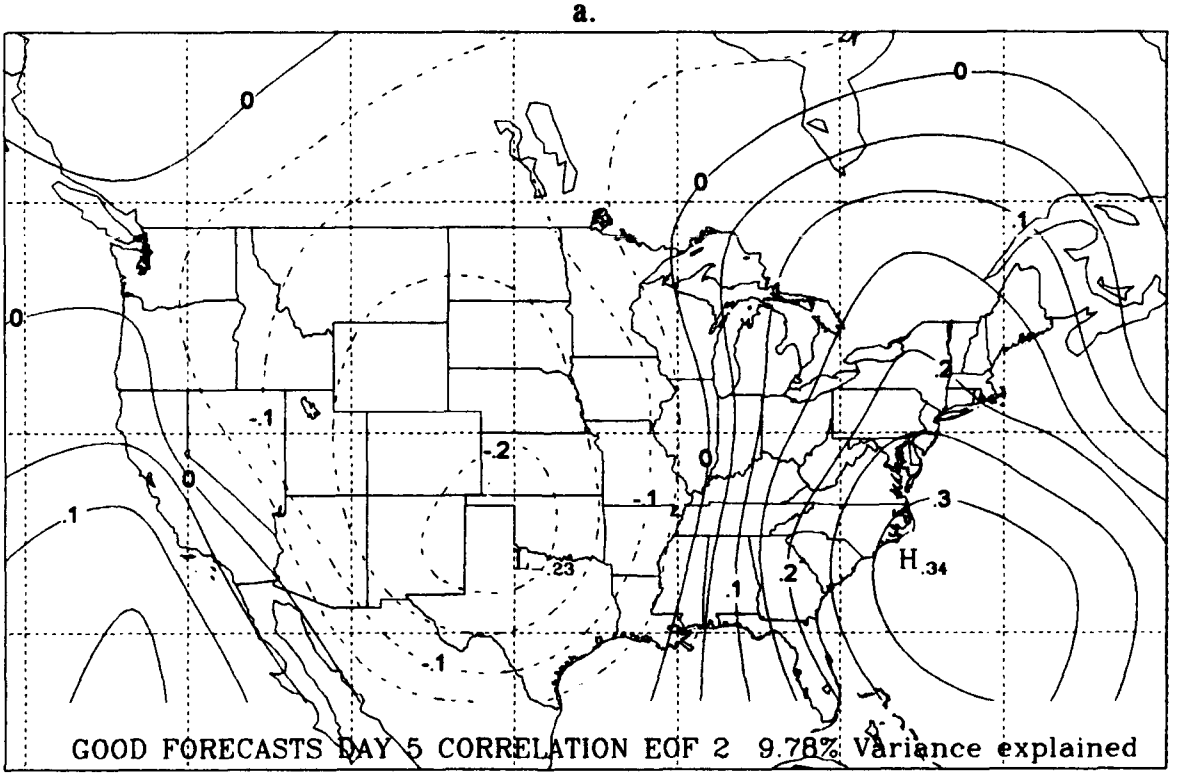

b.

Figure 25. Leading correlation EOFs of the day 5 error field of good forecasts.

On day 1 (Fig. 26), the leading EOF is once again the single phase pattern as before, and as expected. However, the contribution to variance is more pronounced. The second EOF still has some characteristics of the dipole pattern, but its existence is largely confined to the western half of the CONUS, as opposed to the longer length scale found in the covariance EOFs. The single phase remains dominant on day 2 (Fig. 27a), however the presence of a maximum center in Washington resembles the dipolar pattern. The dipole pattern and its quadrature is revealed in EOFs 2 and 3, however the two modes are not well separated, either from each other or from the remaining EOFs, in terms of dominance (Fig. 27b and 27c). On day 3 (not shown) the dipole and quadrature gain dominance as before, with this dominance continuing through day 5 (Fig. 28). Once again, it must be noted that when this analysis is performed, the significance of the dipole/quadrature pattern is shown to be increased.

For good forecasts, the single phase pattern is once again the leading pattern on day 1 (Fig. 29). However, throughout the length of the forecast, the dipole/quadrature combination still never manifests itself as one of the dominant, leading patterns. The pattern is found on day 5 as EOFs 2 and 3 (Fig. 30), but with a low, nondescript percentage of the variance. As with the correlation EOFs, the contributions to variance of the good forecast covariance EOFs are muddled as revealed by their flat distribution in Fig. 31.

The EOFs presented thus far are calculated without correcting for, or removing, the mean error field of each individual forecast day and forecast category, especially the poor forecast category. To complete the EOF analysis, the EOFs are again calculated with the mean error field removed. This mean pattern will be revealed as the leading mode, as was the case of the temporal EOF presented earlier. In this case, the mean pattern would represent the systematic model error associated with the particular forecast day and category.

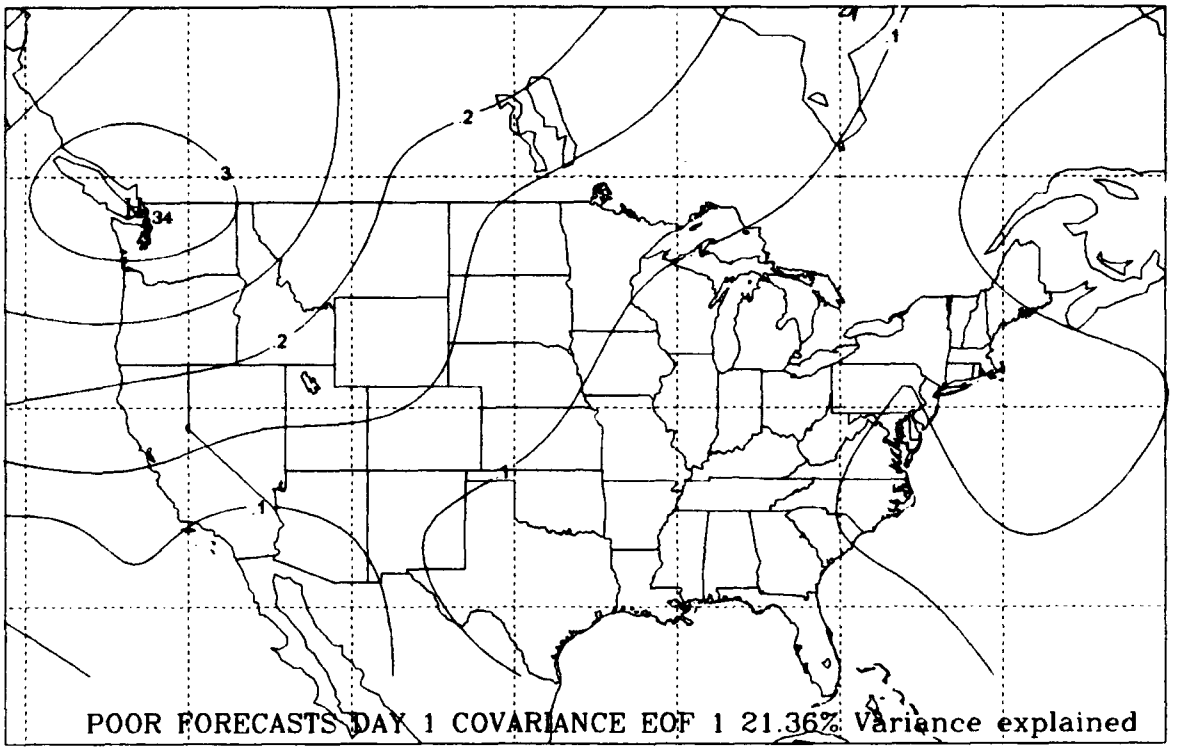

a.

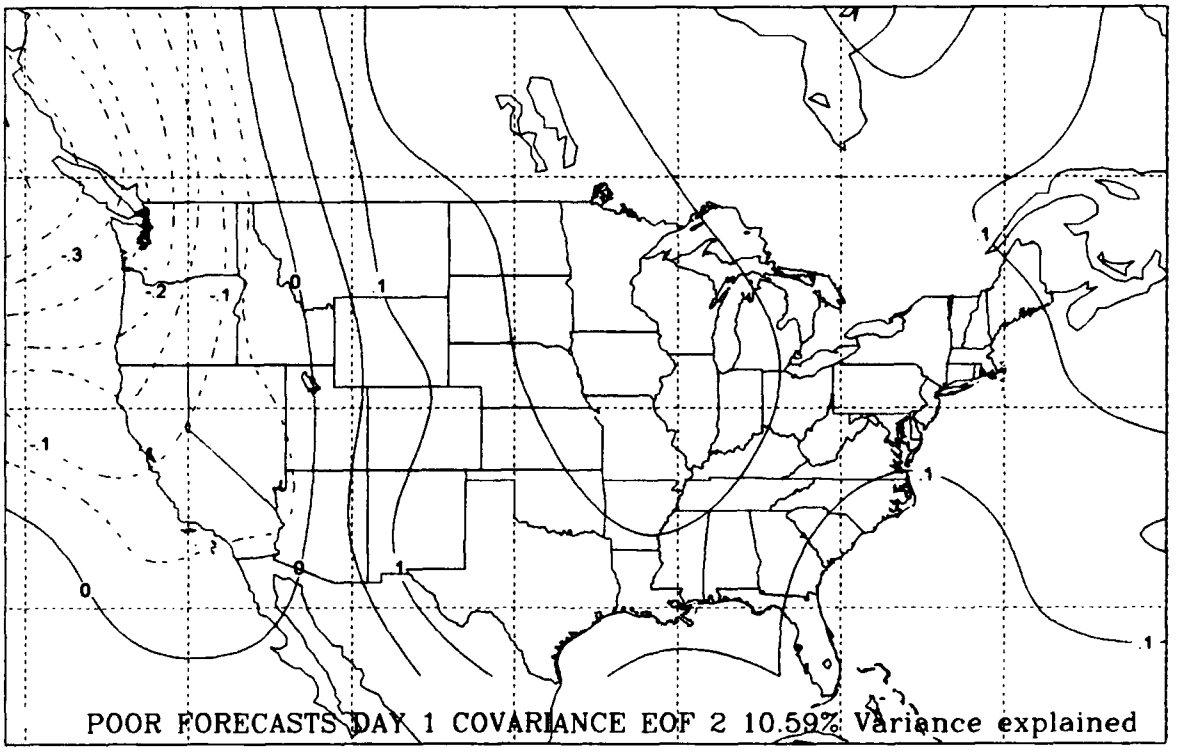

b.

Figure 26. Leading covariance EOFs of the day 1 error field of poor forecasts.

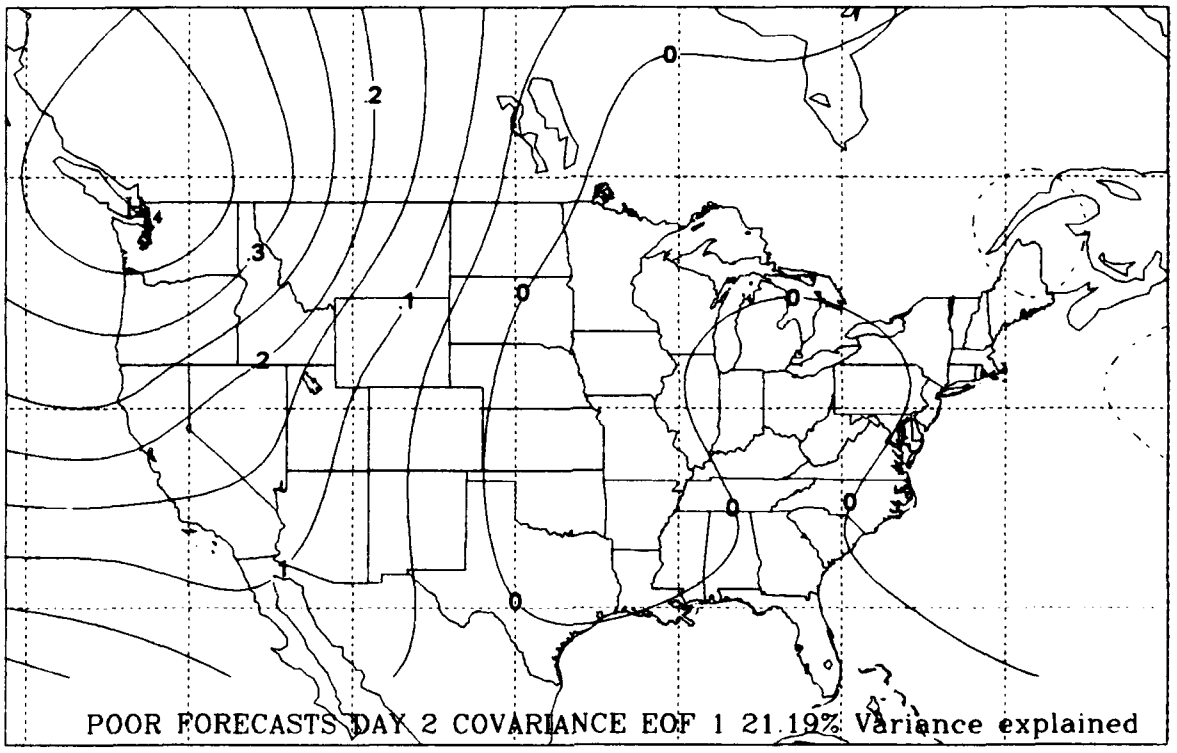

a.

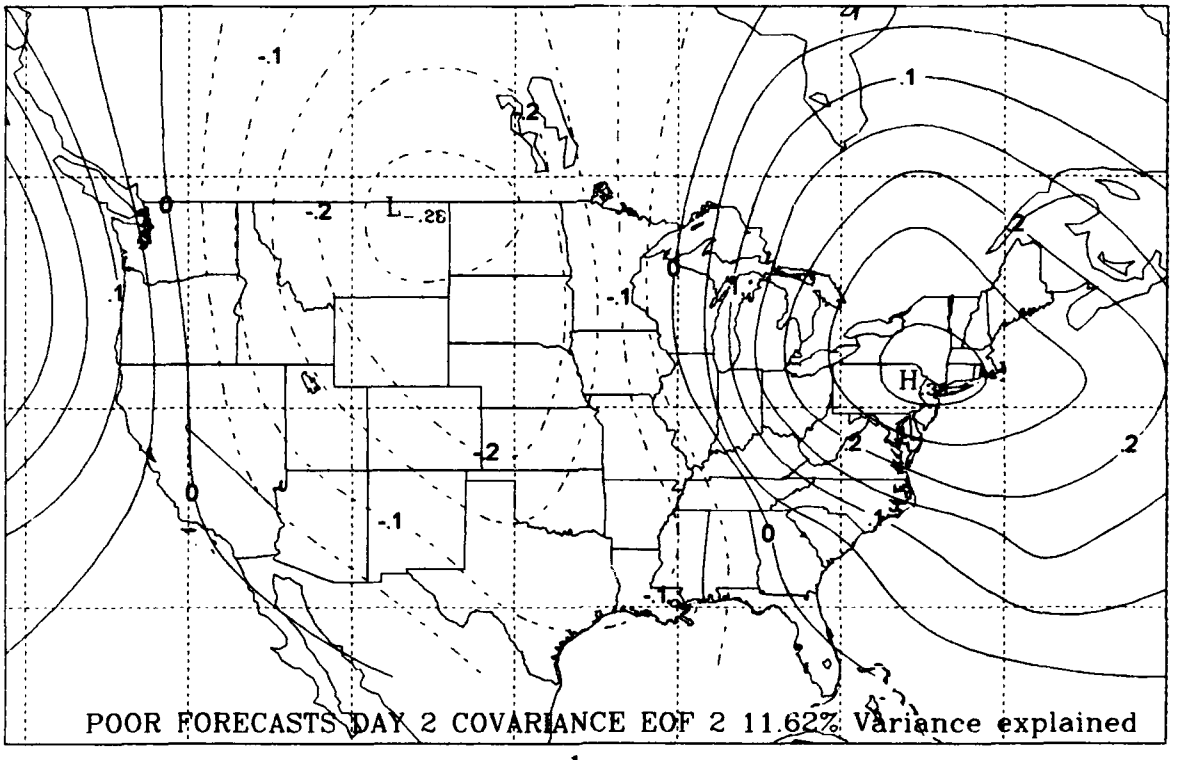

b.

Figure 27. Leading covariance EOFs of the day 2 error fields of poor forecasts.

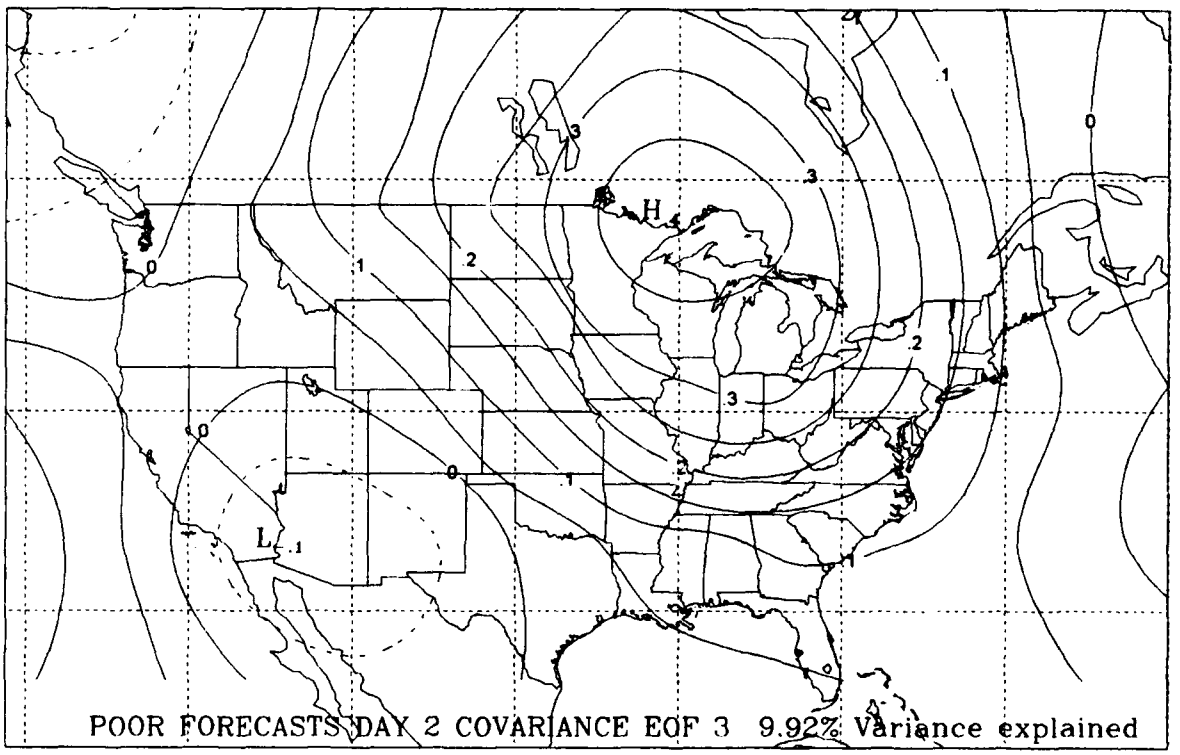

c.

Figure 27. (Continued).

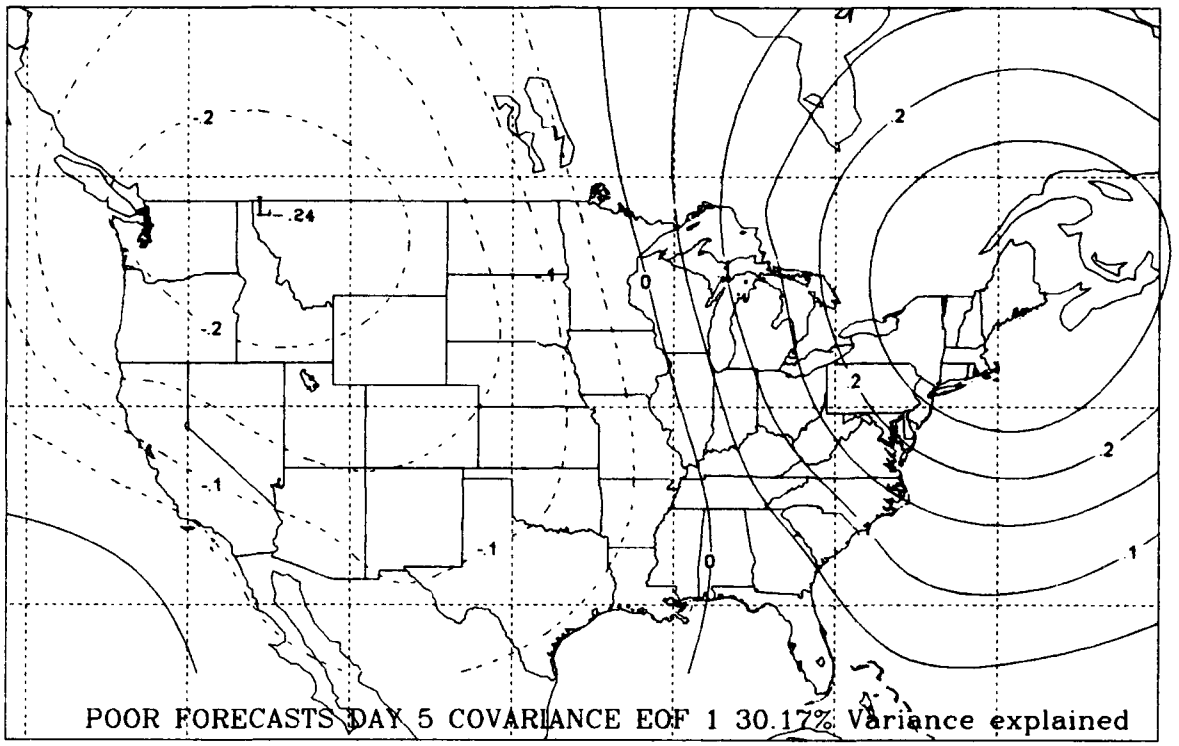

a.

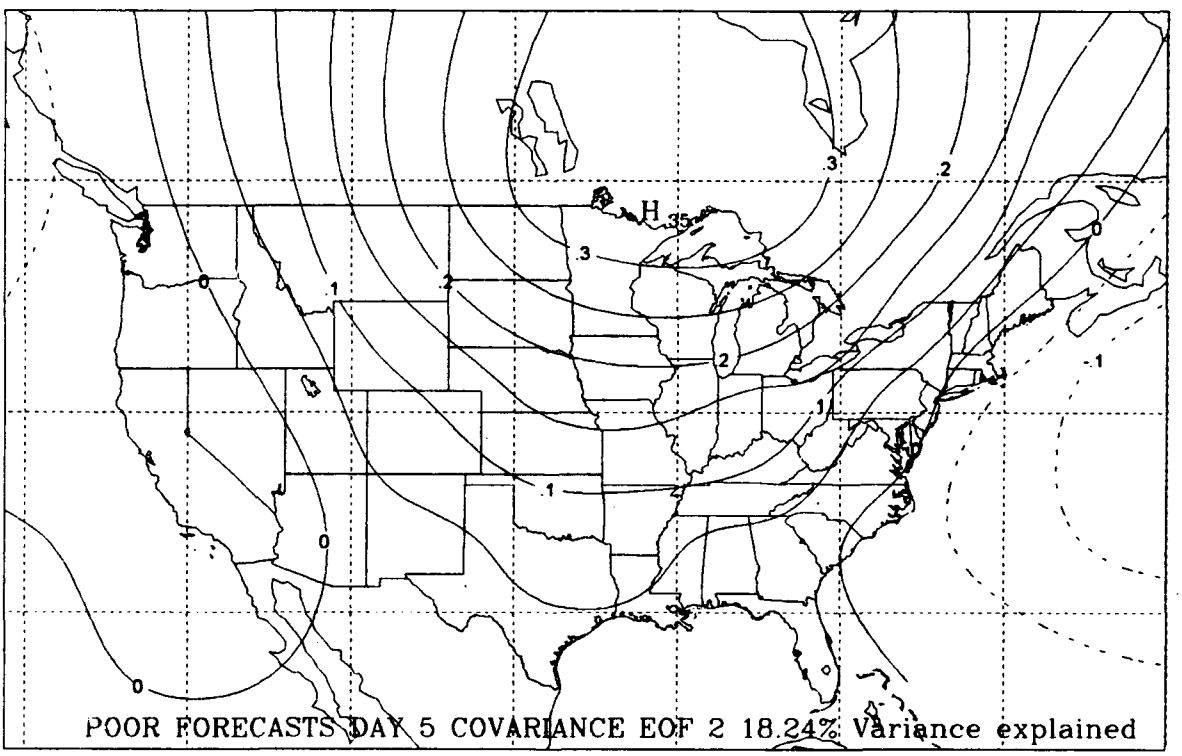

b.

Figure 28. Leading covariance EOFs of the day 5 error field of poor forecasts.

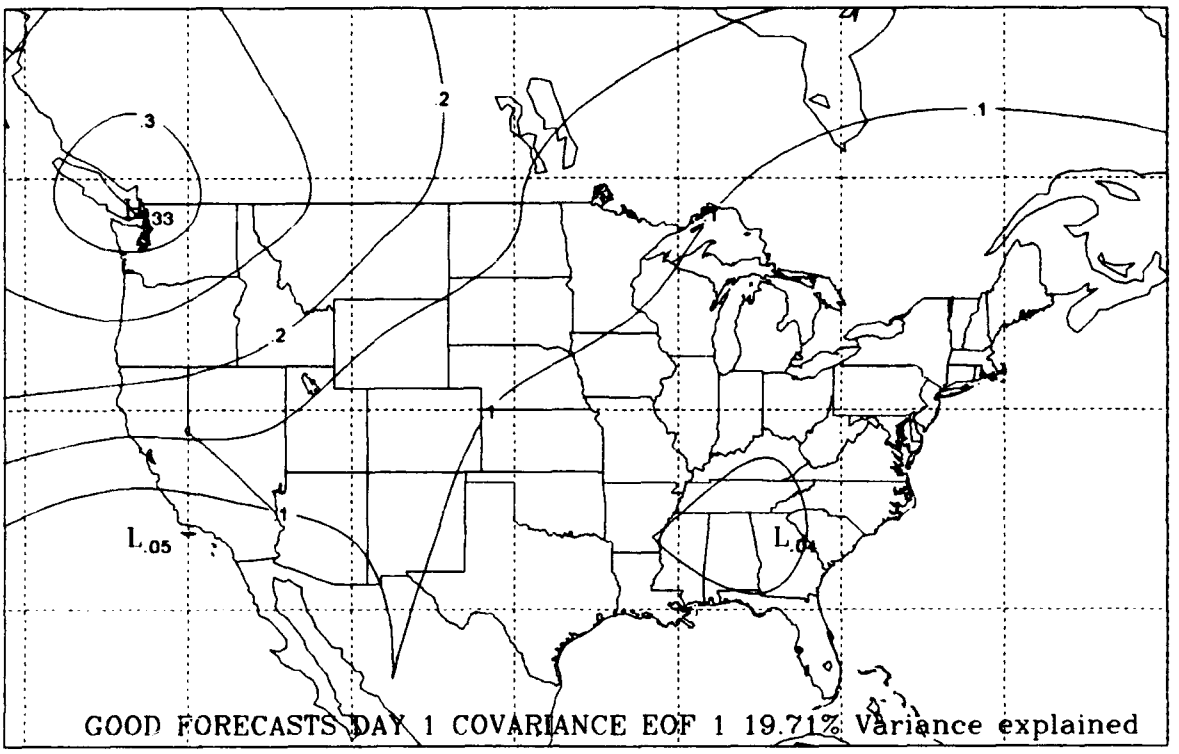

a.

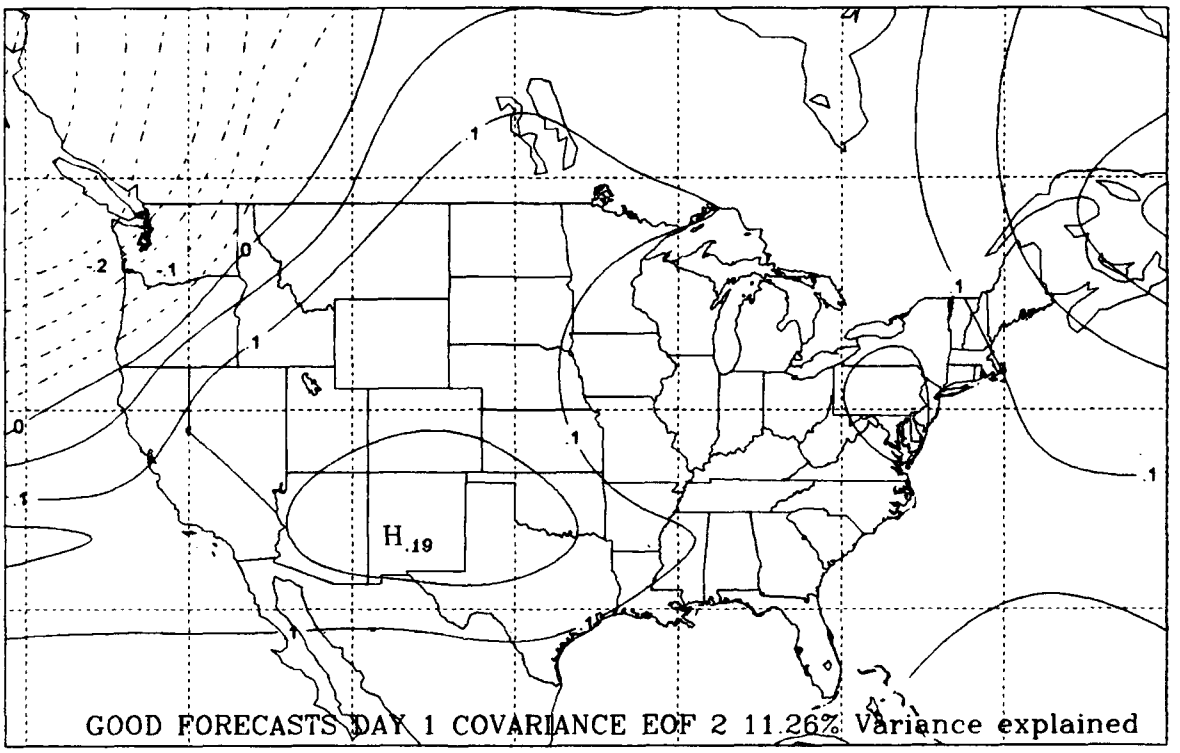

b.

Figure 29. Leading covariance EOFs of the day 1 error field of good forecasts.

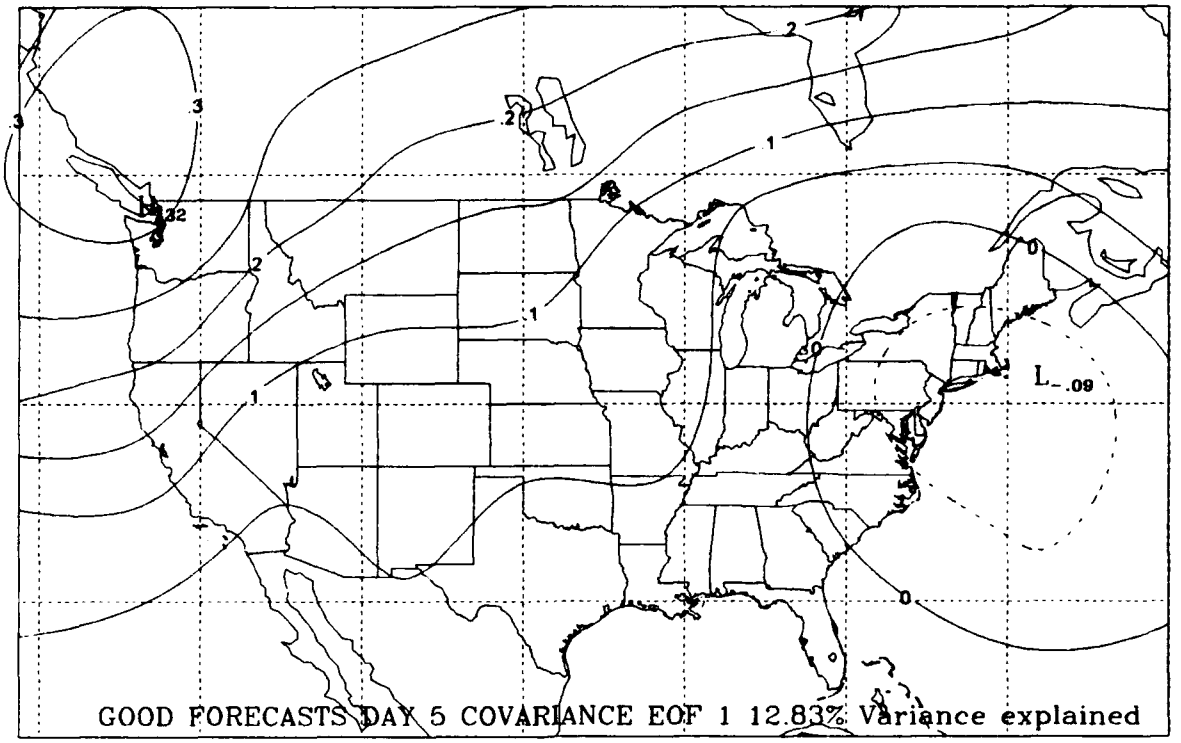

a.

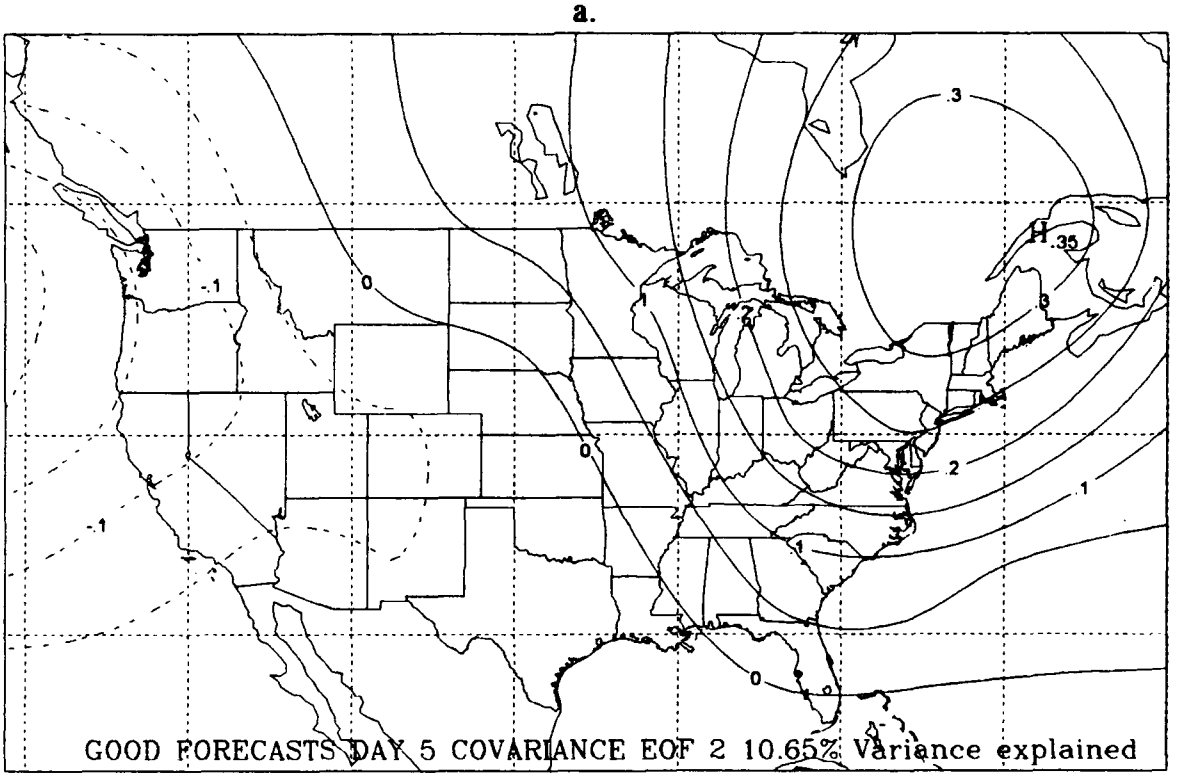

b.

Figure 30. Leading covariance EOFs of the day 5 error field of good forecasts.

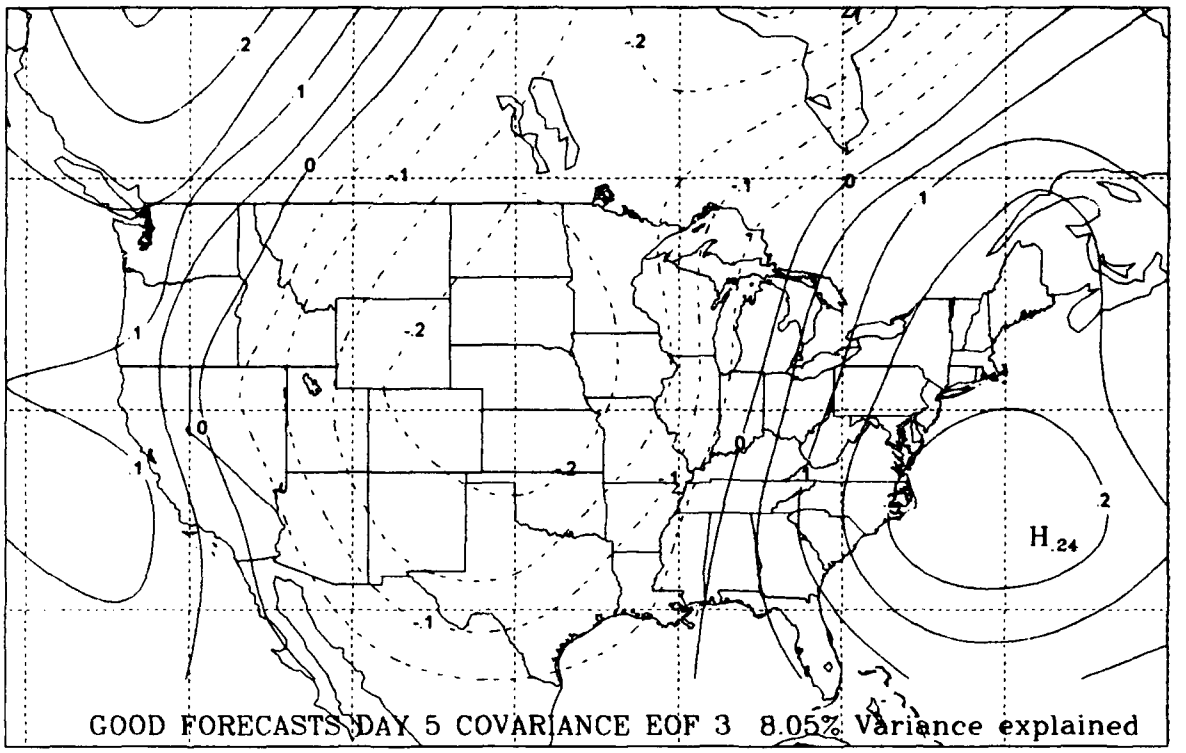

c.

Figure 30. (Continued).

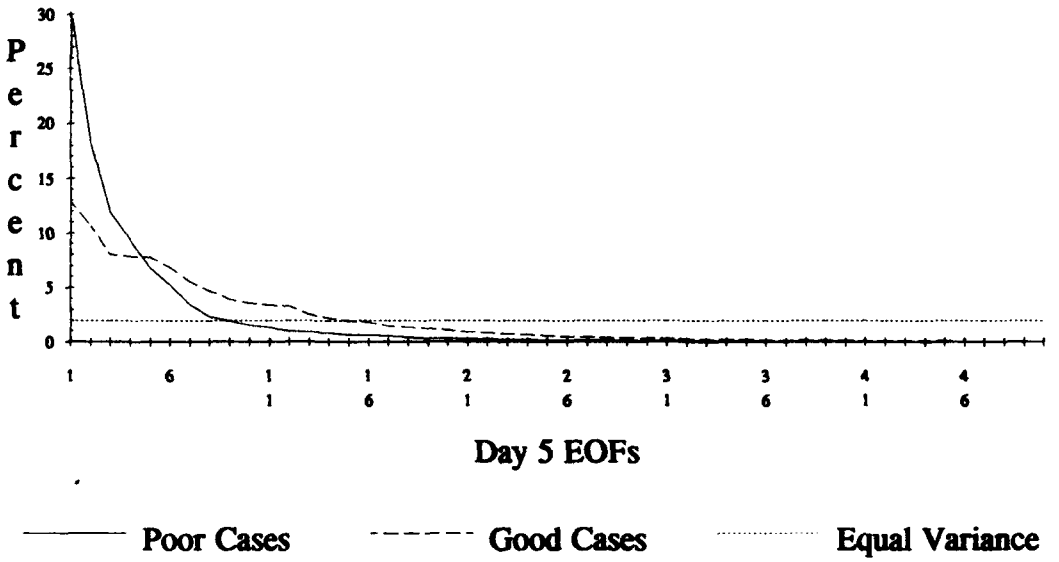

Figure 31. Percentage of variance of the day 5 CONUS error fields explained by the spatial EOFs calculated from the covariance matrix.

When this analysis is accomplished, an interesting result is revealed in the poor forecasts. The mean pattern is essentially a zero field, and is masked in the leading EOF. Inspection of the leading day 5 poor forecast EOFs (Fig. 32) reveals that these EOFs are essentially the same as those which were not corrected for the mean. This similarity extends even to the percentage of variance explained by each EOF. The absence of an identifiable mean pattern through this analysis indicates that the errors in poor forecasts at 5 days do not contain a systematic bias.

As discussed earlier, the fact that RMS performance increased with time over the data period, coupled with the use of 10-year statistics to define forecast categories, introduced some bias into the poor and good forecast data sets. The poor forecast data set is weighted more toward the earlier years of the data period, while the good forecasts are slanted more toward the later years. This means that there may be more contribution to the error modes in poor forecasts from the earlier version of the ECMWF model. To investigate if this is indeed a factor, the EOF analysis is once again performed for each forecast category and length. However, in this analysis the error fields are also segregated on the basis of the operational version of the model used to produce the forecast. In this data set, the winter seasons 1981-1983 represent the grid point version, 1984 and 1985 are from the T63 version and the 1986-1990 winter seasons are from the T106 model.

Figure 33 presents the leading correlation EOFs for day 5 of poor forecasts from the 1981-1983 winter seasons. During this period, the grid point version of the model was the operational version. The familiar dipole pattern is once again the leading EOF at this forecast length and category. This mode contributes 27% of the variance in this case. The quadrature pattern is once again revealed in EOFs 2 and 3. These two modes are also somewhat muddled, as their contributions are rather close (15 and 13.6%, respectively), although EOF 2 looks most like the quadrature. Compare these patterns with the EOFs of Fig. 21. This comparison shows that the dominant modes in this category from this 3 year period are essentially the same as those of the entire 10-year period.

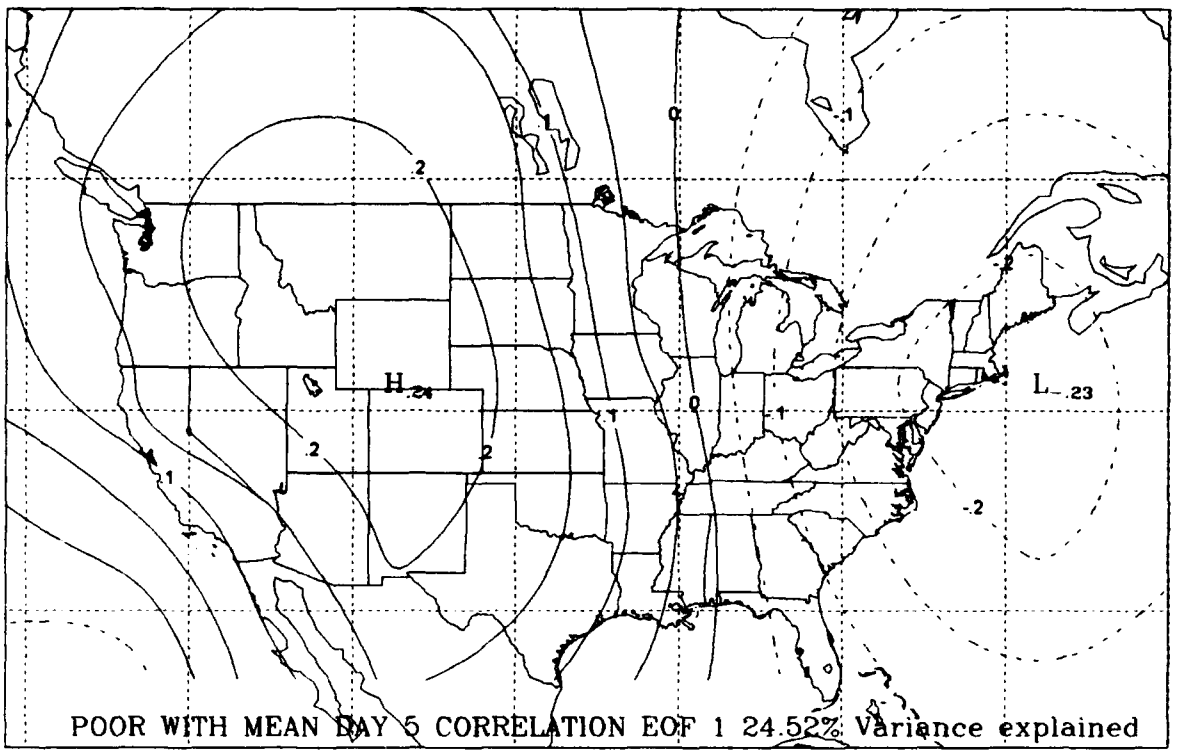

a.

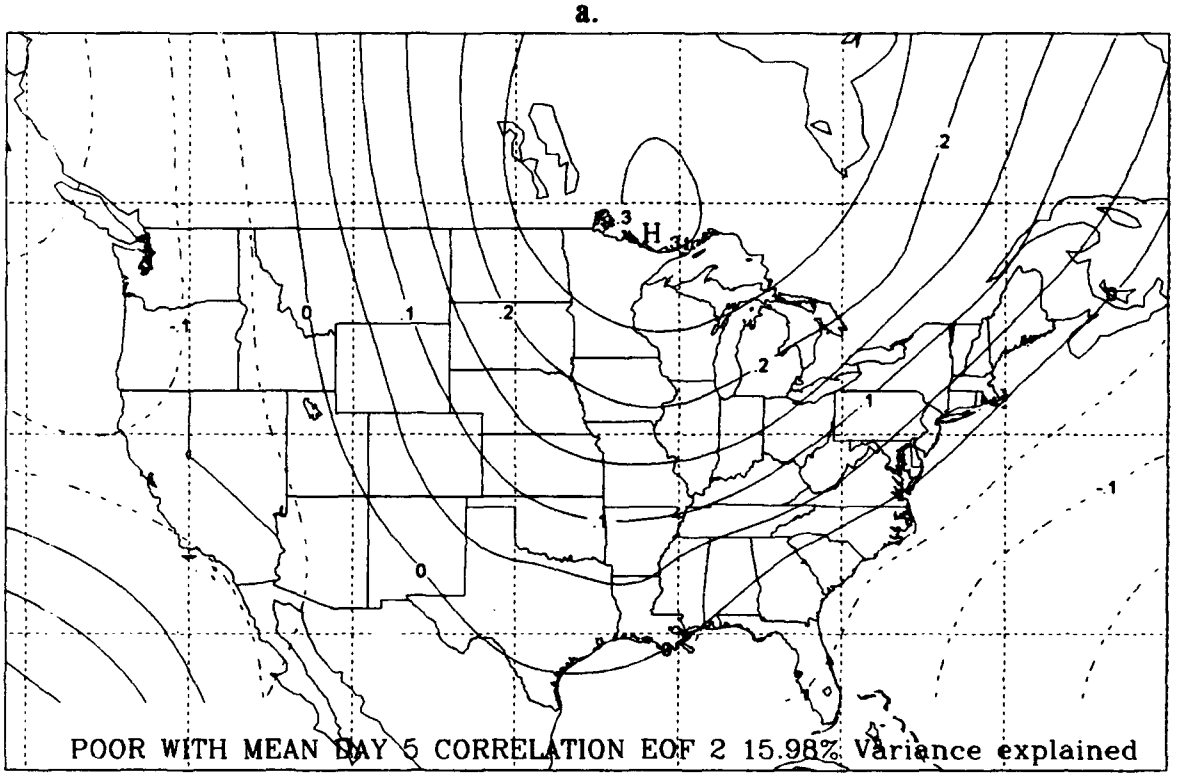

b.

Figure 32. Leading correlation EOFs with mean error field included of the day 5 error fields of poor forecasts.

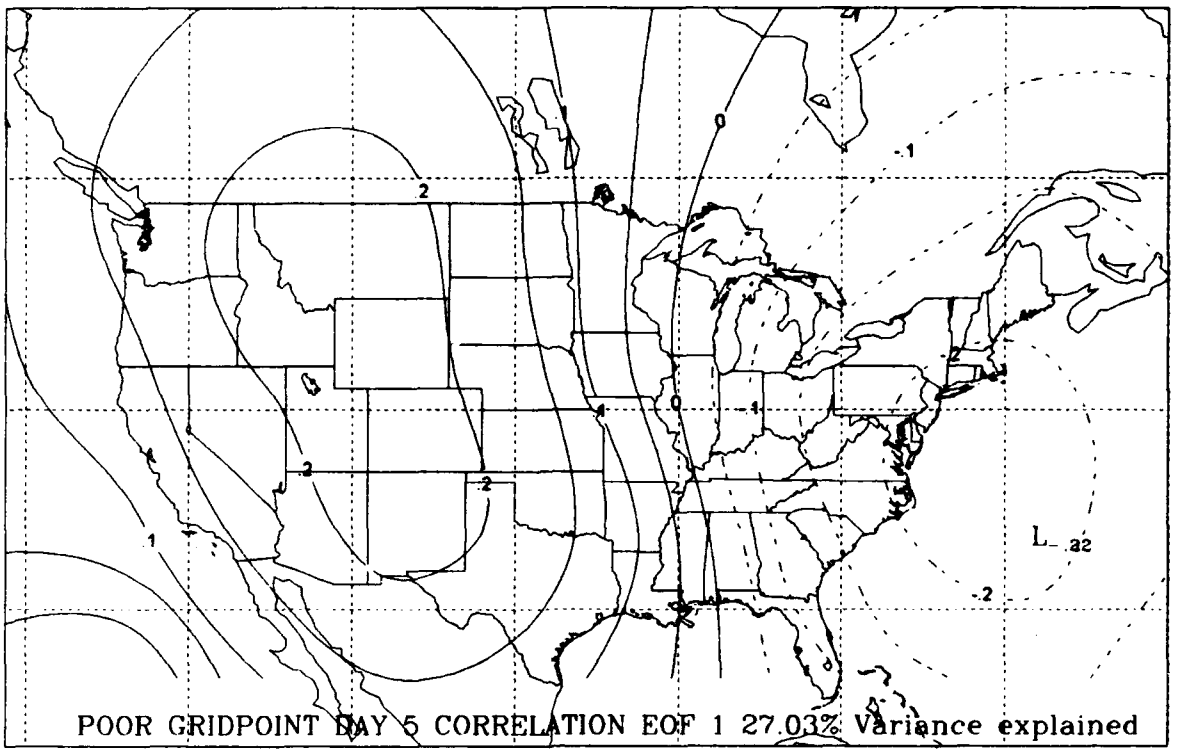

a.

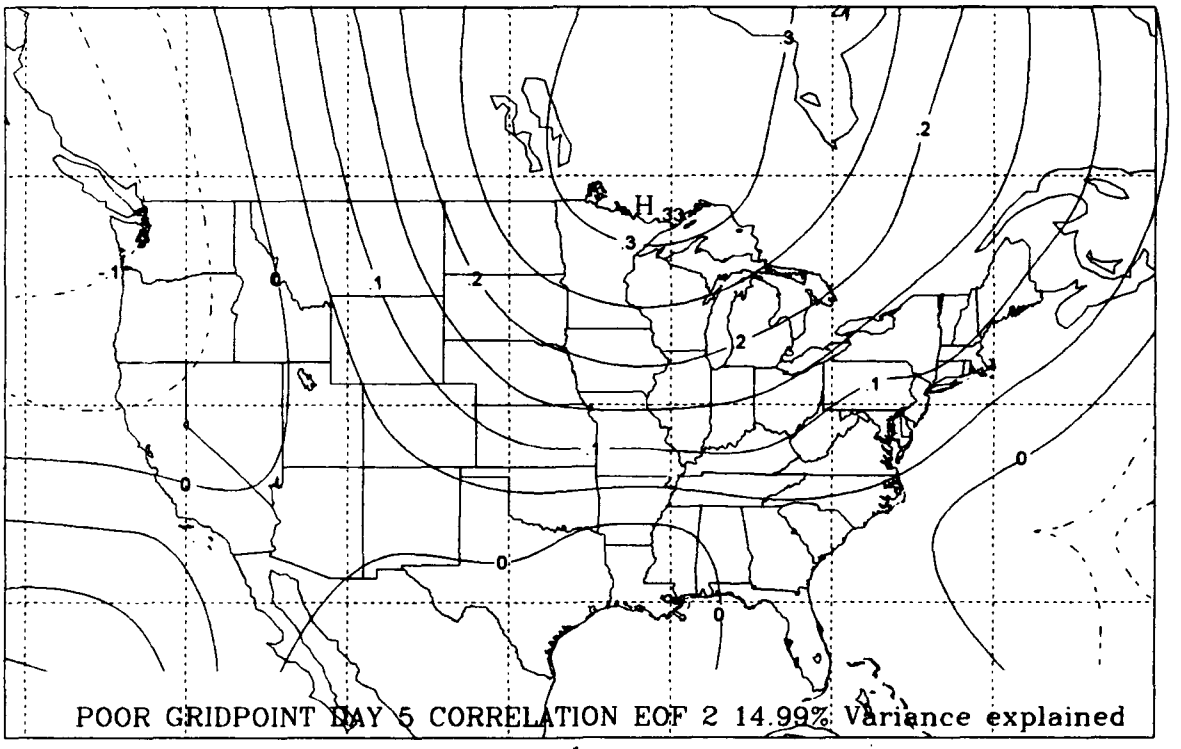

b.

Figure 33. Leading correlation EOFs of the day 5 error field of poor forecasts from the operational grid point version of the ECMWF model.

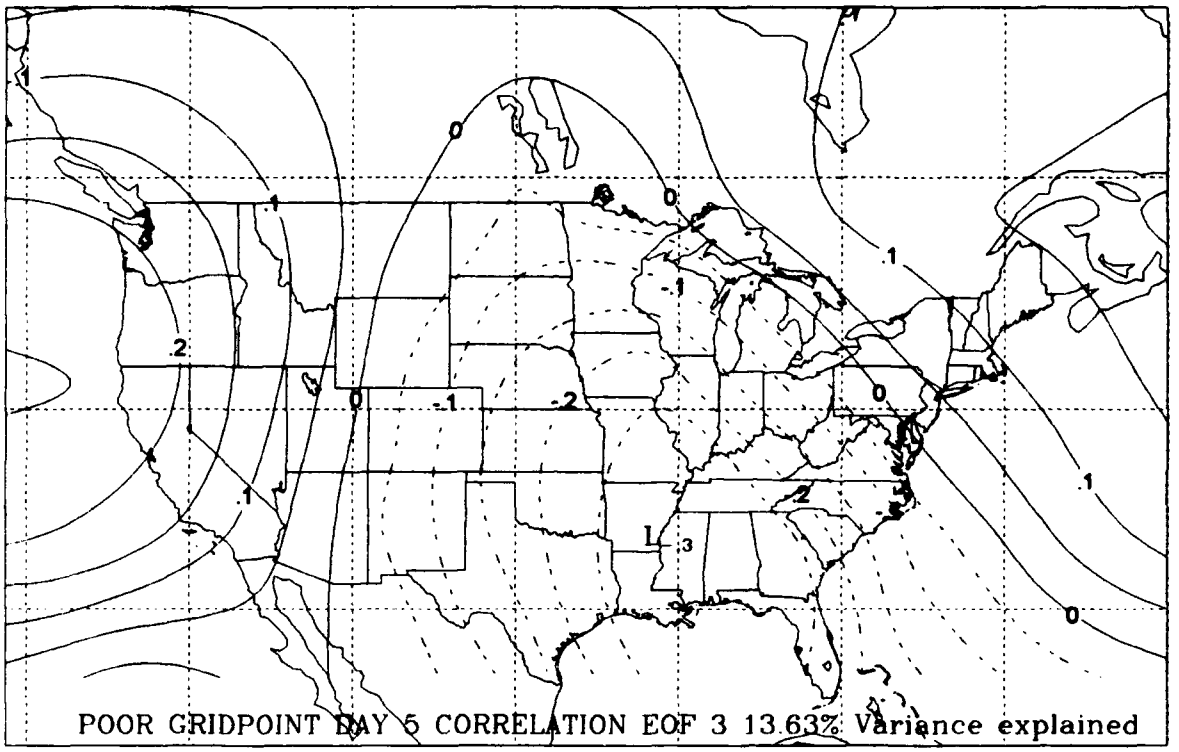

c.

Figure 33. (Continued).

The leading EOFs from the day 5 error field of poor forecasts from the T106 version of the ECMWF are presented in Fig. 34. Once again, the dipole pattern is the leading pattern, explaining about 31.5% of the variance. The quadrature pattern again takes its place as EOF 2. This dipole/quadrature pattern is now revealed as the leading mode in the error fields of poor forecasts of the grid point model and the T106 model, as well as the entire 10-year set of poor forecasts. Earlier in Chapter V, the inherent bias caused by the use of 10-year statistics was discussed. This resulted in the selection of more poor forecasts from the earlier years of the 10-year period, with less poor forecasts selected from the later years of the data set. However, there does not appear to be a serious drawback in using the 10-year statistics to differentiate between poor and good

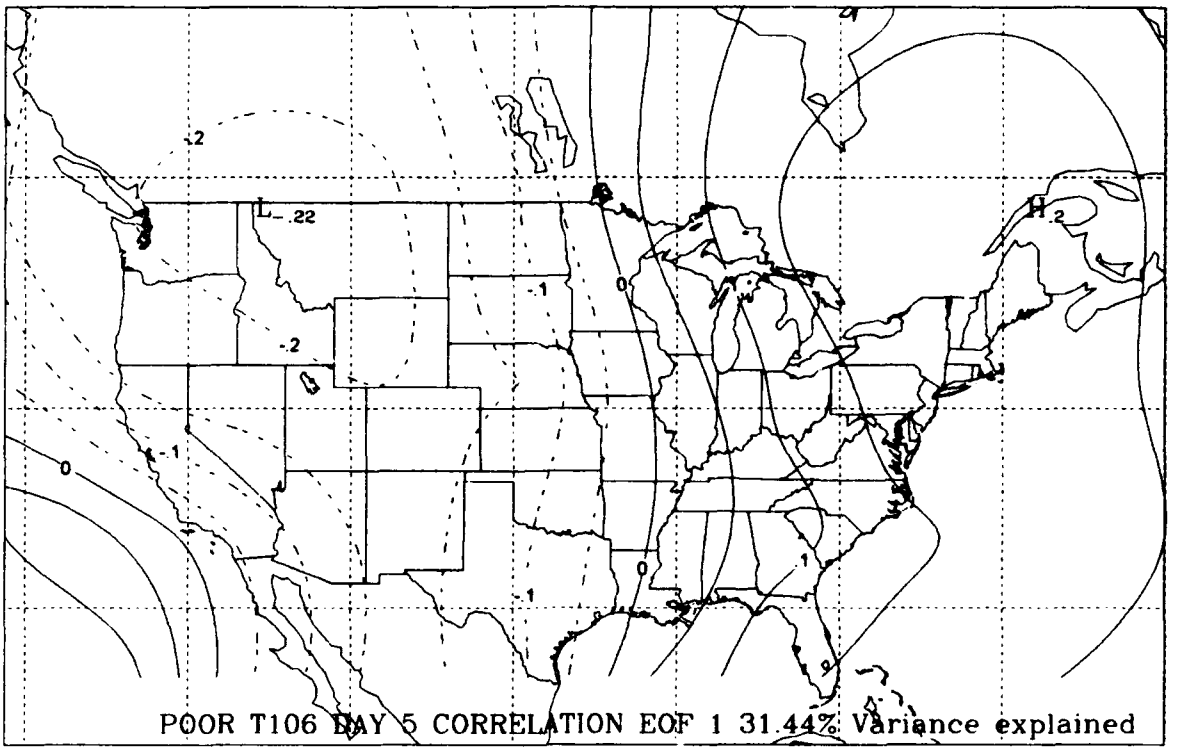

a.

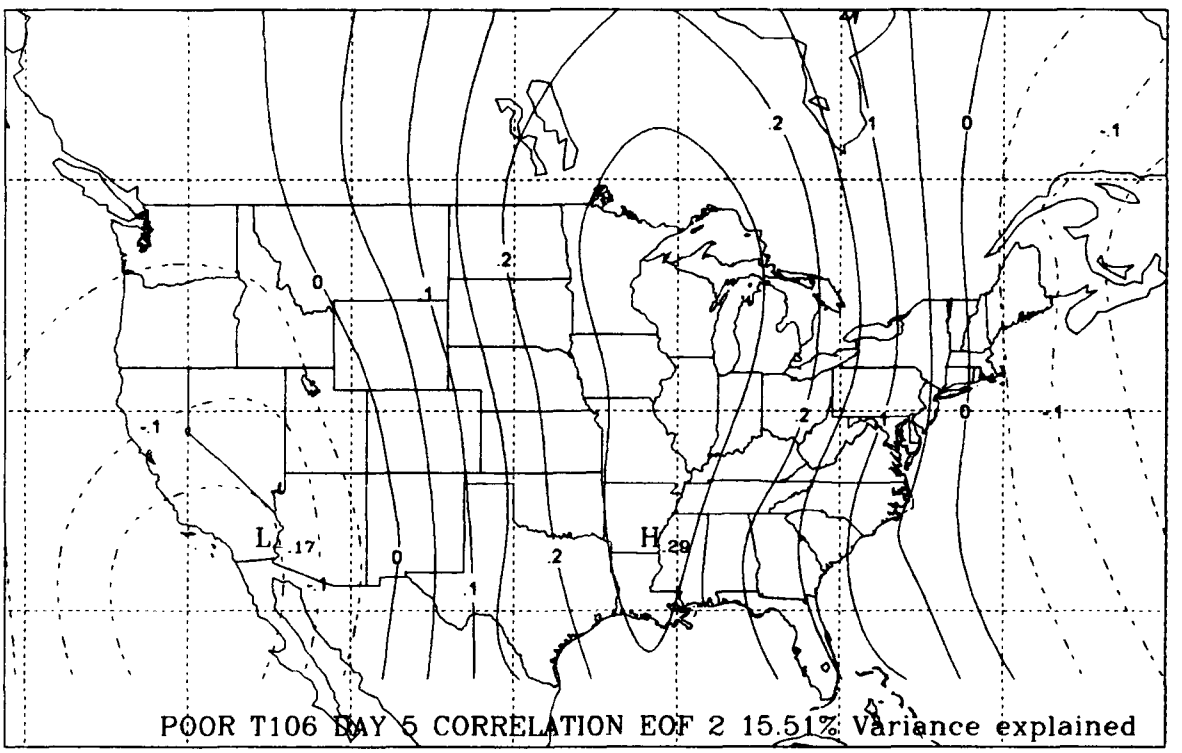

b.

Figure 34. Leading correlation EOFs of the day 5 error field of poor forecasts from the T106 operational version of the ECMWF model.

forecasts, since all three of these data sets exhibit the same error modes in poor forecasts on day 5.

3. Summary

The existence of this quadrature pattern in poor forecasts, but not good forecasts, requires further discussion. The leading dipole pattern, which is centered around the Rockies, resembles that discussed by Arpe and Klinker (1986). However, the existence of its quadrature is important also. When both phases (positive and negative) of these two EOFs are taken in combination, the result is all four phases of what appears to be a standing wave originating due to the Rocky Mountains. The oscillation of this wave is controlled by the daily amplitudes of the respective EOFs. When the pattern is most influenced by the leading EOF, the amplitude maxima of the resulting error field will most resemble the dipole pattern However, when the quadrature portion contributes more to the total pattern, the amplitude maxima of the resulting error field will be shifted further downstream from the Rockies. This apparent movement of this feature develops on the 3 - 5 day time scale. This time scale was also identified by the temporal EOF analysis as the time of maximum RMS growth in poor forecasts. Thus, it appears that the conditions and times of maximum RMS growth are directly related to the appearance of this orographic feature.

This apparent standing wave over the CONUS in the error fields of poor forecasts is tested to determine if it can be associated directly with the occurrence of poor forecasts. Specifically, it is speculated that these two EOFs reveal an orographic instability in the form of a standing downstream wave resulting from the Rockies and that this wave can be related to the mean zonal wind over the CONUS.

Zonal mean 500 mb heights over the sector of the CONUS region are computed at two latitudes (30 N and 48.75 N) for use in the geostrophic wind equation of Holton (1992). These give a value of the mean 500 mb zonal wind between approximately 30 and 50 N. The zonal winds were computed for both the initial conditions of all forecast runs,

as well as for each forecast day. The values of 5-day CONUS RMS were then plotted against the zonal wind speeds of the corresponding initial conditions which produced the forecasts. The results are shown in Fig. 35. If the poor forecasts were related, via the zonal wind, to the standing wave orographic instability, the RMS values of poor forecasts should be restricted to a narrow range of zonal wind speeds. This range should also be exclusive of the wind speeds related to the other categories. However, this separation of good and poor forecasts on the basis of mean zonal winds was not found to be the case, as the distributions of mean zonal wind speeds are essentially equivalent for both poor forecasts and good forecasts (Fig. 36). Similar poor results were obtained when this comparison was made using the mean zonal winds computed over several other geographical regions immediately upstream from the CONUS region.

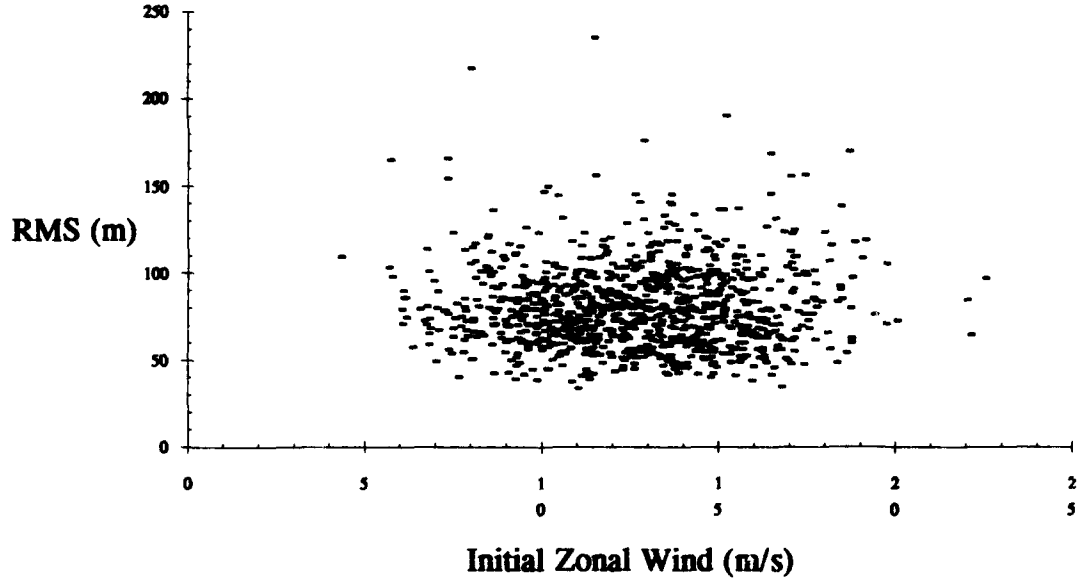

Figure 35. Scattergram of the relationship between the initial condition mean zonal wind speed and the 5-day CONUS RMS value.

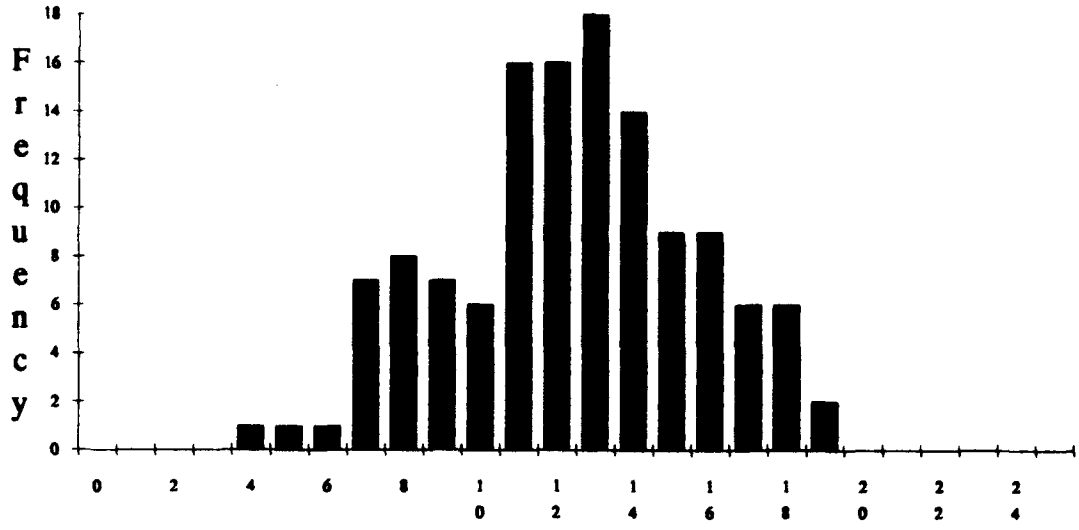

a.

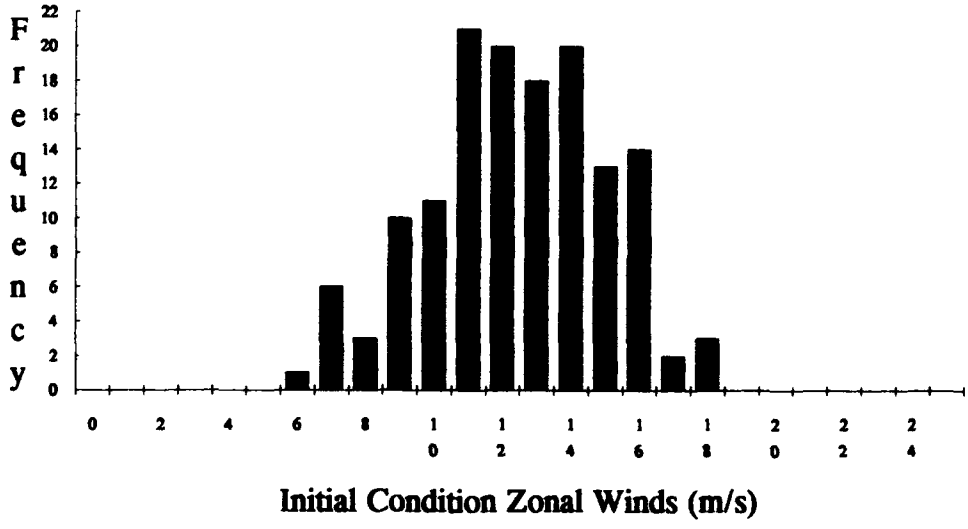

b.

Figure 36. Distribution of CONUS initial condition mean zonal wind speeds. (a.) Poor forecasts subset and (b.) good forecast subset.

CHAPTER VII

SUMMARY

The error fields of poor 5-day CONUS forecasts have been examined in three ways. These examinations have revealed several interesting features about the growth of errors in these forecasts, both from temporal and spatial points of view.

Examination of the raw error data revealed that the CONUS region is in a relative minimum area when measuring the frequency of errors at the 5-day point. The maxima which lie just upstream and downstream of the CONUS are in documented areas of persistent anomalies. The errors over the CONUS are fairly evenly divided between under and over forecasts of the 5-day 500 mb height.

The RMS error value for the CONUS was used as the measure of forecast performance over the region of interest. In keeping with previous work with this data set, a normal distribution of this value was assumed. However, in this study, the 10-year mean and standard deviation were used to provide critical values for poor and good forecasts. This was done to avoid the paradox in which overall forecast performance improves, (as measured by annual RMS values), but the actual number of poor forecasts increased with time. However, this creates a bias in the data due to the general decrease of the RMS error with time. The subset of poor forecasts is weighted more toward the early years of the period, while the subset of good forecasts is slanted more toward the latter portion of the period. A similar study of the RMS distribution was accomplished for the East Pacific Ocean region immediately west of the CONUS region. It was found that the distribution of 5-day RMS values for this region was not significantly different than that over the CONUS.

A subjective analysis of the error growth of a subset of the poor forecasts was accomplished. This revealed no outstanding pattern of raw error growth, location of

error initiation zones or movement of the error action centers with time. In fact, maximum error amplitudes in the poor forecasts were found to occur throughout the entire Northern Hemisphere, rather than in distinct regions. It was also observed that the error action centers exhibited very little transient behavior, but instead seemed to grow *in situ* with time.

Additionally, the same subset of poor forecasts was analyzed to determine the differences between forecasts originating on successive days which verify on the same day four to six days later. Again, for the successive forecasts, the main error centers for the CONUS did not exhibit significant day to day movement. A trend was noted throughout the entire forecast data set for the percentage of poor forecasts for these valid dates to increase with increasing forecast length. This would indicate that the distribution of the RMS error value becomes skewed more with time. On the other hand, 5-day forecasts that were poor were likely to be poor 6-day forecasts started a day earlier or poor 4-day forecasts started a day later. This result is not consistent, however, with the observation that poor forecasts tend not to be episodic.

Due to the limited success of these subjective analyses, a more objective approach was taken through the use of EOF analysis, both in time and space. The temporal analysis used the daily CONUS RMS errors which evolved out of each 5-day forecast run. This procedure showed that there were quantifiable differences in the evolution of the RMS errors between poor and good forecasts. Good forecasts were found to have the majority of their RMS growth on the first day of the forecast run. However, poor forecasts were found to perform as well as all other forecasts for one or two days before experiencing a rapid growth of error on days 3 and 4. With regards to the dominant EOFs, the paths taken by poor and good forecasts are completely opposite. In particular, good forecasts experienced excessively weak error growth on days 3 - 5. The dominant EOFs were found to explain a significant majority of the performance of both poor and good forecast RMS growth.

The spatial EOF analysis of the daily error fields of evolving poor and good forecasts revealed significant differences between the two categories. Initially, both categories were found to exhibit universally typical EOF modes. However, poor forecasts exhibited a pair of EOF modes which combine to define an apparent standing wave which seems to originate due to the presence of the Rocky Mountains. This combination of EOFs becomes dominant on the 3 - 4 day time length indicative of synoptic weather systems. By day 5, the two EOFs combine to explain over 40% of the variance in the error fields. No similar pattern or combination of patterns was found within the analysis of good forecasts.

The pattern evidenced by the leading EOFs of poor forecasts resembles a standing wave which may represent an orographic instability. In an attempt to relate the performance of poor forecasts to the presence of this wave, the RMS value of the poor 5-day forecast was compared to the mean zonal wind speeds over the CONUS. This comparison was made using both the mean zonal wind from the initial conditions and the 5-day forecast. No tendency for poor forecasts to be associated with a restricted range of zonal wind was found. The same poor results were found when the mean zonal winds were computed over other geographical regions upstream of the CONUS.

Many questions remain unanswered regarding the causes of poor forecasts, not only over the CONUS, but on a global scale. This study has focused on diagnosing the patterns which exist in the error fields over the CONUS region. Further investigation is necessary to determine why these patterns produce poor forecasts. It is possible that the leading EOFs and the poor RMS error values are more closely related to the wind fields at other levels of the atmosphere, or even to some combination of levels. Additionally, it has been suggested that the error action centers or the error trains may be related to other dynamic variables such as the vorticity field. Since the leading patterns over the CONUS appear to be linked to the Rocky Mountains, refinements to

the model orography in this region may also yield successful results. Many other possibilities exist and warrant further research.

The objectives of this research have been met. The 10-year climatological distributions of the 5-day RMS values have been examined over different geographical regions in order to define poor and good forecasts. A case study of error evolution was presented. The growth of CONUS RMS with time has been analyzed using EOF analysis and was found to be different for poor and good forecasts. The spatial evolution of the CONUS error fields was investigated with EOFs and the dominant patterns were found. The leading spatial patterns were also found to be different for poor and good forecasts. These EOF results were compared for different time periods in the evolution of the ECMWF model and no significant differences were found. The spatial patterns found in poor forecasts suggested a dynamic-orographic relation between the poor forecasts and zonal winds. However, no strong relation between the two values was found.

APPENDIX A

VALID DATES OF POOR FORECASTS

The subset of poor forecasts used in this study consists of 5-day forecasts valid on the following dates:

801205	820125	840205	870207
801206	820203	840223	870208
801210	820204	841206	870209
801217	820210	841207	870224
810102	820212	841214	871229
810103	820213	841222	871230
810104	820214	841223	880110
810113	820216	841224	880124
810119	820218	841228	880228
810122	820220	850101	880229
810125	820221	850113	881212
810201	821210	850116	881218
810203	821211	850117	890103
810209	821222	850119	890108
810211	821223	850122	890130
810214	821228	850201	890131
810215	821230	850202	890201
810216	830103	850209	890202
810224	830110	850211	890203
810225	830111	850224	890228
810226	830129	850308	890303
810227	830202	851224	900101
811221	830219	851225	900112
820104	830223	851227	900118
820108	831215	851231	900126
820109	831221	860106	900301
820110	831222	860131	900302
820111	831223	860306	900303
820115	831224	860307	900304
820118	831225	861207	
820120	831226	861219	
820121	840117	870123	
820124	840204	870206	

APPENDIX B

VALID DATES OF GOOD FORECASTS

The subset of good forecasts used in this study consists of 5-day forecasts valid on the following dates:

801207	840123	860217	880121
801208	840211	860218	880129
801220	840224	860219	880130
801223	840303	860303	880131
801224	840304	860309	880205
810112	840305	861205	880208
810114	850126	861210	880214
810115	850127	861215	880216
810124	850128	861220	880226
811215	850215	861221	880227
820129	850217	861224	880306
820303	850218	870108	880307
820305	850225	870119	881216
830107	850226	870120	890105
830108	850227	870128	890109
830121	851209	870129	890114
830122	851215	870216	890117
830131	851216	870217	890119
830205	851217	870220	890120
830208	851221	870307	890128
830209	851228	871207	890207
830211	860102	871208	890210
830301	860103	871209	890211
830302	860110	871212	890222
831205	860121	871220	890224
831206	860124	880108	891207
840103	860201	880112	891210
840105	860205	880116	891215
840107	860208	880118	891219
840118	860213	880119	891220
840122	860215	880120	891223

900105
900106
900109
900111
900114
900115
900116
900124
900128
900129
900201
900206
900207
900208
900211
900214
900215
900225
900226
900309

REFERENCES

Alberta, T. L., S. J. Colucci and J. C Davenport, 1991: Rapid 500-mb Cyclogenesis and Anticyclogenesis. *Mon. Wea. Rev.*, **119**, 1186-1204.

Arpe, K., 1990: Impacts of Changes in the ECMWF Analysis-Forecasting Scheme on the Systematic Error of the Model. *Seminar Proceedings Ten Years of Medium-range Weather Forecasting*, 4-8 September 1989 Vol I, 69-114. ECMWF, Shinfield Park, Reading, RG2 9AX, United Kingdom.

Arpe, K. and E. Klinker, 1986: Systematic Errors of the ECMWF Operational Forecasting Model in Mid-Latitudes. *Quart. J. Roy. Meteor. Soc.*, **112**, 181-202.

Dalcher, A. and E. Kalnay, 1987: Error Growth and Predictability in Operational ECMWF Forecasts. *Tellus*, **39A**, 474-491.

Girard, C. and M. Jarraud, 1982: Short and Medium Range Forecast Differences Between a Spectral and a Grid-Point Model. An Extensive Quasi-Operational Comparison. ECMWF Tech. Rep. No. 32, ECMWF, Shinfield Park, Reading, RG2 9AX, United Kingdom.

Holton, J. R., 1992: *An Introduction to Dynamic Meteorology, Third Edition.* Academic Press. 511 pp.

Lorenz, E. N., 1982: Atmospheric Predictability Experiments With a Large Numerical Model. *Tellus*, **34**, 505-513.

_____, 1989: Effects of Analysis and Model Errors on Routine Weather Forecasts. *Seminar Proceedings Ten Years of Medium-range Weather Forecasting*, 4-8 September 1989 Vol I, 115-128, ECMWF, Shinfield Park, Reading, RG2 9AX, United Kingdom.

Lynch, P., 1992: Richardson's Barotropic Forecast: A Reappraisal. *Bull. Amer. Meteor. Soc.* **73**, 35-47.

Lyons, S. W., 1992: Skill and Reliability of Medium Range Numerical Weather Forecasts. NWS Southern Region Forecaster Notes No. 8. NWS Southern Region, Fort Worth, Texas.

Netterville, L. S., 1991: Predictability of ECMWF 5-Day Forecasts Over the Contiguous United States. M.S. Thesis, Texas A&M Univ. College Station, Texas, 72 pp.

Ott, L., 1988: *An Introduction to Statistical Methods and Data Analysis, Third Edition.* PWS-Kent. 835 pp.

Platzman, G. W., 1967: A Retrospective View of Richardson's Book on Weather Prediction. *Bull. Amer. Meteor. Soc.*, **48**, 514-550.

Preisendorfer, R. W., 1988: *Principal Component Analysis in Meteorology and Oceanography.* (C. D. Mobley, posthumous compiler/editor), Elsevier, 425 pp.

Richardson, L. F., 1922: *Weather Prediction by Numerical Process.* Cambridge University Press, 236 pp.

Richman, M. B., 1986: Rotation of Principal Components. *J. Climatology.* **6**, 293-335.

Roebber, P. J., 1984: Statistical Analysis and Updated Climatology of Explosive Cyclones. *Mon. Wea. Rev.*, **112**, 1577-1589.

Simmons, A. J., 1983: Adiabatic Formulation of the ECMWF Forecasting System. *ECMWF Seminar/Workshop Proceedings on Interpretation of Numerical Weather Prediction Products.* 13-24 September 1982, 49-82, ECMWF, Shinfield Park, Reading, RG2 9AX, United Kingdom.

Trenberth, K. E. and J. G. Olson, 1988: ECMWF Global Analyses 1979-1986: Circulation Statistics and Data Evaluation. NCAR Tech. Rep. 300+STR, P. O. Box 3000, Boulder, Colorado.

Uccellini, L. W., 1990: Processes Contributing to the Rapid Development of Extratropical Cyclones. *Extratropical Cyclones: The Erik Palmen Memorial Volume.* C. W. Newton and E. O. Holopainen, Eds. American Meteorological Society, 81-105.

VITA

Norman Ray Modlin was born August 1, 1964 in Williamston, NC. He is the third of five children of Dallas S. and Lorina C. Modlin. He graduated as Class Valedictorian from Jamesville (NC) High School in June 1982.

Norman then enrolled at North Carolina State University, Raleigh, NC. While at NCSU, he was a member of the Gamma Beta Phi Honor and Service Society, serving as the organization's treasurer during his senior year. In May 1986, Norman was awarded the degree of Bachelor of Science in Meteorology, graduating *Cum Laude*.

In October 1986, Norman entered the United States Air Force Officer Training School. He was named a Distinguished Graduate of OTS and commissioned as a Second Lieutenant, USAF in January 1987.

After commissioning, Norman was assigned to Barksdale AFB, LA where he served as a Duty Officer in the Eighth Air Force Weather Support Unit. In October 1989, he was reassigned to serve as 37th Tactical Fighter Wing Weather Officer at the Tonopah Test Range, NV. From August 1990 to April 1991, Norman was deployed to King Khalid AB, Saudi Arabia, where he served as Commander, Detachment 26, 1690th Provisional Weather Group and Staff Weather Officer, 37th TFW Provisional. While in Saudi Arabia, he supported F-117 operations during Operations DESERT SHIELD and DESERT STORM. He was reassigned in August 1991 to Texas A&M University to participate in the Air Force Institute of Technology Master of Science Program in Meteorology. Following this, he will be assigned to the USAF Environmental Technical Applications Center (USAFETAC) at Scott AFB, IL.

Norman was married in November 1988 to the former Lilah M. Gaulden of Ruston, LA. They have a son, Christopher, who was born in April 1990.

Norman's permanent address is that of his parents: Route 1, Box 281-AA Jamesville, NC 27846.